Contributed Talks

Session 1

Wednesday 11.03.2020

10:10 - 12:10

Thermochemical heat storage using alcohol solvates

D.J. Kok, H. Meekes & E. Vlieg

Solid State Chemistry, Radboud University, Heyendaalseweg 135, 6525 AJ Nijmegen,
The Netherlands
E-mail: dirkkok@science.ru.nl

Summary

Renewable energy sources tend to be inflexible: energy is either currently available or not. With the continuing drive towards a larger fraction of renewables in our power mix, the need for energy storage capacity is rising. Since an average household in Europe consumes about 70% of its energy in the form of heat for hot water and space heating [1], storing heat is an attractive option.

Currently, there are three ways of storing heat:

- Sensible heat storage: storing a warm substance
- Latent heat storage: storing heat in a phase transition
- Thermochemical heat storage: storing heat in a reversible chemical reaction, often hydrate or solvate formation

Thermochemical heat storage has several advantages: it has a very high energy density, and the dehydrated compound can be stored indefinitely, whereas sensible heat will always leak away. In addition, latent heat is difficult to partially release while a rehydration reaction stops when the solvent vapor flow ceases.

The general principle of seasonal thermochemical heat storage is shown in fig. 1. The discharged reactor, containing the host-solvent complex, is heated using a solar thermal collector. The solvent is stored, and in winter, the solvent vapor is allowed to flow back to the dry host, exothermically forming the complex again.

Good candidate materials need to have a high energy density (≈ 1 GJ/m^3 or more), release the solvent at a useful temperature (roughly between 70 and 130 °C for domestic applications) and not have any side reactions with the solvent or the reactor. Also, the material should not be highly toxic or too expensive.

Most research into these systems has focused on hydrates (see for example [2]), but the vapor pressure of water is inconveniently low. At 10°C, it is 12 mBar while ethanol has a vapor pressure of 29 mBar and methanol has a vapor pressure of 68 mBar. This makes alcoholate complexes interesting candidates for heat storage systems.

Since alcoholate complexes are not nearly as well studied as hydrates, current work is focusing on determining the energy density and cycle stability of different materials. First, it must be determined whether there is an exothermic solvate formation or not and whether the complex also forms from gaseous solvent or only in solution. The latter is done in a thermogravimetric analysis (TGA) setup with an alcohol bubbler attached. This setup is also used to test how many cycles the compound will last. Alcoholate crystals are grown from solution to determine or confirm their structures. These crystals are then also investigated with differential scanning calorimetry (DSC) and TGA to determine their energy density. Some example curves for $CaBr_2x6MeOH$ are shown in fig. 2. It took between 463 and 544 J/g to remove the methanol from the crystals, which gives an energy density of 0.72-0.85 GJ/m^3.

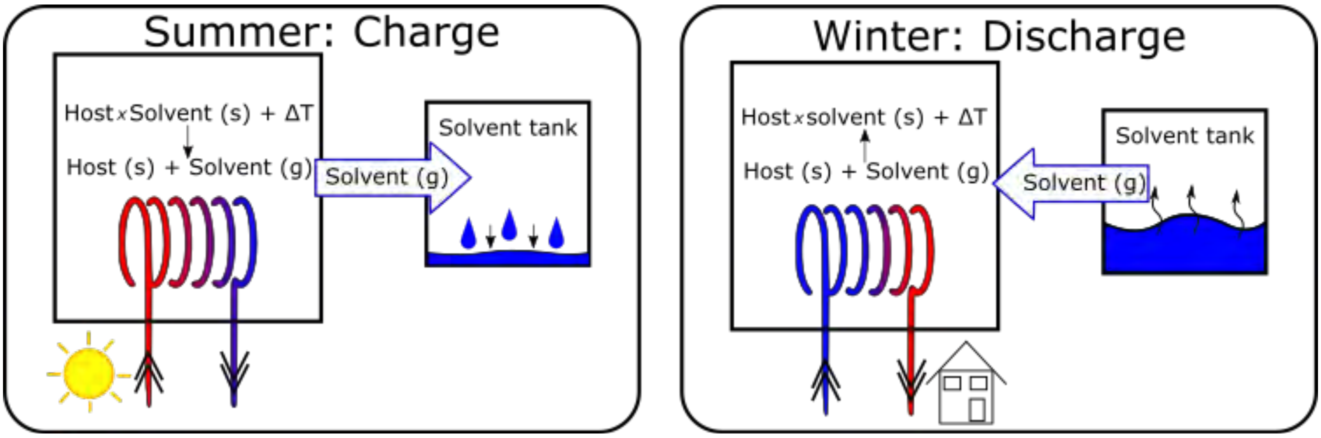

Fig. 1: General principle of seasonal heat storage based on a thermochemical system.

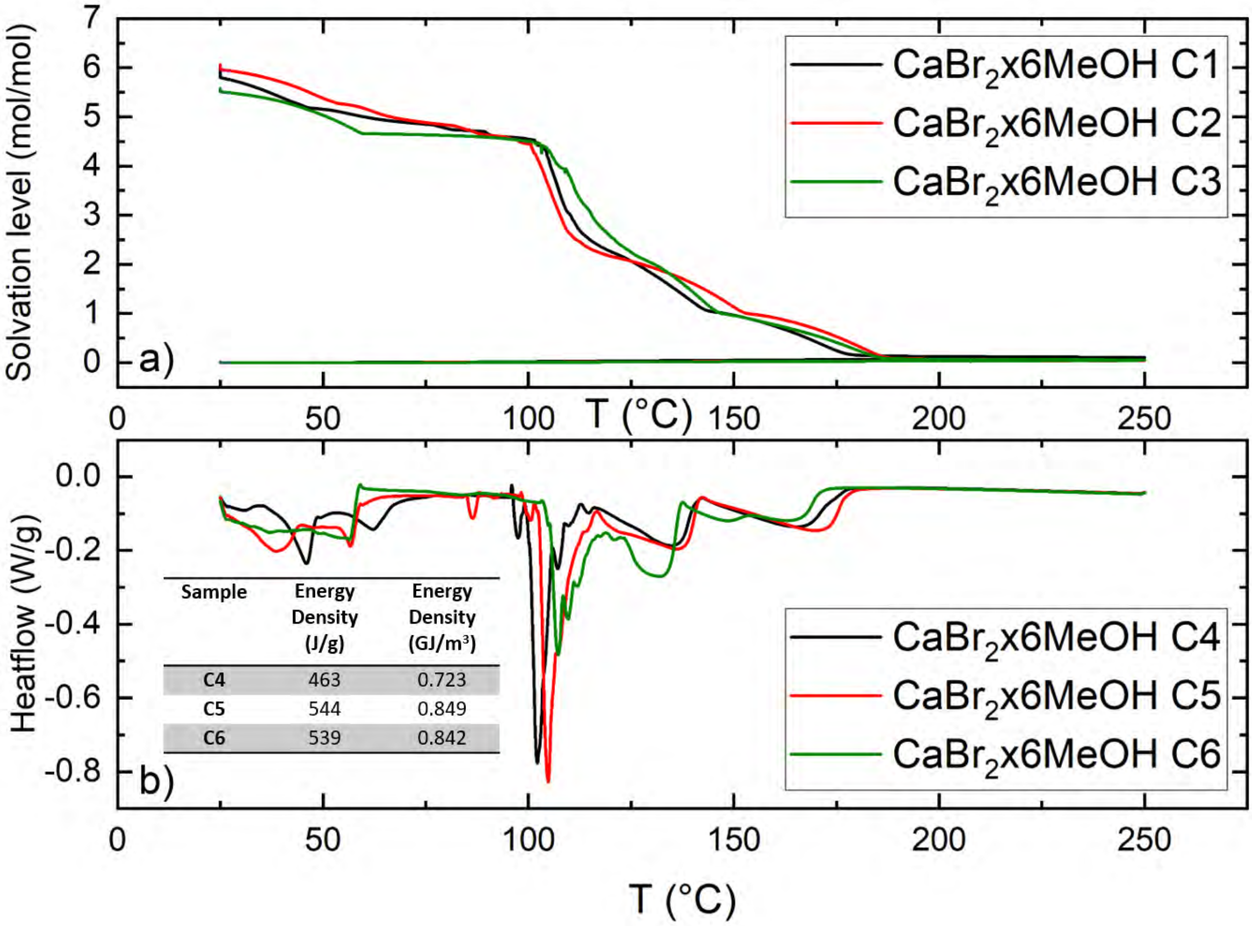

Sample	Energy Density (J/g)	Energy Density (GJ/m³)
C4	463	0.723
C5	544	0.849
C6	539	0.842

Fig. 2: Thermal analysis results for $CaBr_2x6MeOH$. a) Solvation level calculated from TGA measurements b) DSC heating curves.

Acknowledgment
We kindly acknowledge funding by Topsector Energie under project number TEUE117062 (SWeKOS).

[1] F. Belaïd, Energy Policy, **92**, 220-233 (2016)
[2] P.A.J. Donkers, L.C. Sögütogl, H.P. Huinink, H.R. Fischer, O.C.G. Adan, Applied Energy, **199**, 45-68 (2017)

VGF-Growth of Half-Heusler-material for industrial production of Thermoelectric-material

M. Gerrmann[a*], D. Zuckermann[a], A. Fey[a], S. Herbert[a], C. Klingelhöfer[a], V. Macin[a], D. Eirich[a]

[a] Isabellenhütte Heusler GmbH & Co KG, Eibacher Weg 3-5, 35683 Dillenburg, Germany
** Corresponding Author: mathias.gerrmann@isabellenhuette.de*

The industrialization and automation of material and module manufacturing technologies is one of the important topics to reduce the costs of thermoelectric technology. The company Isabellenhütte Heusler GmbH & Co. KG (ISA) is engaged in the industrialization of the thermoelectric (TE) technology based on Half-Heusler-materials (HH).

The ISA has a long tradition in Heusler-compound research. The great grandfather of the actual CEO Dr. Felix Heusler was Dr. Fritz Heusler. Dr. Fritz Heusler developed the first Heusler alloy in 1901 at the Isabellenhütte. Unfortunately there was no economic use for this kind of compounds for the company until today.

Since 2009 the Isabellenhütte is actively involved in Heusler alloy research again. The purpose of the project activities is the development of a melt metallurgical manufacturing process for an appropriate HH-material, which can be industrialized. A second objective in this context is the development of thermoelectric modules using the developed Half-Heusler-material.

In 2017 the Isabellenhütte built up an industrial pilot line production, which starts with the raw material and ends up with thermoelectric modules. The ambition is to demonstrate an industrial scale material manufacturing and an automated assembling process of HH-TE-modules in a constant high quality.

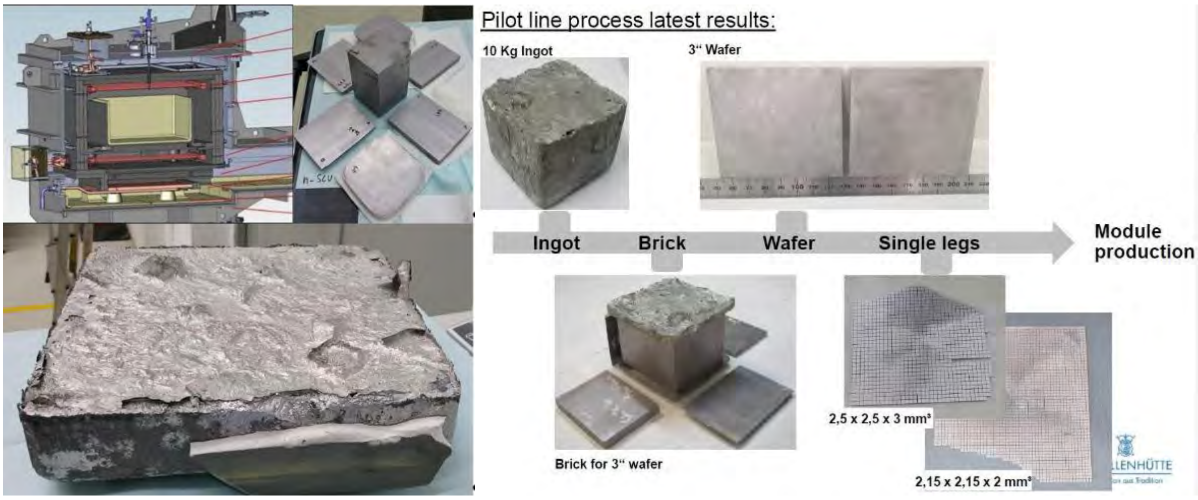

Figure 1 – L: VGF-furnace with a 10kg and the 25kg ingot. R: Pilot line process.

A key feature for the industrial scale material manufacturing is the mass production of the raw material. Following the silicon mass production, for solar cells, etc., the VGF-method got judged as a promising process for the preparation of the HH-materials in an industrial scale. We succeeded to grow 10kg ingots of HH-material with the VGF-method. Both classes of HH-materials, p- and n-type, were grown with a reproducible quality. Additional the process was used to grow ingots up to 25kg (see Fig. 1).

Due the industrialization of the thermoelectric module manufacturing, Isabellenhütte developed a two-step module design concept (see Fig. 2). The first step is the production of an unicouple. The second step is the mounting of many unicouples on the surface of a special cold side substrate without the classical massive ceramic sheet. In this way it is possible to produce different module geometries with one type of unicouple. Additional it´s possible to process different materials.

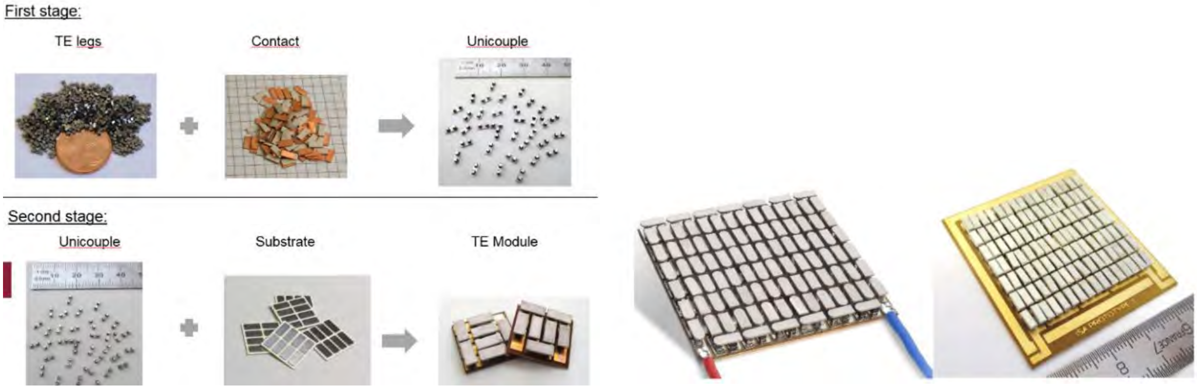

Figure 2 – 2 step manufacturing and prototype modules from an industrial like production.

The raw material for the unicouples are legs cut from the VGF-grown ingots. The VGF-ingot is getting cut with a band saw into a cuboid. Then wafers are cut from the cuboid with an inner diameter saw. The legs for the unicouple are fabricated with a blade saw. Finally one p-type and one n-type leg are getting assembled on top of a hot side contact to a unicouple.

For the second step IH built up an automated production line for a standard type of thermoelectric modules to investigate an industrial manufacturing. The line has a theoretical production capacity of 5.8 million unicouples p.a.. This amount of unicouples is enough to equip 50.000 modules with a size of 40mm by 40mm. Isabellenhütte developed a first standard module with 40 x 40 mm² for qualification testing and customer sampling (figure 3.).

3D interlayer growth in the high temperature vapor phase epitaxy of GaN

T. Schneider[a], M. Förste[a], P. Fischer[b], C. Röder[c], E. Niederschlag[a], O. Pätzold[a], D. Rafaja[b], M. Stelter[a]

[a] *Institute of Nonferrous Metallurgy and Purest Materials, TU Bergakademie Freiberg, Leipziger Straße 34, 09599 Freiberg, Germany*
[b] *Institute of Materials Science, TU Bergakademie Freiberg, Gustav-Zeuner-Straße 5, 09599 Freiberg, Germany*
[c] *Institute of Applied Physics, TU Bergakademie Freiberg, Leipziger Straße 23, 09599 Freiberg, Germany*
E-mail: Tom.Schneider@inemet.tu-freiberg.de

Summary

The growth of GaN by high temperature vapor phase epitaxy (HTVPE) is based on the physical vapor transport of gallium. Thermally evaporated gallium is transported to a substrate, where it reacts with ammonia to form a GaN layer according to $2Ga + 2NH_3 \rightarrow 2GaN + 3H_2$. This method has attracted interest, because aggressive or toxic substances are widely avoided and high growth rates can be reached. In the last years, advanced HTVPE techniques with improved process control and stability were developed [1–6]. The potential of the method for the deposition of GaN seed layers on sapphire substrates [1-4] and for the deposition of GaN bulk layers with a growth rate of up to 200 µm/h [5,6] was demonstrated.

This contribution addresses recent progress in the growth of GaN layers by HTVPE. A novel multi-step process aimed at the in-situ deposition of 3D interlayers to control the dislocation density and the stress level is described. A series of GaN samples deposited on 15 x 15mm^2 sapphire substrates under different growth conditions is presented. The results of SEM, XRD and Raman measurements are shown and the influence of a 3D interlayer on the dislocation density and the residual stress is discussed.

Fig. 1a shows the HTVPE reactor used for the experiments. The main components are made of refractory metals, glassy carbon, pyrolytical boron nitride and fused silica. The reactor provides a flexible setting of the process parameters in wide ranges [3,4]:

- Separate control of the substrate temperature T_S and the temperature of the Ga melt T_{Ga} in the ranges of 500 – 1350°C and 1100 – 1350°C, respectively.
- Variation of the reactor pressure from 20 to 1000 mbar.
- Control of the growth rate between 0.1 – 160 µm/h.

A scheme of the presented GaN samples is shown in Fig. 1b. Starting from a sapphire substrate, the samples are formed by a seed layer – 3D interlayer – top layer sequence. The process steps used for the deposition of the seed layers can be summarized as follows [3,4]:

- Deposition of a nucleation layer with a thickness of about 20 nm at a reactor pressure of 985 mbar, a substrate temperature of 500°C and with a typical growth rate of 240 nm/h.
- Recrystallization of the nucleation layer at the substrate temperature of 1080°C under an ammonia and hydrogen containing atmosphere.
- High-temperature (HT) growth to form a coalesced GaN seed layer with a thickness of about 2 – 5 µm at a reactor pressure of 985 mbar and a substrate temperature of 1100°C with a growth rate of about 2.5 µm/h.

The interlayers were deposited at a reactor pressure of 55 mbar under different substrate temperatures (900°C, 950°C, 1000°C) and Ga melt temperatures (1300°C, 1320°C, 1340°C) with growth rates in the range of 27 – 57 µm/h. Under these conditions, 3D growth dominates leading to a preferred formation of voids and pyramidal facets (see Fig. 1c). In the final process step, the interlayers were coalesced within 90 min at a reactor pressure of 985 mbar, a substrate temperature of 1100°C and a Ga melt temperature of 1300°C to form a 2D top layer (see Fig. 1d). First XRD and Raman investigations of the samples indicate that a 3D interlayer mainly influences the residual compressive stress, whereas the dislocation density remains essentially unchanged in comparison with a reference sample without interlayer.

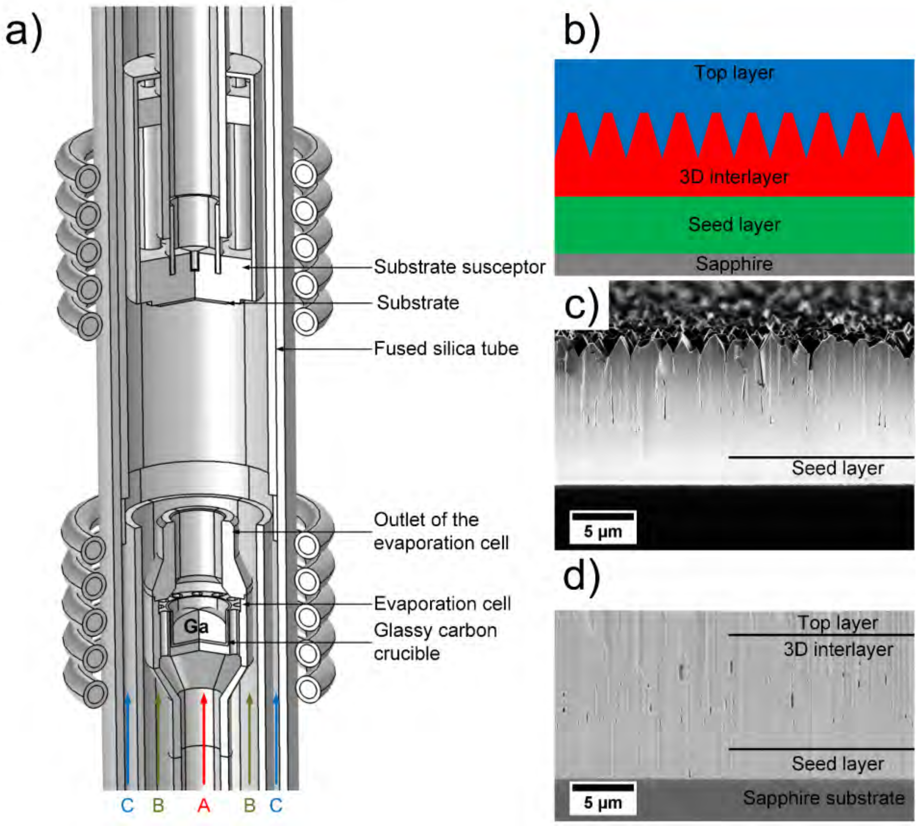

Fig. 1: a) Scheme of the HTVPE reactor. A, B, and C indicate different gas flows: A – Ga transport flow (Ar, H_2), B – separation flow (N_2), C – NH_3 transport flow (H_2, N_2). b) Cross-section scheme of the layer sequence of the presented GaN samples. c)/d) Cross-section SEM images of an interlayer-terminated/a complete GaN sample with a coalesced top layer.

Acknowledgment
The financial support by the German Research Foundation (projects PA 1236/3 and RA 1050/28) is gratefully acknowledged.

[1] G. Lukin, C. Röder, M. Barchuk, G. Schreiber, O. Pätzold, J. Kortus, D. Rafaja, M. Stelter, Physica Status Solidi C , **11**, 491-494 (2014)
[2] G. Lukin, T. Schneider, M. Barchuk, F. Zimmermann, E. Niederschlag, O. Pätzold, M. Stelter, Physica Status Solidi A, **214**, 1600753 (2017)
[3] G. Lukin, T. Schneider, M. Förste, M. Barchuk, C. Schimpf, C. Röder, F. Zimmermann, E. Niederschlag, O. Pätzold, F. C. Beyer, D. Rafaja, M. Stelter, Journal of Crystal Growth, **524**, 125185 (2019)
[4] T. Schneider, M. Förste, G. Lukin, P. Fischer, M. Barchuk, C. Schimpf, E. Niederschlag, O. Pätzold, D. Rafaja, M. Stelter, Journal of Crystal Growth, **533**, 125465 (2020)
[5] D. Nakamura, T. Kimura, Applied Physics Express, **10**, 95503 (2017)
[6] D. Nakamura, T. Kimura, K. Horibuchi, Applied Physics Express, **10**, 45504 (2017)

Growth of ^{28}Si crystals for preparation of Si spheres

N.V. Abrosimov, H. Riemann, H.-J. Rost, L. Lehmann, M. Renner, S. Weiß, R. Menzel

Leibniz-Institut für Kristallzüchtung (IKZ), Max-Born-Straße 2, 12489 Brlin, Germany
nikolay.abrosimov@ikz-berlin.de

Summary The manufacturing chain of ^{28}Si crystals from the enrichment procedure up to the growth of the final 4 inch crystals by the Floating Zone (FZ) technique is described systematically. As a result, six ^{28}Si dislocation free single crystals of 100 mm in diameter were grown in the frame of "Avogadro", "Kg-2" and "Kg-3" projects for preparation of Si spheres used for a more precise determination of the Avogadro constant, which has been crucial for the new definition of the mass unit - kilogram.

On the 16th of November 2018, the General Conference on Weights and Measures in Paris passed a new definition of the kilogram, which has been successfully entered into force on the 20th of May 2019. There are seven fundamental units: meter, second, kilogram, ampere, candela, kelvin, and mole which are organized in the International System of Units (SI). The main idea of metrology in the last decade was to define these units in terms of fundamental natural constants and one of them is the Avogadro constant N_A - the number of atoms contained in a certain quantity of a substance, i.e. in one mole. N_A is used then for determining of the Planck constant as the basis for the new definition of the kilogram standard that was the last unit based on an artefact - the so-called prototype kilogram (Urkilogramm) in Sevre near Paris.
The IKZ was involved in several projects, such as ""Avogadro", "Kg-2" and "Kg-3" under the initiative and management of the Physikalisch Technische Bundesanstalt (PTB; the German National Metrology Institute) aiming at a more precise determination of the Avogadro constant. It was done by counting the atoms in ^{28}Si silicon spheres prepared by PTB with less than 20 nm shape deviation at a diameter of approximately 93.6 mm and with a surface polished free of defects. These spheres were used for measurements to establish a connection between the volume and the number of atoms in the highly ordered crystalline structure. To make Si spheres one needs to grow perfect Si crystals of about 100 mm in diameter. Six ^{28}Si dislocation free single crystals of 100 mm in diameter were grown by FZ technique over the last 12 years (Fig.1).

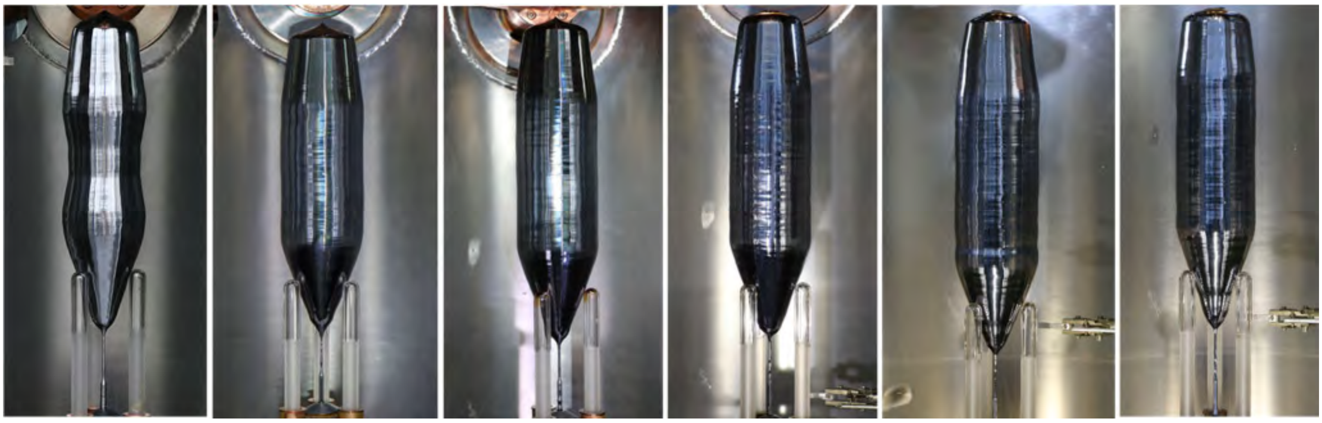

Fig. 1: ^{28}Si dislocation free single crystals of 100 mm in diameter grown by FZ technique in the frame of "Avogadro", "Kg-2" and "Kg-3" projects

Manufacturing chain of the ^{28}Si highly enriched crystals includes five main steps (Fig. 2). A big challenge relating to the production of highly enriched ^{28}Si is saving the isotopic enrichment of the starting material during all technological steps and improving the high chemical purity at the same time.

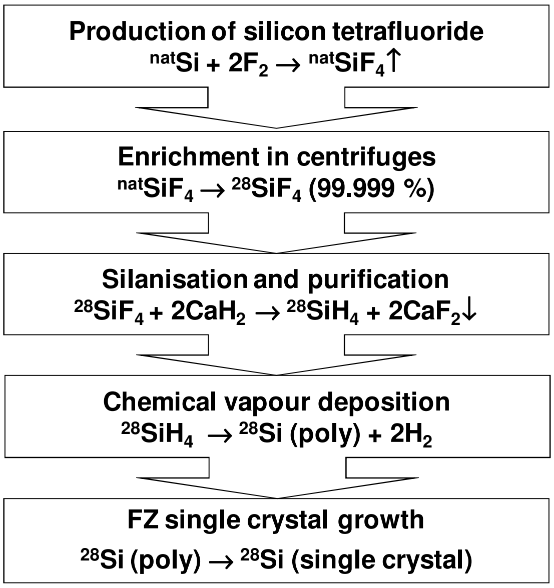

Fig. 2. Main technological steps of the ^{28}Si crystal production [1].

Crystal growth techniques such as FZ, pedestal and Czochralski (CZ) are used for the single crystal growth and recycling of ^{28}Si residues after different steps of the manufacturing chain (Fig. 2) and material characterization. To improve the chemical purity of the starting polycrystalline material several FZ runs, partly in vacuum in order to remove oxygen, were carried out. For the CZ growth, the quartz crucible was coated with $^{28}SiO_2$ to avoid the introduction of other Si isotopes by erosion of the inner crucible surface in contact with molten^{28}Si. As a result, dislocation free ^{28}Si single crystals of about 4” diameter with an enrichment of up to 99.9995 at% and weights of about 5.5 kg could be grown using the FZ technique.

FZ grown ^{28}Si crystals were also used for the investigation of the basic properties of the novel material. In natural Si the stable isotopes ^{28}Si, ^{29}Si, ^{30}Si, mixed in the crystal lattice, influencing the average molar mass, changing the whole phonon spectrum and causing inhomogeneous line broadening. For instance, the thermal conductivity of a ^{28}Si crystal enhances according to the enrichment level from 45.5 Wcm^{-1}K^{-1} to ca. 450 Wcm^{-1}K^{-1} at 24K in a crystal of ^{28}Si (99.995 %) being the highest ever measured value for thermal conductivity of dielectrics at any temperature [2]. The absence of the ^{29}Si nuclear magnetic dipoles enables a spin-free “semiconductor vacuum” making them very promising for quantum information technologies and for the development of Si-based quantum computer [3].

[1] N.V. Abrosimov, D.G. Aref’ev, P. Becker, H. Bettin, A.D. Bulanov, M.F. Churbanov, S.V. Filimonov, V.A. Gavva, O.N. Godisov, A.V. Gusev, T.V. Kotereva, D. Nietzold, M. Peters, A.M. Potapov, H.-J. Pohl, A. Pramann, H. Riemann, P.-T. Scheel, R. Stosch, S. Wundrack, S. Zakel, Metrologia **54**, 599 (2017).

[2] A.V. Inyushkin, A.N. Taldenkov, J.W. Ager III, E.E. Haller, H. Riemann, N.V. Abrosimov, H.-J. Pohl, P. Becker, JApplPhys **123**, 095112 (2018).

[3] M. Steger, K. Saeedi, M.L.W. Thewalt, J.J.L. Morton, H. Riemann, N.V. Abrosimov, P. Becker, H.-J. Pohl, Science **336**, 1280 (2012).

Session 2

Wednesday 11.03.2020

13:20 – 15:00

X-Ray Diffraction Analysis of the Defect Structure of Diamond Substrates and Thick Diamond Films

L. Kirste, J. Engels, T. Fuchs, P. Knittel, J. Langer, M. Prescher, P. Reinke, J. Weippert, V. Cimalla, & V. Lebedev

Fraunhofer Institut für Angewandte Festkörperphysik (IAF),
Tullastraße 72, 79108 Freiburg, Germany
E-mail: lutz.kirste@iaf.fraunhofer.de

Diamond is a wide band-gap semiconductor with a number of extraordinary physical properties promising for emerging devices such as power transistors, high frequency electro-acoustic filters, integrated photonic circuits and quantum-effect sensors.
Defect density and substrate size are still bottlenecks for the development of reliable and cost-effective diamond based devices. In the past years, a number of approaches have been developed to produce larger substrates, as well as substrates with relatively low defect density. Using a bulk crystal growth technique like the high-pressure high-temperature method (HPHT) for diamond, dislocation densities below 5×10^{3} cm^{-2} were demonstrated. However, for the diamond HPHT crystal growth process, the resulting levels of impurities are typically high and additional wafer diameters are still small and the yield of devices is therefore low. On the other side, for larger substrates and low impurity levels, concepts based on heteroepitaxy are used, e.g. chemical vapor deposition (CVD) of diamond on Ir/YSZ/Si (001) template. The drawback of these heteroepitaxial method is that the density of dislocation is typically high (e.g. $\approx 10^{8}$ - 10^{10} cm^{-2}). Since a low content of crystal defects is a critical requirement for the realization of demanding diamond-based devices with high efficiency, performance and lifetime, it is necessary to determine the types of defects and their density in the substrate crystals.

In this work we will present a detailed analysis of the defect structure of freestanding diamond substrates grown by HPHT and CVD and thick (> 10 µm) diamond layers grown by CVD. Aspects such as defect types and defect densities depending on crystal growth method, seed material and doping (e.g. boron doping for power transistors or nitrogen doping for quantum sensing devices based on spin properties of the nitrogen vacancy (NV) center in diamond) will be discussed. X-ray topography (XRT) and high resolution X-ray diffraction (HRXRD) are used for this combined study. XRT in two principal ways is used in the course of this analysis, namely the projection transmission mode and the section transmission mode. HRXRD (reciprocal space mapping, $\omega/2\Theta$-scans and ω-scans) is used for the analysis of subsurface damage, strain and mosaicity of the diamonds. The combination of these analytical methods allows a detailed statement of the nature, density and distribution of typical defects in diamond bulk substrates and epitaxial CVD grown diamond layers.

Fig.1 and Fig.2 show as examples type 220 reflection X-ray topographies (projection mode and section mode, Mo-radiation) of large CVD-grown (001) diamond substrates from two different vendors. The diamond crystal of Fig.1 was grown heteroepitaxially on an Ir/YSZ/Si (001) seed (Vendor: Audiatec). The projection topography (Fig. 1a) of this diamond shows a mosaic-like blurred contrast (orientation contrast) of a mosaic crystal with tilted and twisted grains. No sharp contrast of individual dislocations is observable. However, the projection topography shows some kind of texture (Fig.1b). Important information can be extracted from the section topographies (Fig.1c and 1d). While the image of the $2\bar{2}0$ reflex is very diffuse, the topography of the $\bar{2}\bar{2}0$ reflex shows a lateral domain structure, which suggests an epitaxial lateral overgrowth (ELOG) technique. Fig. 2a shows the projection topography of a diamond grown by CVD on a high quality HPHT diamond seed (Vendor: ElementSix). In the center of the crystal the defect density is low and only single threading dislocations are visible. In contrast, dislocation bundles with a high density appear at the {100} growth sector boundaries. The high material quality in the center of the crystal is confirmed by the visibility of Kato-fringes in the section topographies of Fig.2b.

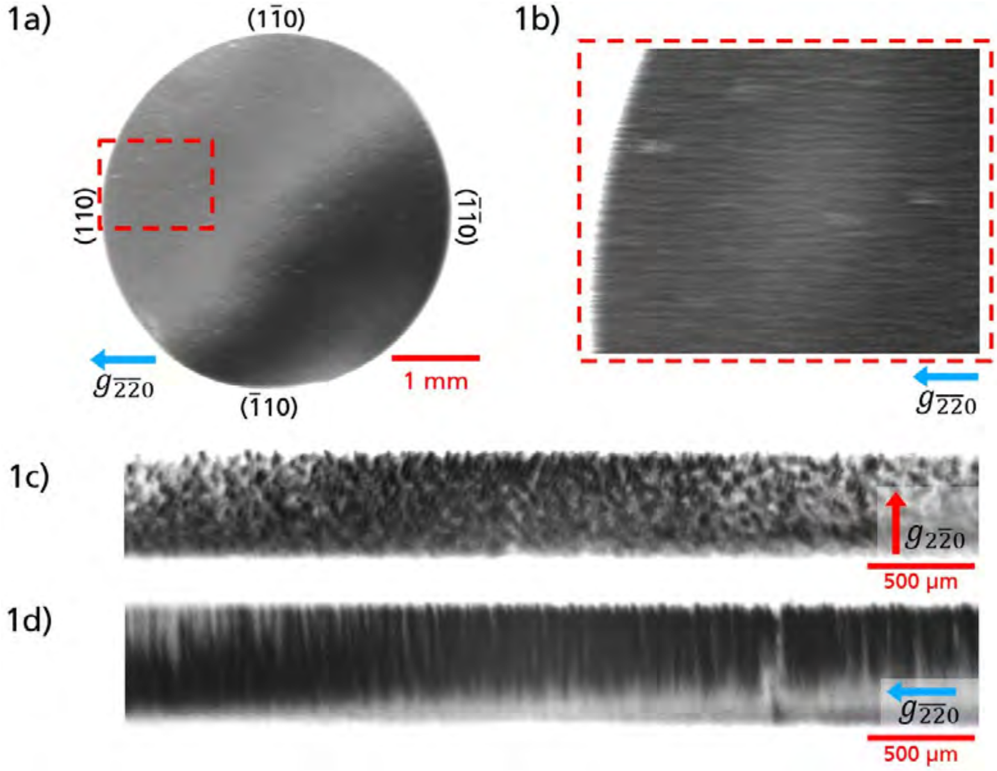

Fig. 1: XRT of a diamond crystal (diameter: 9 mm) grown heteroepitaxially by CVD on an Ir/YSZ/Si (001) seed. The seed was removed after growth. (Fig. 1a and 1b: projection topographies, Fig. 1c and 1d: section topographies)

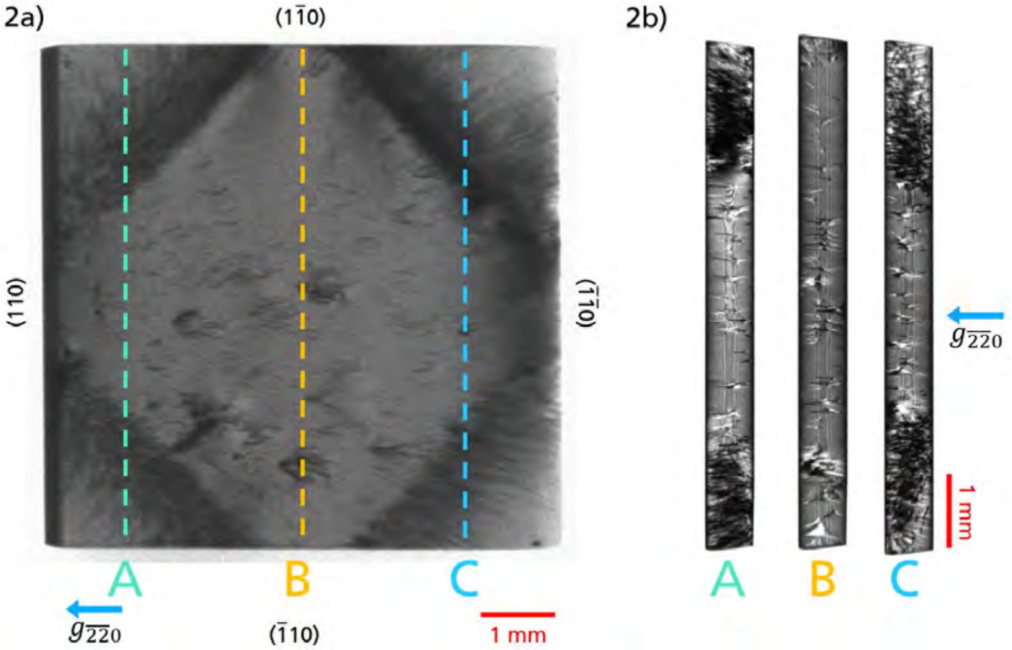

Fig. 2: XRT of a diamond crystal (size: 7 mm × 7 mm) grown homoepitaxially by CVD on a HPHT diamond (001) seed. The seed was removed after growth. (Fig. 2a: projection topography, Fig. 2b: section topographies)

PVT GROWTH OF LARGE FREESTANDING C-DOPED ALN CRYSTALS

S. Müller, B. Epelbaum, T. Wicht, S. Besendörfer, R. Weingärtner, D. Jockel
E. Meissner and J. Friedrich

Fraunhofer IISB, Schottkystr. 10, 91058, Germany
E-mail: stephan.mueller@iisb.fraunhofer.de

Summary

The availability of large size, high quality AlN substrates is critical for a high yielding, cost-effective production process of the next generation of AlGaN devices via homoepitaxy for UV-optoelectronics and power electronics. Despite considerable efforts and recent progress [1], high quality 2" AlN substrates are still far from being widespread commercially available. Moreover, for applications in power electronics, an even larger substrate sizes will be necessary to take advantage of the economy of scale and advanced equipment of existing fab lines. While a slow but steady increase of crystal size by repeated PVT bulk growth has been demonstrated, only very limited data is available on changes of the AlN crystals defect microstructure during growth both within the regular growth direction ($[0001]$ or $[000\bar{1}]$) or within any lateral expansion areas. It is of particular interest, if the new crystal material added by lateral expansion differs in structural quality from the original material in the center area. Possible reasons for such difference include: (i) thermomechanical stress build up in the growing crystal, and (ii) differences in the growth modes for various crystallographic directions. It is well known from other PVT grown semiconductors like SiC, that the diameter expansion geometry needs to be chosen very carefully to avoid stress and any related deterioration of the crystal quality [2].

In order to minimize thermomechanical stress and specifically investigate this aspect (ii) for the AlN material system, we employed a dedicated PVT growth geometry based on the concept of Lely growth [3]. By establishing conditions with low thermal gradients, we were able to investigate the *fundamental* possibility to maintain both, the crystal quality in axial and lateral portions of material grown in quite different growth modes. The seed wafers used for this study were cut from previous bulk AlN crystals grown in our laboratory with approximately one inch diameter and mainly wafer halves. The seed thickness was about 600 µm, with both surfaces polished mechanically with 1 µm diamond slurry. On some of seed wafers we added differently oriented edge flats in order to facilitate the formation of side facets and to investigate lateral growth (Fig. 1). All seed wafers were annealed at temperature of 2250-2300°C in isothermal conditions in slightly undersaturated AlN vapor during 2-5 hours prior to setting them into the growth cell. Thermal anneal was essential for the removal of residual surface damage, in particular on seed edges and added flats. These seeds were mounted in a Lely-type growth assembly shown schematically in Fig. 1A. Hereby the main structure used for growth was a central cavity build by sintered blocks of coarse grained (1 to 3 mm) AlN of high purity inside of a loosely-closed TaC crucible, also acting as background C-source for doping. All charge material was carefully purified by repeated re-sublimation in W-crucibles in a carbon-free reactor, resulting in slightly Al-rich material. The seeds were clamped at a targeted position with tungsten or tantalum stripes. Growth experiments were performed during 24-48 hours runs at $T > 2300$°C and 700-900 mbar of nitrogen pressure in a growth reactor with indirect heating of a dense graphite susceptor via an induction coil. Due to the very low T-gradients in our system, the habitus of grown crystals clearly reflects differences in the growth rates in various crystallographic directions (Wulff shape), with the biggest portion of new material always grown in $[000\bar{1}]$-direction on the N-polar face (normally facing towards the hotter crucible bottom), and only 200-400 µm grown on Al-polar face. As-grown crystals (Fig. 1 B, C) were first evaluated using optical microscopy, while the crystal surfaces morphology, formed in the course of the growth process, have been investigated in more details by AFM and SEM. The dislocation structures in the grown crystals were analyzed by X-ray diffraction (XRD), X-ray

topography (XRT)) and defect selective KOH/NaOH etching. The diffraction vectors chosen for XRT were $\vec{g} = [0004]$ (reflection geometry.), $\vec{g} = \langle 1\bar{1}00 \rangle$ (transmission geomentry) and $\vec{g} = \langle \bar{2}021 \rangle$ (transmission).

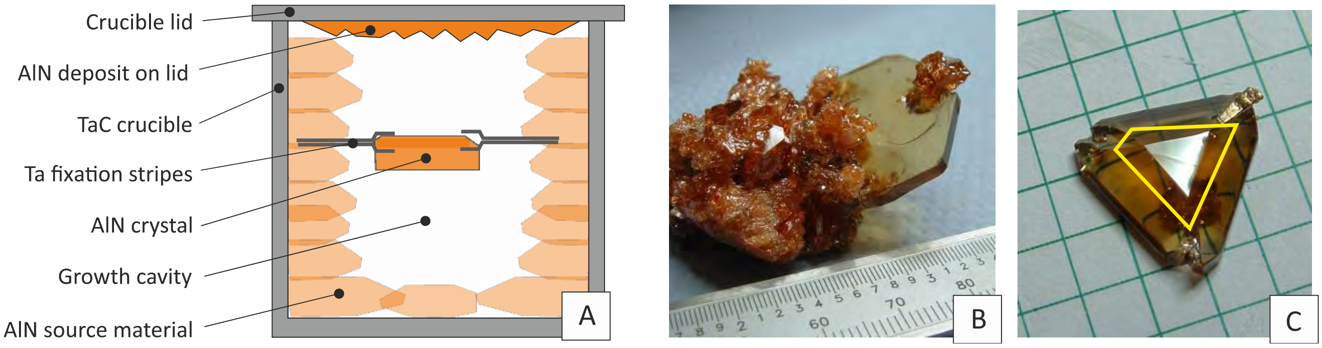

Fig. 1: Growth assembly for growth of unstrained AlN crystals (A) and some characteristic examples: crystal seeded on round wafer grows into hexagonal prism (B); triangle-shaped seed (marked yellow) produces large amount of lateral growth (C), grid scale in C is 5 mm.

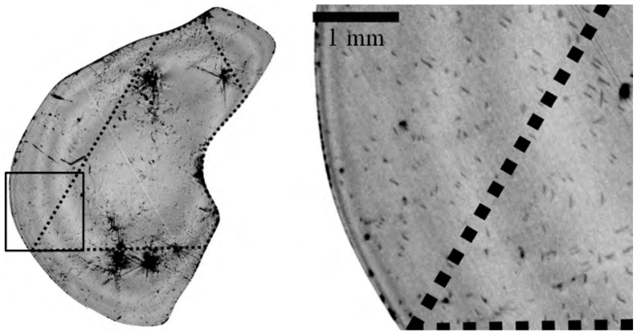

Fig. 2: XRT $\vec{g} = [\bar{2}021]$ measurements of an AlN wafer in transmission. The dotted triangle illustrates the border between material grown axially on top of the seed, and the lateral expansion area

XRD $(0\bar{1}10)$-rocking-curve mappings result in a mean FWHM of 13-17 arcsec which is in line with a low density of Basal Plane Dislocations (BPDs) as well as 2Θ-shift values in between ±15 arcsec, again in line with a low density of Threading Edge Dislocations (TEDs) in the range of $2\text{-}4 \cdot 10^3$ cm^{-2} for the great majority of the crystal volume i.e. for both regions the axially and the laterally grown crystal portions (excluding the areas of parasitic nucleation). These results are within the expectation for the low thermal gradient conditions employed for the growth. The comparison of XRT images of subsequent wafers sliced from the same crystal resulted in an identical Total Dislocation Density (TDD), demonstrating no deterioration of the high crystal quality during axial growth on N-polar (000-1)-face. On the other hand, locally increased FWHM and 2Θ-shift are found for parasitic grains and defect clusters. It is shown, that the latter were accommodated by both grain boundaries and by the formation of Basal Plane Screw Dislocations (BPSs) in adjacent areas during growth, identified as such for the first time in AlN bulk material. Most significantly, the crystal quality was typically the same in expansion areas compared to the center of the crystal (Fig. 2), despite the rather large laterally added area within a single growth run. In summary, it was shown, that fundamentally the high structural quality of bulk AlN material could be preserved within both, axial and lateral growth, independent on very strong differences in growth morphologies characteristic for differently oriented facets of carbon-doped AlN. Important differences in surface morphologies and their influence on growth rate, resulting crystal habit and defect formation will be presented as well.

[1] Dalmau, R., Craft, H. S., Britt et al. Materials Science Forum, **924**, 923–926 (2018)
[2] Drachev, R. V.; Hansen, D.; Loboda, M. J. *MRS Proc. 1246* (2010) K2.18.1.
[3] Lely, J. A., US Patent US2854364A, March 7, (1955)

Growth of bulk AlN crystals: Influence of the temperature field on growth rate, optical absorption and dislocation density

T. Straubinger, *C. Hartmann, L. Matiwe, J. Wollweber, I. Gamov, K. Irmscher, M. Bickermann*

Leibniz-Institut für Kristallzüchtung (IKZ), Max-Born-Str. 2, 12489 Berlin, Germany
E-mail: thomas.straubinger@ikz-berlin.de

Summary

Light emitting diodes (LEDs) for ultra-violet (UV) applications are typically processed on sapphire substrates and typically show threading dislocation densities (TDD) in the range of 10^9 cm^2 in the light emitting AlxGa1-xN multi-quantum well layers strongly reducing the radiative recombination efficiency [1]. One solution to overcome this issue is to use native aluminum nitride (AlN) substrates to grow device layers with TDD multiple orders lower compared to AlN on sapphire, typically < 10^5 cm^2 [2, 3].

AlN bulk crystals (Fig. 1, left) are grown with the physical vapor transport (PVT) method [3, 4] by evaporation of an AlN-powder source with low impurity level at temperatures of approx. 2250 °C and recrystallization at a colder AlN-seed at temperatures of approx. 2200 °C.

One key for successful AlN bulk growth is a fundamental understanding of the correlation of temperature field and growth rate which was investigated by growing crystals at five different growth conditions (T_{seed}, Delta-T) and comparing the results to a simple model based on diffusion and step-flow-growth [5]. The growth rate R is directly proportional to the absolute supersaturation S_{Al} (excess partial pressure of gaseous Al at the seed) and increases with both the temperature T_{seed} and the temperature difference Delta-T between source and seed.

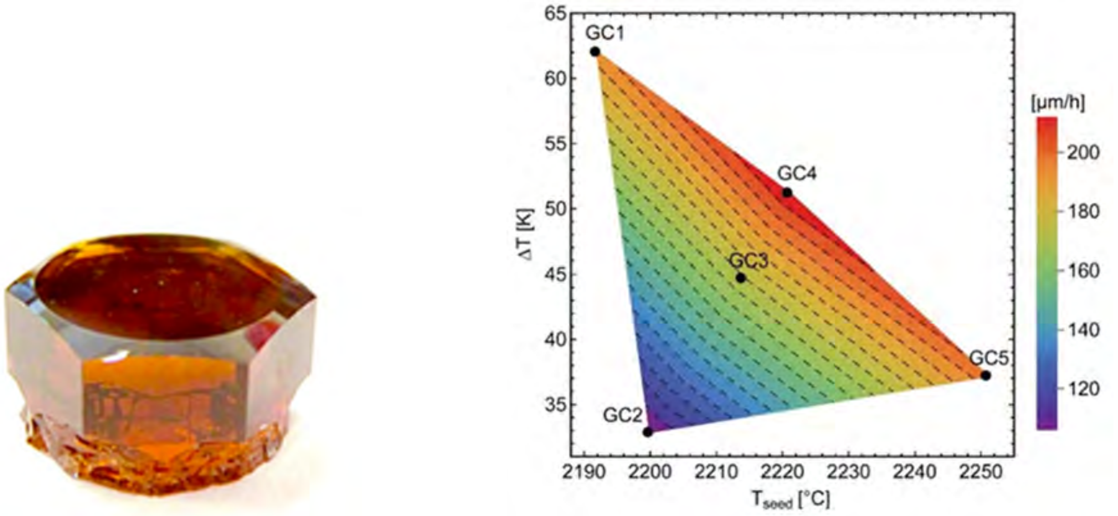

Fig. 1: Left - typical AlN crystal grown in c-direction with m-facets on side walls and 8 mm diameter. Right - contour plot of experimentally observed growth rates R (Tseed, Delta T). The five growth conditions (GC-x) used in the investigation are marked with black data points.

Prior to the analysis of structural and optical properties the AlN-crystals were sliced with an inner diameter saw and both side polished using diamond and SiO_2 (chemo mechanical polishing) abrasives. The absorption in AlN is mainly determined by the concentrations of the elements O, C and Si and their ratios. In all samples [Fig. 2] the carbon related absorption at 4.7 eV [6] is completely quenched due to the shift in the Fermi level because [O] + [Si] > 3 [C] [7]. The lowest absorption in the crucial wavelength range for, e.g., water disinfection (265 nm) is achieved for the crystal grown at the highest T_{seed}.

For the determination of the dislocation densities defect selective etching was performed using molten KOH. The dislocation density was then exclusively counted in the central area as the crystal rims showed defect clusters caused by contact to polycrystalline AlN which was nucleated next to the seed rim. The dislocation density significantly decreases with increasing T_{seed} while it seems not to be influenced by the growth rate and the temperature difference between source and seed.

In conclusion growth of AlN-crystals at high temperatures and low axial temperature gradients is favorable to gain AlN-substrates with low dislocation density (< 10^4 cm^{-2}) and high UV-transparency for AlGaN-based deep-UV emitters.

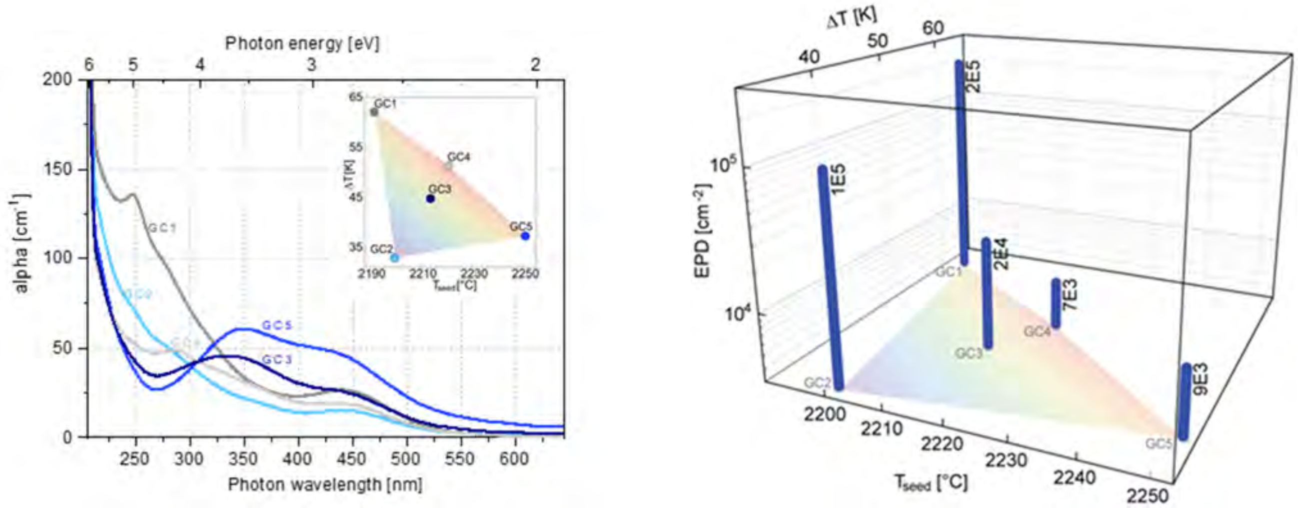

Fig. 2: Left - UV/VIS absorption spectra for the five crystals grown with different T-field and subsequent growth rates. Right - etch pit density (EPD) (z-axis) and subsequent growth rates (xy-plane) for the same crystals.

Acknowledgment

This work is financially supported by the Bundesministerium für Bildung und Forschung (Zwanzig20 Advanced UV for Live, 03ZZ0112A and 03ZZ0138A). This work is financially supported by the Bundesministerium für Bildung und Forschung (Zwanzig20 Advanced UV for Live, 03ZZ0112A and 03ZZ0138A). Parts of the work were also performed using funding from the German Research Foundation under grant no. BI781/11-1.

[1] M. Kneissl et al., Nature Photonics, **13**, pp. 233-244 (2019)
[2] R. Dalmau et al., Journal of the Electrochemical Society, **158 (5)**, pp. 530-535 (2011)
[3] R. Dalmau et al., Materials Science Forum, **924**, pp. 923-926 (2018)
[4] C. Hartmann et al., CrystEngComm, **18**, pp. 3488-3497 (2016)
[5] B. Epelbaum et al., Materials Science Forum, **457-460**, pp. 1537-1540 (2004)
[6] R. Collazo et al., Applied Physics Letters, **100**, p. 191914 (2012)
[7] K. Irmscher et al., Journal of Applied Physics, **114**, p. 123505 (2013)

Session 3

Wednesday 11.03.2020

16:30 – 18:10

MAGNETO-OPTICAL BISMUTH SUBSTITUTED RARE-EARTH IRON GARNET SENSOR FILMS FOR CHARACTERIZATION OF ELECTRICAL STEEL SHEETS

T. Reimann [a], M. Lindner [a], B. Wenzel [a], R. Holzhey [a]

[a] *INNOVENT e.V. Technologieentwicklung, Dept. Magnetic and Optical Systems, Prüssingstr. 27B, 07745 Jena, Germany*
E-mail: tr@innovent-jena.de

Summary

Bismuth-substituted rare-earth iron garnets (Bi-REIG) are well known for their high specific Faraday rotation of few degrees per micrometer film thickness. The principle of magneto-optical (MO) imaging using Faraday rotation (MOIF) is shown in Fig. 1. The local magnetic north and south pole of the magnetic sample results in an antipodal direction of the magnetic polarization of the Bi-REIG sensor film. The resulting opposing rotation of the polarized light leads to an optically visible black-white contrast. Therefore, the magnetic domain structure can be observed using a standard camera. The low optical absorption, high sensitivity for weak magnetic stray field strengths and high lateral resolution of Bi-REIG materials enables MOIF of magnetic domains in grain oriented electrical steel sheets (GOES). These are widely used as core material for inductive power transformers [1].
The investigation of the correlation between the magnetic properties and the crystallographic orientation of the GOES grains, was subject to research activities within the last years [2] [3]. In this work, the magnetic domain structure of a GOES (thyssenkrupp AG) was characterized by MOIF technique and the results were compared with texture measurements from XRD.

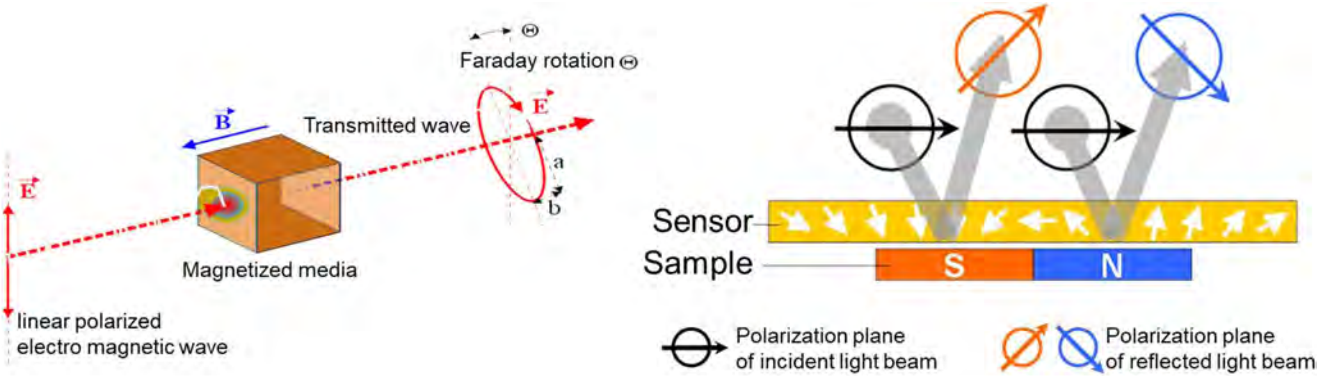

Fig. 1: Faraday effect of magnetized material (left) and illustration of the MO imaging principle (right).

Bi-REIG films were made by liquid phase epitaxy (LPE), with dipping technique in $PbO-Bi_2O_3-B_2O_3$ based flux. Single crystalline $Gd_3Ga_5O_{12}$ garnet disks ([111] oriented) with very low surface roughness and a diameter up to three inches were used as substrates. The deposition process was done under air atmosphere in a 3 zone furnace using platinum crucibles. After the LPE process, the coated substrates were cleaned and the BI-REIG layer was removed from one side by polishing. For use as MO sensor, the residual Bi-REIG film was coated with an additional mirror layer and a hard coating layer, in order to increase the scratch resistance. The MO sensor was cut into chips of size 20 mm x 15 mm. This sensor chips are used in a camera based measuring system for MOIF (CMOS Magview S, Matesy GmbH).

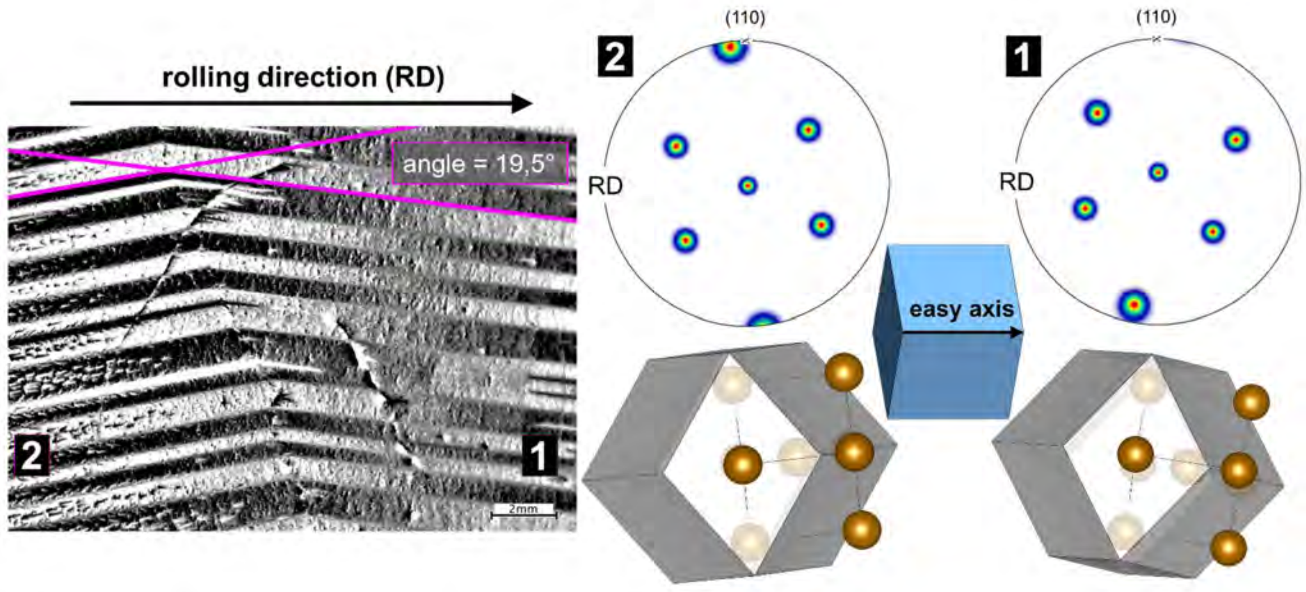

Fig. 2: MO image of grain oriented electrical steel (left), via CMOS-MagView technique and pole figures with illustrated crystal orientation of the two grains, measured by XRD texture analysis (right).

The measured magnetic domain structure of two grains of the GOES sample, is shown in Fig. 2. The XRD texture analysis (Bruker Discover, Co-K-alpha radiation) of these grains shows a typical rolling texture of the GOES. This is called Goss texture, where the (110) plane is ideally parallel to the surface and the magnetic easy axis [001] is oriented in the rolling direction (RD) (Fig. 2.). The XRD data was evaluated by MTEX toolbox for Matlab [2]. However, a misorientation of the easy axis according to the rolling direction in the x-y-plane can be detected by the XRD and MOIF analysis. As a result, the angle between the two domain directions in die MO image was 19.5°. Evaluation of the XRD data revealed the same angle between the intersection lines of the (110) planes of the two grain orientations with the x-y-plane. Because the magnetic domain structure is determined by the direction of the [001] axis, the MO image also gives a information on the actual crystallographic orientation of the GOES grains. This could be very suitable for the quality management of GOES production process. The MOIF techniques enables a very fast and sample preparation free measurement of the domain structure, compared to structure analysis techniques like XRD or EBSD.

Acknowledgment

We would like to thank Mr. Arne Bochmann from the Ernst-Abbe-University of applied Science Jena for providing support at the XRD texture measurements and evaluation.

[1] Hendryk Richert, Heidemarie Schmidt, Sandra Lindner, Morris Lindner, Benjamin Wenzel, Rocco Holzhey, and Rudolf Schäfer, steel research int., **No. 2**, 232-240 (2016)
[2] I. Gutierrez-Urrutia, A. Bottcher, L. Lahn, D. Raabe, J Mater Sci, **49**, 269-276 (2014)
[3] A. Nadouma, F. Robinsonb, S. Birosca, Journal of Magnetism and Magnetic Materials **Volume 494**, 165772 (2020)
[4] F. Bachmann, R. Hielscher, H. Schaeben, Solid State Phenomena, **Vol. 160**, 63-68 (2010)

Self-flux Growth of Single Crystals of BaCoSO

Y.H. Song [a], D.C. Peets [a,b], X.S. Liu [a], Maxim Avdeev [c], and D.L. Feng [a,d]

[a] *Department of Physics and Advanced Materials Laboratory, Fudan University, 2005 SongHu Road, Yangpu District, Shanghai 200438, China*
[b] *Institut für Festkörper- und Materialphysik, Technische Universität Dresden, Häcklstr. 3, 01169 Dresden, Germany*
[c] *Australian Nuclear Science and Technology Organisation, Lucas Heights, NSW 2234, Australia*
[d] *Hefei National Laboratory for Physical Science at Microscale and Department of Physics, University of Science and Technology of China, Hefei, Anhui 230026, China*
[e] *Collaborative Innovation Center of Advanced Microstructures, Nanjing 210093, China*
E-mail: darren.peets@tu-dresden.de

Summary

Doped BaCoSO was recently predicted to be a high-temperature superconductor in an entirely new class based on Co and Ni. BaCoSO has been recently prepared as a powder [1,2], but crystals have not been available. Based on its layered crystal structure, significant anisotropy would be expected in its electronic and magnetic response, which will require single-crystalline samples to elucidate. Single crystals will also be a prerequisite for several doping and measurement schemes in the quest to verify the prediction of superconductivity. We were unable to inject carriers or induce superconductivity in this study.

Using a Co-S self-flux method with a 5:1 flux ratio, we synthesized the first single crystals of the antiferromagnetic insulator BaCoSO from BaO, Co, and S. The growth was performed in a sealed quartz tube between 1000 and 880°C using an alumina crucible. Excess flux was removed at the conclusion of growth using a centrifuge. The resulting single crystals were up to $2\times2\times0.2$ mm^3 in size, black, with mirror surfaces largely free of flux [see Fig. 1(b) for an example].

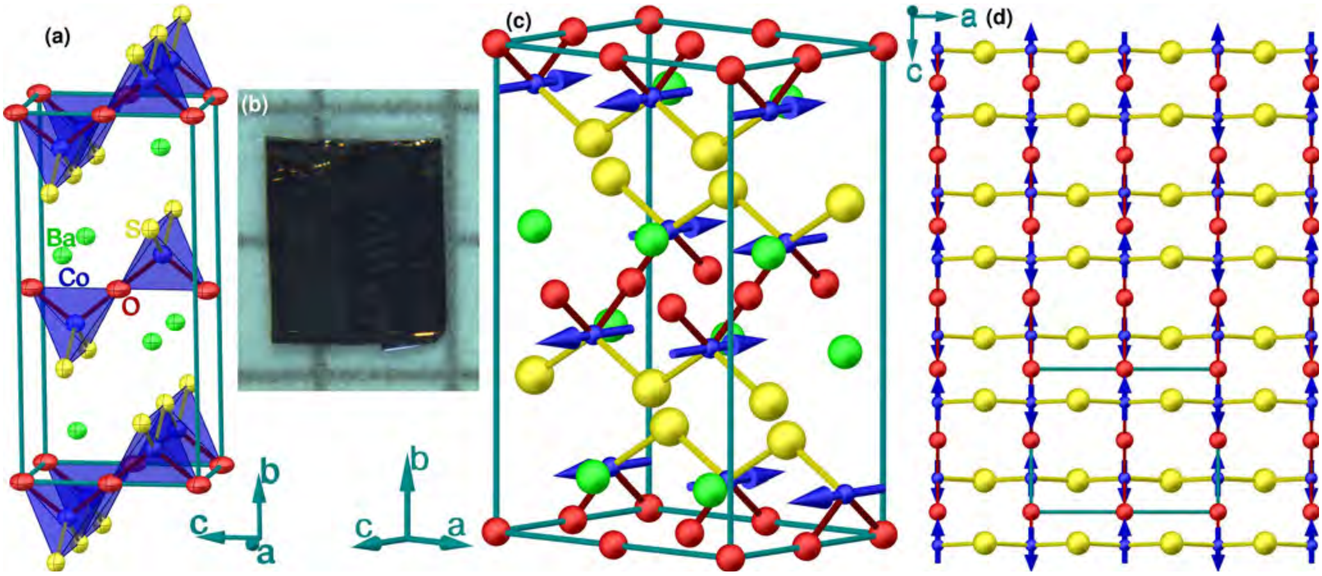

Fig. 1: Crystal and magnetic structure of BaCoSO, also now reported in our Ref. [3]. (a) Crystal structure of BaCoSO. (b) An example of one of the single crystals grown in this study, on millimetre-ruled graph paper. (c,d) Magnetic structure of BaCoSO.

Our magnetic and specific heat measurements and neutron single-crystal diffraction results provide previously-unavailable details of its magnetic anisotropy and order. The refined crystal and magnetic structure are shown in Fig. 1. We find a different magnetic space group from that reported previously, and a rather different magnetic response for fields along *c* than *a* or *b*. The vast majority of magnetic entropy is not released near the transition, suggesting the survival of significant short-range order to far higher temperatures. Our white-beam neutron Laue diffraction experiment was not sensitive to diffuse scattering, and was unable to confirm this.

Acknowledgment
This work is supported by the Science Challenge Project (grant No. TZ2016004), the National Key R&D Program of the MOST of China (grant No. 2016YFA0300203), the German Science Foundation from the project C03 of the Collaborative Research Center SFB 1143 at the TU Dresden (project-ID 247310070), and the National Natural Science Foundation of China (projects No. 11650110428, 11421404, U1532266, 11790312, and 11674367). D.C.P. is supported by the Chinese Academy of Sciences through 2018PM0036.

[1] M. Valldor, U.K. Rößler, Y. Prots, C.-Y. Kuo, J.-C. Chiang, Z.W. Hu, T.-W. Pi, Rüdiger Kniep, and L.H. Tjeng, Chem. Eur. J., **21**, 10821–10828 (2015)
[2] E.J.T. Salter, J.N. Blandy, and S.J. Clarke, Inorg. Chem., **55**, 1697–1701 (2016)
[3] Y.H. Song, X.S. Liu, D. Wu, Q. Yao, C.H.P. Wen, M. Avdeev, R. Peng, H.C. Xu, J. Miao, X. Lou, Y.F. Fang, B.L. Pan, N.L. Wang, D.C. Peets, and D.L. Feng, Phys. Rev. B, **100**, 205130 (2019), also available as arXiv:1911.03076

Crystal growth of the valence fluctuating system $EuPd_2Si_2$

Marius Peters, Doan-My Tran, Eunhyung Cho, Franz Ritter, Kristin Kliemt, and Cornelius Krellner

Kristall- und Materiallabor, Physikalisches Institut, Goethe-Universität Frankfurt, Max-von-Laue-Str. 1, 60438 Frankfurt am Main

E-mail: marius.peters@stud.uni-frankfurt.de

The study of collective phenomena raising from enhanced coupling between electrons and phonons is focussed on materials exhibiting phase transitions involving both electronic and lattice-degrees of freedom. One system providing such a strongly coupled phase transition is $EuPd_2Si_2$ of the $ThCr_2Si_2$ structural type, showing a temperature induced valence transition of europium between the energetically vicinal valence states Eu^{2+} and Eu^{3+} at about 160 K [1]. First reports on the synthesis of single crystals came up only recently [2], but a deep investigation of the valence transition in this compound is still missing.

We approached the ternary Eu-Pd-Si system using differential thermal analysis to map the local composition phase diagram. The target compound, its melting temperature and the remainders for certain starting stochiometries could be identified and utilised to conduct larger scaled growth experiments.

We used the Bridgman method to gain a seed of $EuPd_2Si_2$ for an iterative Czochralski method for the successful growth of mm-sized single crystals of $EuPd_2Si_2$ (see Fig. 1). These experiments were performed testing various levels of Europium excess in the starting composition.

Fig. 1, left to right: Czochralski growth, sample MP401 (generation 1), sample MP411 (generation 3).

The characterisation of this system is highly interdependent between the three pillars of stochiometrical, structural and physical characterisation. Structural characterization was done by powder X-ray diffraction (XRD). With this technique, we determined the temperature dependence of the lattice parameters by measuring XRD down to 50 K. The respective curves are depicted in Fig. 2a. We first focus on the (004) reflection at $2\Theta = 36.3°$. It is apparent that this peak is nearly temperature independent with a tendency of a shift to smaller angles at low temperatures, which corresponds to a constant *c* parameter through the valence transition with only a slight increase at low temperature (see Fig. 2c). In contrast, the *a* parameter decreases strongly (around 2%) when cooling through the valence transition, visible in the raw data as a significant shift of the (200) reflection and in the refined lattice parameter in Fig. 2b.

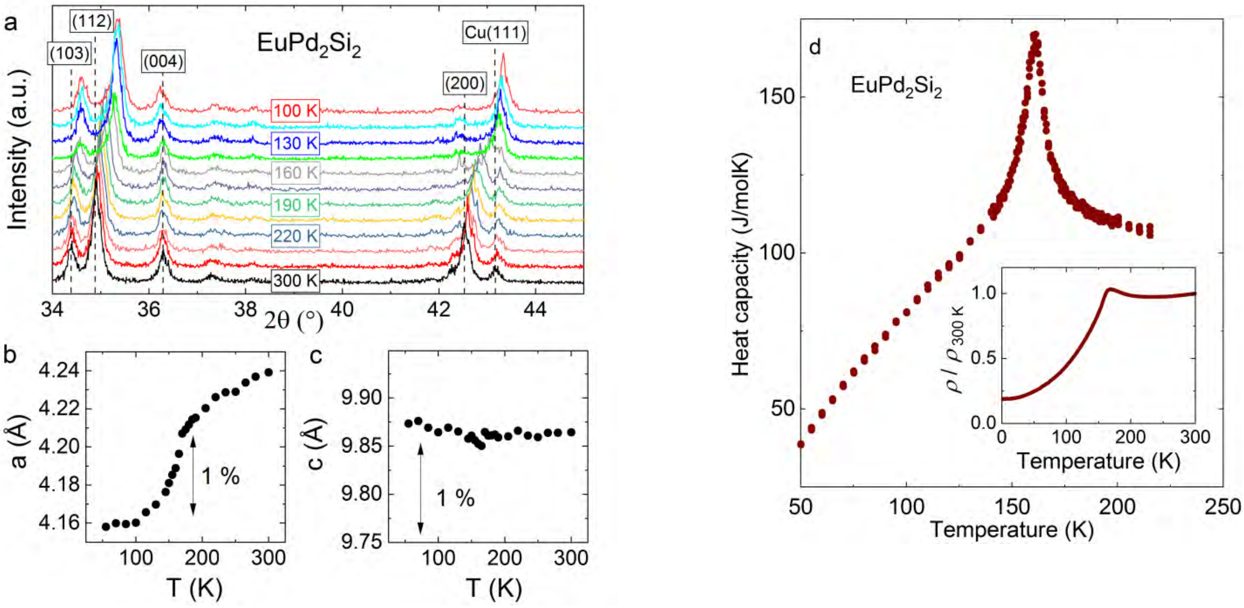

Fig. 2: a) Temperature-dependent powder XRD data of $EuPd_2Si_2$. The refined lattice parameters as function of temperature are shown in b) and c). The change of the *a* parameter is very large with relative changes of about 1%, whereas the $_c$ parameter is nearly temperature independent. d) Heat capacity of an $EuPd_2Si_2$ single crystal. A sharp anomaly is visible at the valence transition, T_V = 160 K. The inset presents the resistivity for current along the crystallographic *c* direction. Also there a pronounced anomaly is apparent at T_V .

The valence transition was further investigated by temperature-dependent measurements of the heat capacity and the resistivity using the standard options of a Physical Property Measurement System (PPMS). In Fig. 2d we present the heat capacity of a single crystal, grown using the Czochralski technique described above. A pronounced anomaly is visible around T_V = 160 K. As the standard option of the PPMS determines the heat capacity with a relaxation method, where one easily can miss first-order transitions, we carefully checked the temperature-time curves but did not find any evidence of latent heat. Therefore, we can exclude a first-order phase transition for this particular crystal.

The resistivity of that sample is shown in the inset of Fig. 2d and also there a pronounced anomaly is visible at T_V . The residual resistivity ratio (RRR = 5) of that sample is comparable to what was reported by Onuki *et al*. [2].

Acknowledgment

We acknowledge funding through the Deutsche Forschungsgemeinschaft (DFG), grant No. KR3831/5-1 and Fermi-NESt.

[1] E. V. Sampathkumaran *et al*., Journal of Physics **C14**, L237 (1981).
[2] Y. Onuki *et al*., Philosophical Magazine **97**, 3399 (2017).

Session 4

Thursday 12.03.2020

8:30 – 10:10

Growth of $CuFeO_2$ single crystals by the optical floating-zone technique

N. Wolff [a,b], T. Schwaigert[a], D. Siche [a], D. G. Schlom[c,d], D. Klimm[a]

[a] *Leibniz-Institut für Kristallzüchtung, Max-Born-Str. 2, 12489 Berlin*
[b] *Helmholtz-Zentrum Berlin für Materialien und Energie, Hahn-Meitner-Platz 1, 14109 Berlin*
[c] *Department of Materials Science and Engineering, Cornell University, Ithaca, NY 14853-1501, USA*
[d] *Kavli Institute at Cornell for Nanoscale Science, Ithaca, NY 14863-1501, USA*
E-mail: nora.wolff@helmholtz-berlin.de

Oxide materials based on the ABO_2 delafossite structure are of particular interest due to the novel properties that accompany their cation variation at A and B sites. Usually the semiconductor delafossites consists of Ag or Cu at A-site and several trivalent cations as Al, Fe or Ga at B-site. Pd and Pt-based compositions are the metallic delafossite oxides where B-site cations are transition metals like Co, Cr or Rh [1-3]. Among these, the growth of single crystalline $PdCoO_2$ came in our focus due to its ultra-high conductivity at room temperature. An in-plane resistivity of ρ_{ab} = 2.6 µΩ·cm at 295 K makes this material the most conductive oxide known, comparable to the best metallic conductors Ag, Cu, Au and Al [4]. [5]

So far, epitaxial layers of $PdCoO_2$ have mainly been grown on sapphire substrates with degraded quality resulting from the not well matched crystallographic lattice [6-8]. For the growth of high quality epitaxial layers, isostructural single crystalline substrates with similar lattice constants are required. $CuFeO_2$ is the only delafossite compound, which can be grown on a larger scale and has suitable lattice parameters ($PdCoO_2$: a = 2.830 Å, c = 17.743 Å [9] and $CuFeO_2$: a=3.0351 Å, c = 17.166 Å). [5]

The aim of this work was to grow $CuFeO_2$ single crystals, which can be used as substrates for the growth of high quality $PdCoO_2$ films. Crystals with diameters up to 10 mm were grown from stoichiometric sintered rods by the optical floating-zone technique (Fig. 1). Due to the incongruent melting behavior of $CuFeO_2$ and redoxprocesses of iron- and copperoxide during growth (Fig. 2), low growth rates of 0.4 mm/h are necessary. [5]

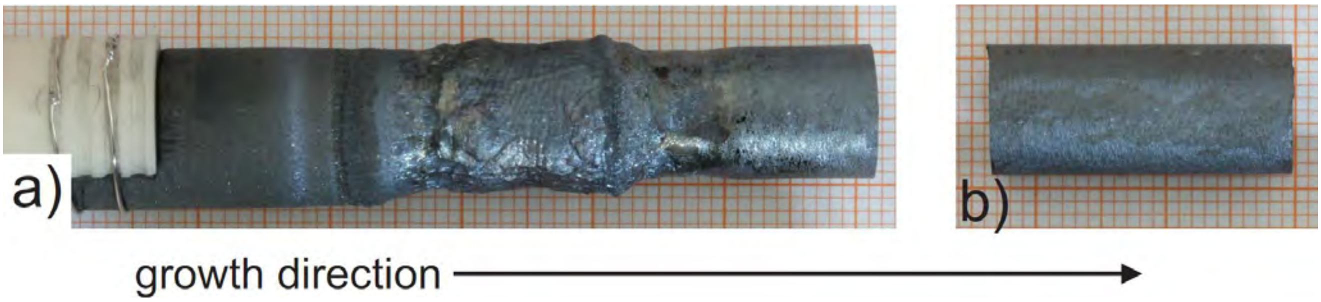

Fig. 1: (a) Unstable growth of $CuFeO_2$ in the initial growth state. (b) Single crystal part of the same rod. [5]

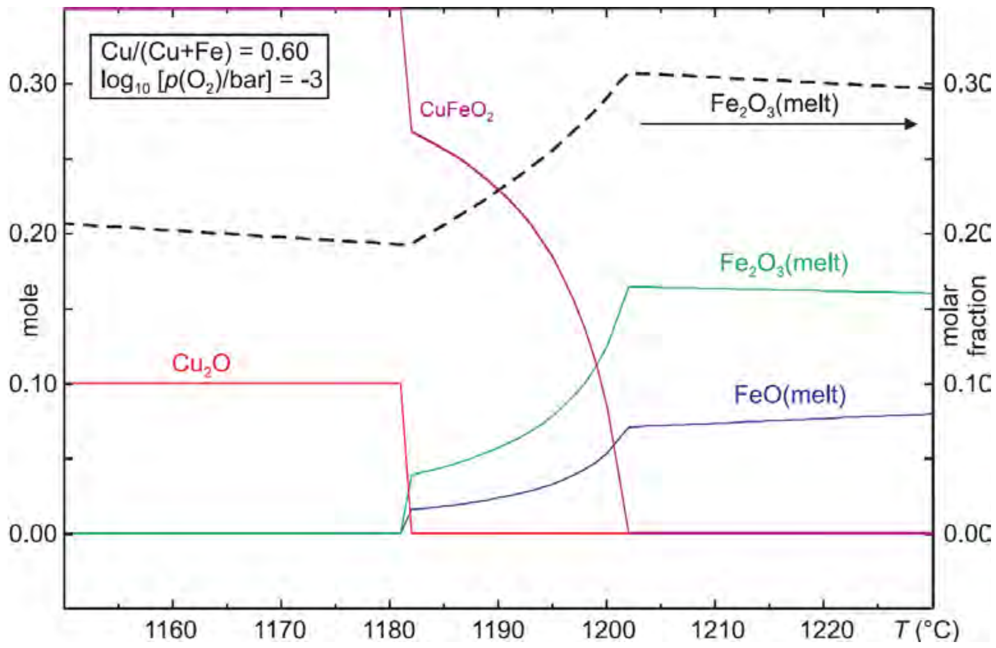

Fig. 2: Crystallization of the Cu-Fe-oxide melt under a constant oxygen fugacity of 1mbar. Even if only $CuFe^{3+}O_2$ starts to crystallize around 1200 °C, the amount of $Fe^{2+}O$ in the melt drops. [5]

Acknowledgment

A. Kwasniewski is acknowleged for performing X-ray powder analysis and Laue measurements. We are indebted to C. Guguschev who performed energy-dispersive Laue mappings and X-ray fluorescence spectroscopy and to S. Ganschow for continuous support of this work. The authors acknowledge funding by the German Research Foundation (DFG) under project SI 463/9-1. D.G.S. acknowledges funding provided by the Alexander von Humboldt Foundation for his sabbatical stay at the Leibniz-Institut für Kristallzüchtung and support from the U.S. Department of Energy, Office of Basic Sciences, Division of Material Sciences and Engineering, under Award No. DE-SC0002334

[1] R.D. Shannon, D.B. Rogers, C.T. Prewitt, Chemistry of noble metal oxides. I. Syntheses and properties of ABO_2 delafossite compounds, Inorg. Chem. 10 (1971) 713–718.
[2] C.T. Prewitt, R.D. Shannon, D.B. Rogers, Chemistry of noble metal oxides. II. crystal structures of $PtCoO_2$, $PdCoO_2$, $CuFeO_2$, and $AgFeO_2$, Inorg. Chem. 10 (1971) 719–723.
[3] D.B. Rogers, R.D. Shannon, C.T. Prewitt, J.L. Gillson, Chemistry of noble metal oxides. III. electrical transport properties and crystal chemistry of ABO_2 compounds with the delafossite structure, Inorg. Chem. 10 (1971) 723–727.
[4] C.W. Hicks, A.S. Gibbs, A.P. Mackenzie, H. Takatsu, Y. Maeno, E.A. Yelland, Quantum oscillations and high carrier mobility in the delafossite $PdCoO_2$, Phys.Rev. Lett. 109 (2012) 116401.
[5] N. Wolff, T. Schwaigert, D. Siche, D.G. Schlom, D. Klimm, Growth of $CuFeO_2$ single crystals by the optical floating-zone technique, J. Cryst. Growth. 532 (2020) 125426.
[6] M. Brahlek, G. Rimal, J.M. Ok, D. Mukherjee, A.R. Mazza, Q. Lu, H.N. Lee, T.Z. Ward, R.R. Unocic, G. Eres, S. Oh, Growth of metallic delafossite PdCoO2 by molecular beam epitaxy, Phys. Rev. Mater. 3 (2019) 093401.
[7] T. Harada, K. Fujiwara, A. Tsukazaki, Highly conductive PdCoO2 ultrathin films for transparent electrodes, APL Mater. 6 (2018) 046107.
[8] P. Yordanov, W. Sigle, P. Kaya, M.E. Grunder, R. Pentcheva, B. Keimer, H.U. Habermeier, Large thermopower anisotropy in PdCoO2 thin films, Phys. Rev. Mater. 3 (2019) 085403.
[9] H.Takatsu, S.Yonezawa, S.Mouri, S.Nakatsuji, K.Tanaka, Y.Maeno, Roles of high frequency optical phonons in the physical properties of the conductive delafossite $PdCoO_2$, J. Phys. Soc. Japan 76 (2007) 104701.

Investigation of orthorhombic and tetragonal phases of $Cs_2CuCl_{4-x}Br_x$ mixed system

Natalija van Well [a]

[a] *Department of Earth and Environmental Sciences, Crystallography Section, Ludwig-Maximilians-University Munich, D-80333 Munich, Germany*
E-mail: Natalija.vanwell@lrz.uni-muenchen.de

Low-dimensional quantum spin systems are a large class of materials, which have been studied intensively in condensed matter physics for the last decades [1]. These systems also include the $Cs_2CuCl_{4-x}Br_x$ mixed system, which exists in orthorhombic and tetragonal polymorphs [2,3]. For this mixed system, the centre of interest are the different Cu^{2+} environments and their influence on the magnetic properties of the orthorhombic and tetragonal compositions. Additionally, the understanding of such influence is important to understand the change of magnetic behaviour by applying magnetic field.

The crystals are grown from aqueous solution using the evaporation method and different temperatures for growing orthorhombic and tetragonal phases. The compounds of the orthorhombic phase of this mixed system can be grown in the full Br concentration range for $0 \leq x \leq 4$ from aqueous solution at a temperature of 50°C [4]. The structure was analysed by x-ray powder diffraction and showed the orthorhombic symmetry *Pnma* in the full Br concentration range [4]. The compositions of the tetragonal phase are grown for a Br concentration range between $1 \leq x \leq 2$ at a temperature of 24°C. At 8°C, the mixed system can be supplemented with the tetragonal realization of Cs_2CuCl_4 [2]. The compositions of the tetragonal phase show the tetragonal symmetry *I4/mmm* in x-ray powder diffraction analysis. Fig. 1 presents a schematic phase diagram of this mixed system.

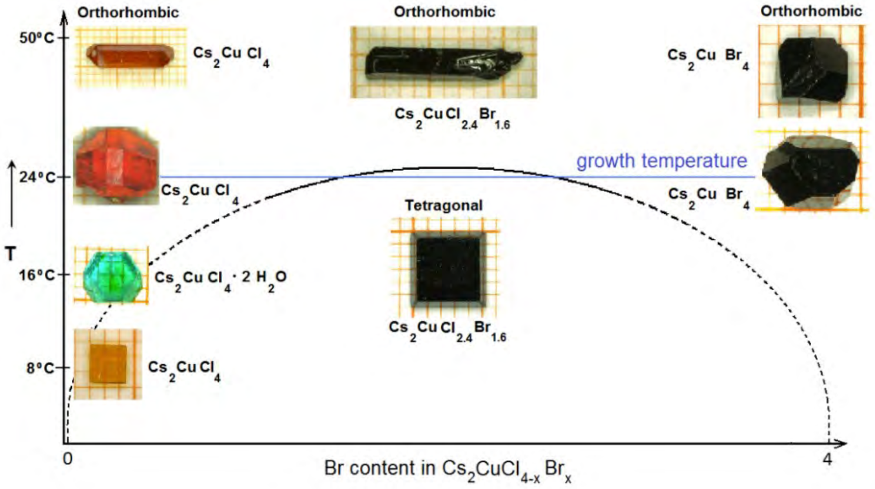

Fig. 1: Schematic phase diagram of the $Cs_2CuCl_{4-x}Br_x$ mixed system grown from aqueous solution.

The physical properties demonstrate differences for the orthorhombic and the tetragonal phases. The investigation of the orthorhombic compounds with neutron diffraction results in a rich magnetic phase diagram, based on four regimes, which is shown in Fig. 2. The regimes are characterized by different exchange coupling mechanisms [3]. In Fig.2, a long-range antiferromagnetic order at lower temperatures is observed for some compositions (red circles) in regimes I and IV. The black circles show the data from literature for Cs_2CuCl_4 and Cs_2CuBr_4 [5,6]. The horizontal arrow bars ±0.1 represent the uncertainties of the EDX results of the chemical composition. In the magnetic phase diagram, the two ordered magnetic phases in regimes I and IV seem to be separated by quantum critical

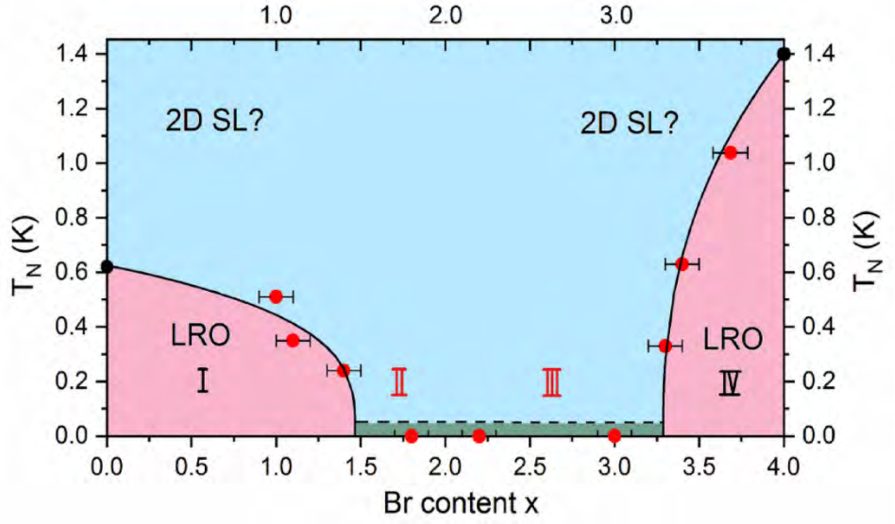

Fig. 2: Magnetic phase diagram of orthorhombic compounds of $Cs_2CuCl_{4-x}Br_x$.

points (QCP), QCP1 near x = 1.5 and QCP2 near x = 3.2, respectively. Whereas in regimes I and IV (with a long-range antiferromagnetic order) investigations in a magnetic field show new results, in regimes II and III no magnetic order was observed. 2D spin liquid (2D SL) might exist for a still to be defined Br concentration range of this mixed system. As this still has to be confirmed with inelastic neutron scattering, 2D SL are marked in Fig. 2 with "?".

For the compounds of the tetragonal phase, the magnetic behaviour remains antiferromagnetic down to 1.5 K, evidenced by neutron diffraction experiments [2]. One of the key points for understanding the magnetic structure of the investigated tetragonal compounds is, to clarify, whether there is a relationship between the spin ordering and the crystallographic ordering of the [CuX6] octahedra. To answer this question, single crystal neutron diffraction measurements are envisaged.

Subject: Abstract Oral

Acknowledgment

The author thanks W. Aßmus from Goethe-University, Frankfurt am Main. The neutron diffraction experiments were performed on ZEBRA with crystals orientated on ORION at PSI, Villigen, Switzerland and on D23 with crystals orientated on OrientExpress at ILL, Grenoble, France, and on MIRA with crystals orientated on the neutron-laue diffractometer RESI at FRM II of MLZ, Garching. This work was supported by Paul Scherrer Institute, Institut Laue-Langevin, University of Bayreuth, Heinz Maier-Leibnitz Zentrum and Physik Department E21, Technische Universität München, and the Deutsche Forschungsgemeinschaft through the research fellowship for the project WE-5803/1-1 and WE-5803/2-1, and through the fellowship A 4576 – 1/3 of the University of Bayreuth. This work was additionally supported by the Swiss State Secretariat for Education, Research and Innovation (SERI) through a CRG-grant.

[1] M. Vojta, *Rep. Prog. Phys.*, 81, 064501 (2018); [2] N. van Well, C. Eisele, S. Ramakrishnan, T. Shang, M. Medarde, A. Cervellino, M. Skoulatos, R. Georgii, S. van Smaalen, *Cryst. Growth Des.*, 19, 11, 6627-6635 (2019); [3] van Well, N.; Zaharko, O.; Delley, B.; Skoulatos, M.; Georgii, R.; van Smaalen, S.; Rüegg, Ch., *Ann. Phys.* (Berlin, Ger.), 530, 201800270 (2018); [4] N. Kruger, S. Belz, F. Schossau, A. A. Haghighirad, P. T. Cong, B. Wolf, S. Gottlieb-Schoenmeyer, F. Ritter, W. Assmus, *Cryst. Growth Des.*, 10, 4456 (2010); [5] Ono, H. Tanaka, T. Nakagomi, O. Kolomiyets, H. Mitamura, F. Ishikawa, T. Goto, K. Nakajima, A. Oosawa, Y. Koike, K. Kakurai, J. Klenke, P. Smeibidle, M. Meißner, H. A. Katori, *J. Phys. Soc. Jpn.*, 74, 135 (2005); [6] R. Coldea, D. A. Tennant, R. A. Cowley, D. F. McMorrow, B. Dorner, Z. Tylczynski, J. Phys., *Condens. Matter*, 8, 7473 (1996)

Investigation of facet growth in heavily doped silicon single crystals grown in the mirror furnace

S. Gruner [a,b], S. Hürner [b], C. Kranert [a,b], T. Jauß [c], T. Sorgenfrei [c], C. Reimann [b], J. Friedrich [b]

[a] *Fraunhofer THM, Am St. Niclas Schacht 13, 09599 Freiberg, Germany*
[b] *Fraunhofer IISB, Schottkystraße 10, 91058 Erlangen, Germany*
[c] *University of Freiburg, Crystallography, Hermann-Herder-Str. 5, 79104 Freiburg, Germany*

E-mail: Sebastian.Gruner@iisb.fraunhofer.de

Summary

When an atomically rough and atomically smooth interface coexist simultaneously during growth of a crystal, their growth kinetics differ, which will affect the properties of the grown crystal like dopant homogeneity or content of extended crystal defects e.g. in form of dislocations or twins. The atomically smooth interface regions form typically along the (111) facets at a certain supercooling during growth of silicon or germanium crystals either at the crystal periphery known as edge facet or growth ridge or as central facet in the bulk for <111> crystal orientation.

In order to obtain a deeper understanding of the relationship between facet growth, growth conditions and the resulting crystal properties, systematic investigations have been carried out in the present work. For that purpose, heavily As-doped, <100>- and <111>- oriented silicon crystals with 8 mm in diameter were grown by the floating zone technique in a mirror furnace at translation speeds of 1 mm/min up to 8 mm/min. Partially the crystals were grown with a free melt surface, partially the melt surface was covered by an oxide layer to prevent Marangoni convection. The grown crystals were characterized with regard to the length of the central facet, the width of the growth ridge, the shape of the phase boundary, the emergence of constitutional supercooling, and the presence of dislocations and twins.

It was found that the macroscopic deflection of the growth interface decreases with increasing growth velocity in the <100>-oriented crystals because the temperature gradient in the crystal becomes steeper. As a result the diameter of the central facet in the <111>-oriented crystals becomes smaller. The diameter of the central facet is also influenced by dislocations. In some experiments it was not possible to apply a dash necking procedure. Therefore, dislocations are present in the crystal already at the beginning of the growth process. As a result, the central facet is shorter compared to the dislocation free crystals because a smaller supercooling is sufficient for the facet to grow when dislocations and therefore growth steps at the facet are present. In some cases an irregular instability of the central facet diameter has been observed apart from periodically oscillations (Fig. 1).

Edge facets appear only when the crystal surface is not covered by an oxide layer. The width of the growth ridge is shorter for <111>-orientation than for <100>-orientation which can be explained simply by the geometrical relation of the (111) edge facet with respect to the growth orientation. However, no influence of the growth velocity and the axial temperature gradient on the width of the growth ridge was found. In addition, the edge facet grows deeply into the bulk of the small diameter crystal and is not limited to the growth ridge, as it is for large diameter crystals. Both findings cannot be explained by the existing theory of Voronkov.

In agreement to our theoretical considerations, interface instability due to constitutional supercooling was found only during final solidification in the atomically rough interface region at the crystal periphery, when the growth velocity exceeds 10 mm/min and the temperature gradient

becomes very small with reducing the heating power. The facetted region showed to be more stable and was not affected by the starting morphological instabilities.

In addition to the experimental investigations, a global numerical model with Ansys Fluent was developed to describe the temperature field in the mirror furnace (Fig. 2). For that purpose experimental data from facet length analysis, phase boundary deflection in etched cross-sections and temperature measurements were used for its validation. The model is applied to analyze the influence of buoyant convection e.g. on the interface shape and to predict a possible influence of microgravity conditions on the growth behavior.

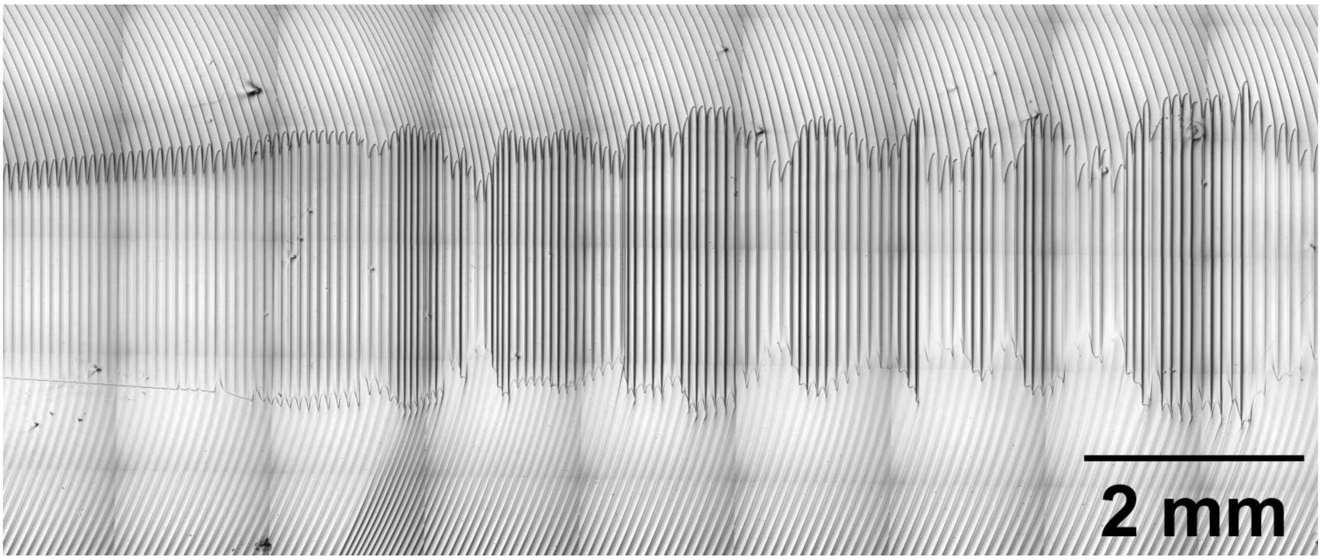

Fig. 1: Instability of the central facet diameter in heavily As-doped silicon

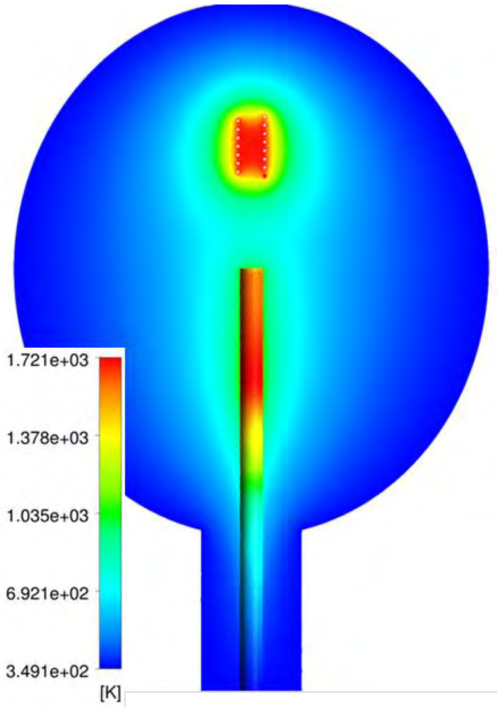

Fig. 2: Modelling of the temperature field for the mirror furnace with Ansys Fluent

Acknowledgment

This work is supported by the DLR within the project „Einfluss der Stabilität des Facettenwachstums auf die Entstehung von Kristalldefekten bei der Halbleiterkristallzüchtung", FKZ50WM1844 and FKZ50WM1845.

Session 5

Thursday 12.03.2020

10:40 – 12:00

CONTROL OF AlInN COMPOSITION IN CLOSED COUPLED SHOWERHEAD MOCVD REACTORS

M. Heuken [ab], D. Meyer [b], F. Sandbaumhüter [ab] , O. Rockenfeller [b], C. Mauder [b], and A. Boyd [b]

[a] RWTH Aachen University, Compound Semiconductor Technology, 52074 Aachen, Germany
[b] AIXTRON SE, Dornkaulstraße 2, 52134 Herzogenrath, Germany
E-mail: m.heuken@aixtron.com

Nitride-based electronic devices continuously gain attention and are envisioned as driving force for next-generation of RF-HEMT for G5 applications. Therein, InAlN is most promising as barrier material. However, it has been reported that InAlN suffers from gallium contamination if grown in a reactor based on the Close Coupled Showerhead (CCS) architecture. Yet, a conclusive picture explaining the presence of Ga in the InAlN has not emerged. We have intensively studied the mechanism of the reported gallium incorporation as a function of precursor materials, process conditions and reactor hardware. In order to investigate the mechanism of the incorporation of gallium in InAlN, we studied the growth of InAlN on GaN templates, either with or without in-situ re-grown GaN, in a 3x2 CCS reactor in a 1x4 inch configuration. To grow InAlN and GaN layers, trimethylaluminum (TMAl), trimethylgallium (TMGa), trimethylindium (TMIn) and ammonia (NH_3) have been used to deposit Al, Ga, In, and N, respectively. The growth of the epitaxial layers have been in-situ monitored using LayTec EpiTT optical reflectance measurement. It is known, that opening and cleaning the reactor between the growth steps of GaN and InAlN results in Ga-free barrier layers. Growing InAlN directly on a GaN template or cleaning the reactor between these two steps are facile options to avoid Ga carry over in InAlN [1]. It also indicates that the origin of Ga cannot be explained by a diffusion of atoms from the GaN layer into InAlN. Moreover, opening the reactor without any additional cleaning of the reactor (for 20 minutes inside the Glovebox) has led to only 0.5% Ga in InAlN, indicating that a volatile and reactive process coating of the reactor affects the purity of InAlN. Residual amounts of oxygen in the glovebox seem to be sufficient to passivate this process coating. In addition, Mrad and co-workers could also show that the amount of Ga in InAlN scales with the thickness of the GaN layer [2].

To further shed light into the mechanism of the contamination, we have investigated the roles of the precursors for In and Ga. We can confirm the vital role of TMIn from an experiment, in which AlN is grown on GaN under conditions equal to those for InAlN, except no TMIn is introduced into the reactor. Growing AlN on in-situ re-grown GaN showed no difference to a sample grown on a GaN template. It is thus unlikely that condensed TMGa molecules slowly desorb during the process subsequent to GaN growth, as this should also affect AlN. We have furthermore investigated the Ga uptake in InAlN when using the precursors TEGa during GaN growth and TEIn during InAlN growth. Both experiments revealed no significant difference to the standard precursors with a Ga pollution in the range of 20-30%, so the fundamental mechanism of the contamination remained and its origin stems from reactants that are present for both trimethyl- and triethyl-based precursors.

We already concluded that desorption of condensed, unreacted TMGa molecules during InAlN growth unlikely cause the Ga uptake. It is also known that metallic Ga covers the Showerhead surface during GaN growth [3]. The effect of metallic gallium on the growth of InAlN has been investigated by an etching experiment, in which the GaN layer has been etched in H_2. This generates free Ga atoms, which agglomerate on the Showerhead [4]. Starting with a cleaned reactor, we have applied this method to coat the initially clean Showerhead with metallic gallium without introducing any Ga precursor to the reactor. After etching approx. 2 µm of GaN from a template sample, we subsequently grew InAlN without opening the reactor using conventional process parameters. Growth rate and elemental analysis then revealed a high Ga contamination of more than 22%. Apparently, the combination of metallic gallium with the precursor for indium in the reactor plays a key role for the unintentional Ga incorporation. Metallic gallium is generated in both processes using TMGa and TEGa. Based on the low vapor pressure of metallic gallium, we can explain that gallium does not simply evaporate during subsequent processes, as evidenced by the missing Ga uptake in AlN grown on GaN. Instead, a chemical reaction takes place between gallium and the precursor for indium, upon which methyl units are exchanged. This reaction is energetically favorable based on the calculations published in ref. [5]. Molecules of TMIn in the vicinity of metallic gallium in the reactor then lead to spontaneous formation of Ga precursor, which travel back into the gas phase and efficiently incorporate during the growth of InAlN.

Avoiding gallium to be incorporated into InAlN thus requires a method to inhibit the reaction between gallium and TMIn. Changing the surface temperature of the Showerhead displays one route to transform the metallic gallium into a more stable coating. Due to its low thermal conductivity, a quartz-based deposition shield fixed to the Showerhead is a facile way to achieve a hot surface above the wafer. Not only reduces a hot surface the condensation rate of gallium, it also seems to enable the formation of a low-quality GaN composition on the deposition shield. As a result, a contamination of InAlN by Ga is almost entirely suppressed when using a quartz-based deposition shield with traces of gallium in the order of 0.1%.

With our current study, we discuss a contamination of InAlN by gallium if the barrier layer is grown subsequent to GaN. Here, we present a concise experimental study that reveals the Ga uptake in InAlN to originate from a metallic gallium coating, which diffuses back into the gas phase upon an alkyl exchange reaction with the precursor for In (e.g., TMIn or TEIn). A quartz-based deposition shield fixed to the Showerhead leads to a high surface temperature, which enable the formation of a more stable coating during GaN growth, which is unaffected by the presence of TMIn during InAlN growth. Thus we can provide Ga-free InAlN barrier layers, grown directly subsequent to GaN.

[1] Kim, et al. "Effect of Group-III precursors on unintentional gallium incorporation during epitaxial growth of InAlN layers by metalorganic vapor deposition," Journal of Applied Physics, **no. 118**, p. 125303 (2015)

[2] M. Mrad, et al. "Understanding and controlling Ga contamination in InAlN barrier layers," Journal of Crystal Growth, **no. 507**, pp. 139-142 (2019)

[3] J. Kim, et al. "Origings of unintentional incorporation of gallium in InAlN layers during epitaxial growth, part II: effects of underlying layers and growth chamber conditions," Journal of Crystal Growth, **no. 388**, pp. 143-149 (2014)

[4] E. E. Zavarin, et al. "In-situ investigations of GaN chemical instability during MOCVD," Proceedings of the EUROCVD-15, p. 299 (2005)

[5] B. H. Cardelino et al. "Dissociative Chemisorption of Trimethylgallium, Trimethylindium, and Ammonia on Gallium and Indium Nitride Substrates. A computational Study," The Journal of Physical Chemistry C, **no. 115**, pp. 9090-9104 (2011)

Growth of modulation-doped ß-Ga_2O_3 multilayers by MOVPE

A. Popp[a], S. Bin Anooz[a], R. Grüneberg[a], A. Fiedler[a], Z. Galazka[a], R. Schewski[a],
M. Albrecht[a], K. Irmscher[a] and G. Wagner[a].

[a] Leibniz-Institut für Kristallzüchtung (IKZ), Member of the Forschungsverbund Berlin e.V,
Max-Born-Str. 2, 12489 Berlin, Germany
E-Mail: andreas.popp@ikz-berlin.de

Summary

The wide bandgap (4.8 eV) oxide material β-Ga_2O_3 is characterized by a breakdown field strength of 8MV/cm [1]. Transistors based on β-Ga_2O_3 benefit from a low on-resistance at a given breakdown voltage, which leads to less power losses. Due to these properties β-Ga_2O_3 meets the requirements to become the next generation of high-performance material for power electronic applications.

In this contribution we report on the growth of homoepitaxial β-Ga_2O_3 layers by metal-organic vapor phase epitaxy (MOVPE) on (010) and (100) oriented substrates. To avoid the formation of twin lamellae for the (100) orientation substrates with a miscut of 6° towards the [00-1] direction were used [2, 3]. At IKZ two inch diameter bulk β-Ga_2O_3 single crystals were grown by the Czochralski method [4]. Out of these crystals the (100) oriented substrates were prepared. (010) oriented substrates were grown by the EFG method and supplied by Tamura Corp., Japan.

The focus of this work was the deposition of modulation Si-doped layer structures. To use the promising material properties of β-Ga_2O_3 the epi layers have to have a high structural perfection, a smooth surface morphology and a low defect density to achieve the best electrical properties. To meet the requirements for modern devices multilayer structures with different doping regimes are necessary. The interfaces between the substrate and layers, and especially between the single doped epi layers play an important role for the device performance. Figure 1 shows the comparison for a 200 nm layer grown on a (010) oriented substrate and a (100) 6° off oriented substrate.

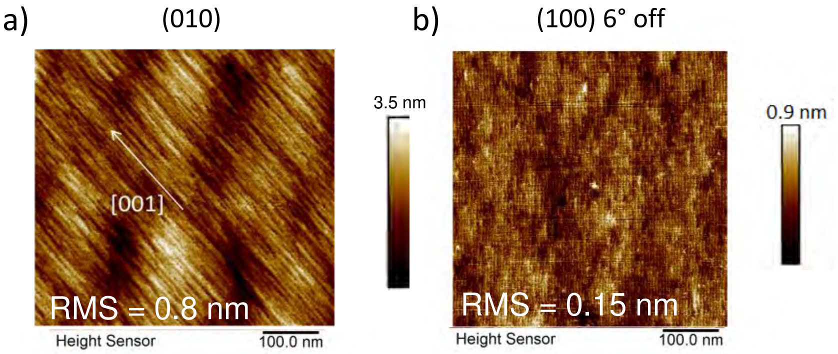

Figure1: AFM pictures of the layer morphology grown by MOVPE on a) a (010) oriented substrate and b) on a (100) 6° off oriented substrate.

The layer grown on the (010) oriented substrate shows elongated two dimensional islands, indicating a faceted surface morphology with a roughness of about 800 pm. In contrast to that, the layer grown on (100) 6° off oriented substrate is characterized by a smooth step flow growth with a surface roughness of < 200 pm, a quarter the value of the (010) layer. This is a good prerequisite to achieve very sharp interfaces for multilayer structures with different doping regimes. In contrast to that, gradual transition of doping regimes between layers will result in scattering of free charge carries that leads to a decrease of the carrier mobility and overall device performance. Therefore, it is crucial to

ensure that the interfaces are as sharp as possible. This depends strongly on the orientation of the β-Ga_2O_3 substrate.
We demonstrated in this work that β-Ga_2O_3 Si-doped multilayer structures homoepitaxialy grown by MOVPE in the same run on (100)6° off oriented substrates and (010) substrates revealed sharper interfaces in the Si-depth profile for the (100) orientated substrates (see Fig. 2).

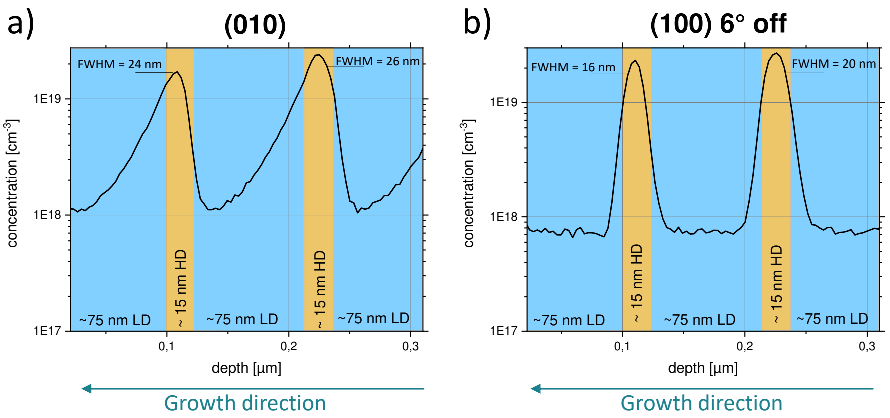

Figure 2: Si-depth profile measured by secondary ion mass spectroscopy (SIMS) of a multilayer structure grown by MOVPE on a) a (010) oriented substrate and b) on a (100) 6° off oriented substrate. The nomenclature LD and HD denotes "Low Si-Doping" and "High Si-Doping", respectively.

The SIMS Si-depth profile for the multilayer grown on the (010) substrate shows a gradual transition from a high to the low Si doping regions. The reason seems to be the surface morphology. For the faceted (010) layer surface the incorporation of Si is inhomogeneous resulting in blurred interfaces. The Si depth profile of the multilayer grown on (100) 6° off substrate instead shows sharp interfaces between the high and low doping regions since the (100) orientation is a cleavage plane with the lowest surface energy [3]. The use of (100) oriented substrates may, therefore, reduce the leakage current and improve the device performance, pointing out at the same time a direction for the device development.
The surface morphology and electrical properties of the obtained layers were analyzed by AFM and Hall Effect measurements, respectively. Ellipsiometry measurements of the layers were performed with the use of Al_2O_3 substrates in the same run to determine the layer thickness. The depth profile and the silicon concentration of the multilayer stack was measured by using secondary ion mass spectroscopy (SIMS). The shape of the interfaces between the layers and the structural perfection were analyzed by SIMS and high resolution transmission electron microscopy (HRTEM), respectively.

Acknowledgment

This work was performed in the framework of GraFOx, a Leibniz ScienceCampus. The work was partially funded by the BMBF under grant number 03VP03712, the European Community (Europäische Fonds für regionale Entwicklung- EFRE) under grant number 1.8/15 and by the Air Force Office of Scientific Research under award number FA9550-17-1-0279.

[1] M. Higashiwaki et al., Semicond. Sci. Technol. **31**, 034001, (2016)
[2] A. Fiedler et al., J. Appl. Phys., **122**, no. 16, 165701, (2017)
[3] R. Schewski et al., APL Mater. **7**, 022515 (2019)
[4] Z. Galazka, Semicond. Sci. Technol., **33**, no. 11, 113001, (2018)

NANOMETER-THIN IRON GARNET FILMS GROWN BY LIQUID PHASE EPITAXY

C. Dubs, [a] O. Surzhenko, [a] R. Thomas, [b] J. Osten, [b] T. Schneider, [b] K. Lenz, [b] J. Grenzer, [b] R. Hübner, [b]
E. Wendler [c]

[a] *INNOVENT e.V. Technologieentwicklung, Prüssingstr. 27B, 07745 Jena, Germany*
[b] *Institut für Ionenstrahlphysik und Materialforschung, Helmholtz-Zentrum Dresden-Rossendorf, Bautzner Landstr. 400, 01328 Dresden, Germany*
[c] *Institut für Festkörperphysik, Friedrich-Schiller-Universität Jena, Helmholtzweg 3, 07743 Jena, Germany*
E-mail: cd (ad) innovent-jena.de

Summary

Future magnonic components for data processing technology could be used as an integral part of magnon spintronics concepts. They are necessary for large-scale integrated circuit technology beyond standard CMOS applications, since the manipulation of spin waves rather than electron transport processes plays the key role here (see, e.g., [1]).

The ferrimagnetic insulator yttrium iron garnet (YIG) is a promising candidate. Its ultra-low ferromagnetic resonance losses allow long spin wave lifetimes in prospective nanoscopic magnonic waveguide structures in the GHz and THz frequency range. For magnonic applications, however, nanometer-thin epitaxial films, with perfect structural and magnetic properties and large diameters, are required to enable efficient wafer-scale circuit fabrication for a future YIG planar technology.

In our contribution we report on the structural and magnetic properties of 10 to 100-nm-thin YIG films grown by liquid phase epitaxy (LPE) on (111) gadolinium gallium garnet (GGG) substrates [2]. High-resolution X-ray diffraction analysis (HR-XRD), Rutherford backscattering spectrometry (RBS), high-resolution transmission electron microscopy (HR-TEM), and magneto-static and dynamic characterization techniques such as vibrating sample magnetometry (VSM) and ferromagnetic resonance spectrometry (FMR) were used to characterize the sample performance. The results show that both the expected high structural perfection of epitaxial YIG films, and the well-known low magnetic damping of YIG single crystals, are preserved for LPE films down to a film thickness of 20 nm.

Our sub-100-nm-thin LPE YIG films reveal RMS values ranging between 0.2 and 0.4 nm, independent of the film thickness. Sometimes, however, partial remnants of dendritic overgrowth increase the surface roughness to RMS values above 0.4 nm for inspection areas larger than 400 μm^2.

HR-XRD measurements confirm a fully strained pseudomorphous film growth with perfect coherent in-plane lattice match to the GGG substrate. Besides the nearly symmetrical intensity distribution along the [111] out-of-plane direction, only a very weak diffuse scattering is visibly close to the Bragg peaks; pointing towards a nearly perfect crystal lattice without significant compositional strain or geometric mosaicity. Using the best fit of both, the (444) and (888) reflections, the out-of-plane lattice misfit values $\delta d^{\perp}_{\mathrm{film}}$ were determined and a weak monotonous increase of $\delta d^{\perp}_{\mathrm{film}}$ with decreasing film thickness was observed for films with thicknesses between 106 nm and 21 nm.

For all LPE films studied, the Fe to Y ratio determined by RBS measurements was $R = 1.67$. This corresponds to the ideal iron garnet stoichiometry of $Y_3Fe_5O_{12}$.

HR-TEM investigations show that the LPE technology is suitable for growing nm-thin YIG films without lattice defects and without significant interdiffusion at the film/substrate interface (Fig. 1).

FMR measurements, within a frequency range of 1 to 40 GHz, were carried out to investigate the magnetostatic and dynamic behavior of the nanometer-thin films. A key parameter is the so-called Gilbert damping parameter α, which can be interpreted as the viscous damping contribution of

the movement of the magnetization vector in an external magnetic field. The Gilbert damping coefficient, obtained for sub-100-nm films, is $\alpha \leq 1.3 \times 10^{-4}$ and corresponds to the best values previously reported for 100 nm LPE YIG films [3]. No significant increase in Gilbert damping at room temperature with decreasing film thickness down to 11 nm was observed for LPE films. This correlates with the high microstructural perfection and homogeneity of the volume and interfaces of LPE-grown films with film thicknesses larger than 11 nm.

The magnetic hysteresis loops obtained by VSM measurements show extremely small coercivity fields with H_c values of $\sim$ 0.2 Oe. The determined saturation moments are independent of thickness except for the thinnest sample and are very close to the YIG volume values (4Ms ~1800 G). The most likely explanation for the observed reduction of the $4\pi M_s$ for the 11-nm-thin film is that the YIG layers at the substrate/film interface exhibit a reduced saturation magnetization due to a magnetically diluted iron sublattice. We assume that the reason for this could be a high-temperature diffusion of gallium ions from the GGG substrate into the YIG film. Curie temperature measurements and SIMS investigations confirm this assumption.

In summary, we are able to show that LPE technology can be used to fabricate sub-100-nm YIG films with high microstructural perfection, smooth surfaces and sharp interfaces, as well as excellent microwave properties down to a minimum film thickness of 21 nm. We expect, that these results will provide the basis for a possible application of nanometer-thin LPE films for the fabrication of nano- and microscaled circuits, such as nano-sized magnonic conduits [4], magnon transistors [5], directional couplers [6] etc. This deposition technique is easily scalable for future YIG sample diameters of several inches.

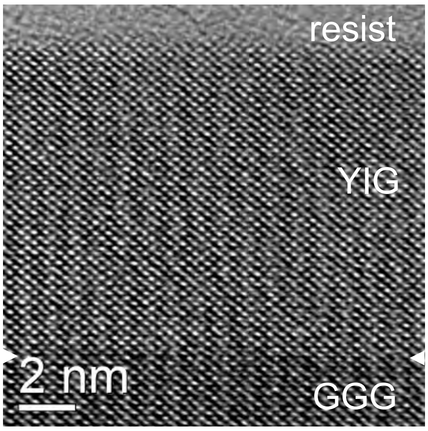

Fig. 1: Cross-sectional HR-TEM image of an 11-nm-thin YIG/GGG (111) LPE film (see also [3]).

Acknowledgment

C. D. and O. S. thank R. Köcher for AFM measurements, A. Hartmann for the DSC measurements and R. Meyer and B. Wenzel for technical support. This research was financially supported by the Deutsche Forschungsgemeinschaft (DFG), via Grant No. DU 1427/2-1.

[1] A.V. Chumak, V.I. Vasyuchka, A.A. Serga, B. Hillebrands, Nature Physics, **11,** 453 (2015)
[2] C. Dubs et al, J. Phys. D : Appl. Phys., **50**, 204005 (2017)
[3] C. Dubs et al.; arXiv: 1911.09400 (2019)
[4] B. Heinz et al.; arXiv: 1910.08801 (2019)
[5] A.V. Chumak, A.A. Serga, B. Hillebrands, Nature Communications, **5:4700** (2014)
[6] Q. Wang et al.; arXiv 1905.12353 (2019)

Status of 3C-SiC bulk growth using sublimation epitaxy

M. Kollmuß [a], M. Schöler [a], *P. Schuh* [a], *F. La Via* [b], *M. Mauceri* [c], *M. Zielinski* [d], *P. Wellmann* [a]

[a] Crystal Growth Lab, Materials Science Department 6, Friedrich-Alexander-Universität Erlangen-Nürnberg, Martensstraße 7, 91058 Erlangen, GERMANY
[b] CNR-IMM, sezione di Catania, Stradale Primosole 50, I-95121 Catania, Italy
[c] LPE S.P.A., Sedicesima Strada, I-95121 Catania, Italy
[d] NOVASiC, Savoie Technolac, BP267, F-73375 Le Bourget-du-Lac Cedex, France
E-mail: manuel.kollmuss@fau.de

Summary

The cubic polytype of silicon carbide (3C-SiC) has attracted particular interest for decades. 3C-SiC is a promising candidate for power electronic device applications, as well as applications in the field of energy saving, such as intermediate band solar cells (IBSC) [1] and photo-electrochemical water splitting [2]. Some point defects in 3C-SiC are even investigated for future quantum applications [3]. However, the lack of high-quality material with reasonable size and in relevant quantities hinders the breakthrough of this material. High numbers of defects and considerable amounts of stress are still an obstacle and subject of current research.

Since Nishino et al. [4] proposed the pioneering work about a multi-step chemical vapor deposition (CVD) process, significant progress has been made in the growth of high-quality 3C-SiC by CVD. Using such material as seed for a subsequent vapor growth process, thickness as well as quality of the 3C-SiC can be further improved [5-7]. In this work, the growth of high-quality 3C-SiC by sublimation epitaxy (SE) on CVD-grown 3C-SiC-on-Si seeding layers is presented.

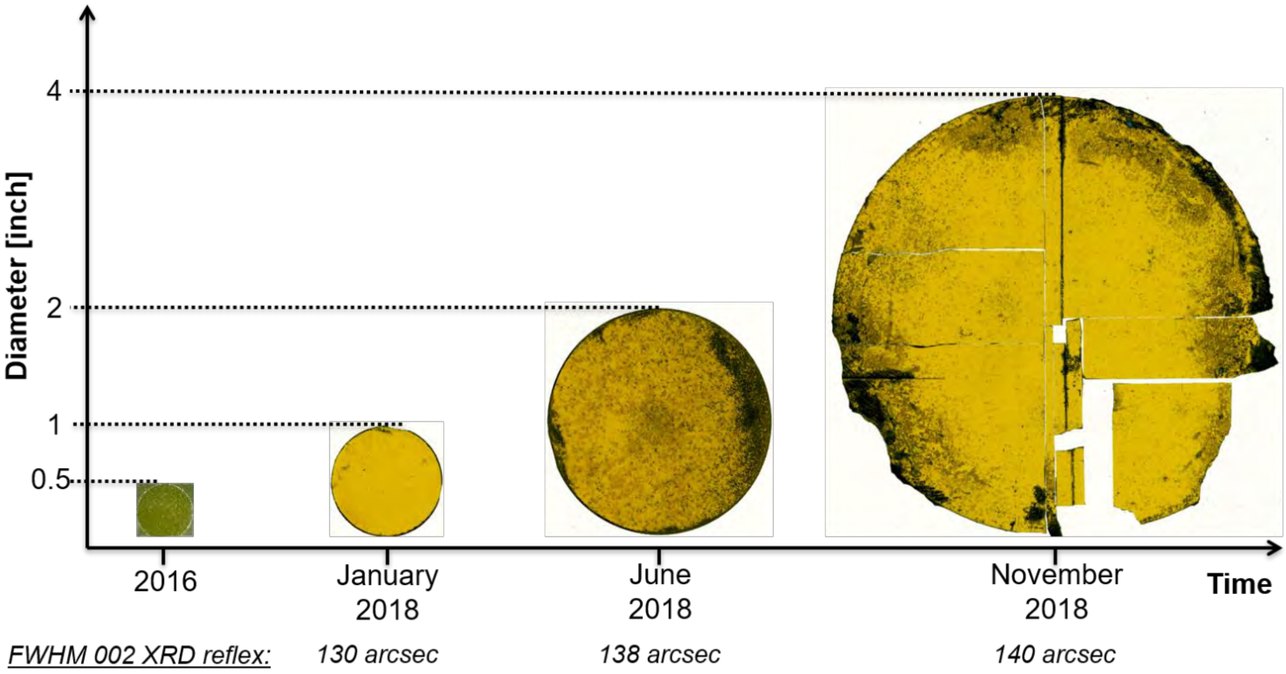

Fig. 1: Evolution of diameters for bulk 3C-SiC crystals grown by sublimation epitaxy. The timeline and the full-width-at-half-maximum (FWHM) values from XRD-rocking curve measurements are indicated.

A method for the reproducible growth of free-standing epitaxial layers up to 52 x 52 mm^2 using a laser ablation process is presented. The path towards growth of four inch material is presented, too. However, for increased dimensions, cracking of the seeds occurred during wet-chemical etching. The resulting vapor grown layers exhibit a thickness between 320 µm and 520 µm and were grown at growth rates between 190 µm/h and 320 µm/h. All crystals exhibit a bright yellow color which is typical for cubic silicon carbide. XRD analysis and Raman spectroscopy confirmed the growth of the 3C-SiC polytype. Moreover, the analysis of the bulk material proved the growth of stress-free-material. Typical defects in (100) oriented 3C-SiC are stacking faults and protrusions. While the number of stacking faults decreases with increasing thickness of the SE-layer, protrusions can be considered as one of the most critical defects when it comes to the growth of thick, “bulk-like” layers. Protrusions increase in size with increasing layer-thickness. This effect limits the achievable maximal thickness and leads to a surface roughening of the crystal.

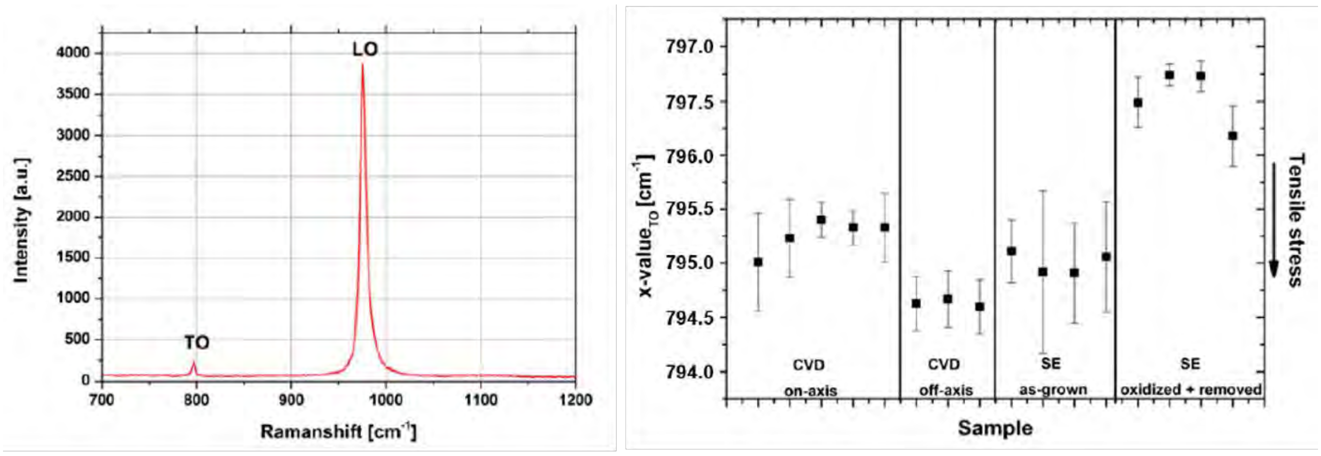

(a) (b)

Fig. 2: (a) Raman spectrum of typical sublimation grown material acquired in a protrusion-free surface area. (b) Comparison of the x-value for the transverse optical (TO) Raman mode of 3C-SiC epitaxial layers grown by chemical vapor deposition (CVD) on on-axis and 4° off-axis substrates, homoepitaxial as-grown material produced by epitaxial sublimation growth (SE), and SE-material after temperature treatment.

Acknowledgment

Financial support by the European Union in the frame of the Horizon 2020 program (CHALLENGE project, grant number 720827) is greatly acknowledged.

[1] M. Syvajarvi et al., Solar Energy Materials and Solar Cells, vol. 145, pp. 104-108, (2016).
[2] N. Ichikawa, M. Kato, and M. Ichimura, Applied Physics Express, vol. 8, no. 9, (2015).
[3] D. J. Christle et al., Physical Review X, vol. 7, no. 2, (2017).
[4] S. Nishino, J. A. Powell, and H. A. Will, Applied Physics Letters, vol. 42, no. 5, pp. 460-462, (1983).
[5] P. Schuh et al., Journal of Crystal Growth, vol. 478, pp. 159-162, (2017).
[6] F. La Via et al., Materials Science in Semiconductor Processing, vol. 78, pp. 57-68, (2018).
[7] M. Schöler, P. Schuh, J. Steiner, and P. J. Wellmann, Materials Science Forum, vol. 963, pp. 157-160, (2019).

Session 6

Thursday 12.03.2020

13:00 – 14:20

CRYSTAL GROWTH OF OXIDES AND FLUORIDES AT THE IKZ

Matthias Bickermann, Zbigniew Galazka, Christo Guguschev, Detlev Schulz, Hiroki Tanaka, Detlef Klimm, Steffen Ganschow, Christian Kränkel, and Thomas Schröder

Leibniz-Institut für Kristallzüchtung (IKZ), Max-Born-Str. 2, 12489 Berlin, Germany
E-mail: matthias.bickermann@ikz-berlin.de

Summary

The growth of volume crystals of oxides and fluorides has a long tradition at the IKZ but is also characterized by modern topics with outstanding international visibility. Our publications on the Czochralski method to grow big gallium oxide (β-Ga_2O_3) bulk crystals from the melt are “highly cited” in the field of bulk crystal growth [1,2]. The former head of the IKZ team, Reinhard Uecker, was awarded the IOCG Frank Prize in 2019 (together with Darrell Schlom) for pioneering "strain engineering" by providing substrates for “lattice mis-matched” films [3,4]. Recently, we succeeded in the growth of the first KTb_3F_{10} bulk crystals that can be used as optical isolators for high-power near infrared lasers.

In the presentation we will show how the preparation of β-Ga_2O_3 substrates of highest structural quality helped to provide a breakthrough in demonstration of novel power electronics devices [5]. Regarding crystal growth, the control of the local oxygen partial pressure is crucial to minimize the formation of suboxides and metallic gallium in the melt that would attack the crucible [2]. The growth of highly n-conductive β-Ga_2O_3 with large diameter remains a challenge, not only due to the self-absorption of heat radiation [1]. Current research is focused on the investigation of the segregation and doping of various elements during growth [6,7]. Also, the preparation and potential applications of gallates with spinel structure such as $ZnGa_2O_4$ [8] are discussed.

Perovskite-type substrates, originally used to prepare superconducting thin films, have been employed to push the limits of novel ferroelectric, superconducting, ferromagnetic, piezoelectric, multiferroic or high-mobility oxide electronic materials [9]. The rare earth scandates $REScO_3$ (RE = Dy...Pr) grown at IKZ are in worldwide use to cover any desired pseudo-cubic lattice parameter in the range from about 3.95 to 4.02 Å [3,4]. Recently, novel promising materials with lattice constants in the range of 4.08–4.15 Å have been developed at IKZ jointly with Cornell University [10,11] to accommodate promising thin film materials such as La:$BaSnO_3$, $BiScO_3$, $BiFeO_3$ or $PbZrO_3$ with high structural quality. This success was strongly based on thermochemical assessments of stability of compounds such as Ba_2ScNbO_6 and $BaSnO_3$ under melt growth conditions and phase diagram calculations in the La_2O_3–Lu_2O_3–Sc_2O_3–Nd_2O_3 system. We will present these results and also highlight perovskite-type crystals $SrHfO_3$ and $SrZrO_3$ grown by the IKZ in collaboration with the Institute of Physics CAS in Prague [12].

Regarding fluorides, we will briefly introduce our activities and demonstrate first crystals of KTb_3F_{10} that can be used to prepare superior optical isolators. The crystal growth is impeded by a peritectic phase transition slightly below the melting point, while accurate thermodynamic data is not available [13]. Formation of scattering centers as well as oxygen contamination must be mitigated by employing the right off-stoichiometry and purified starting materials.

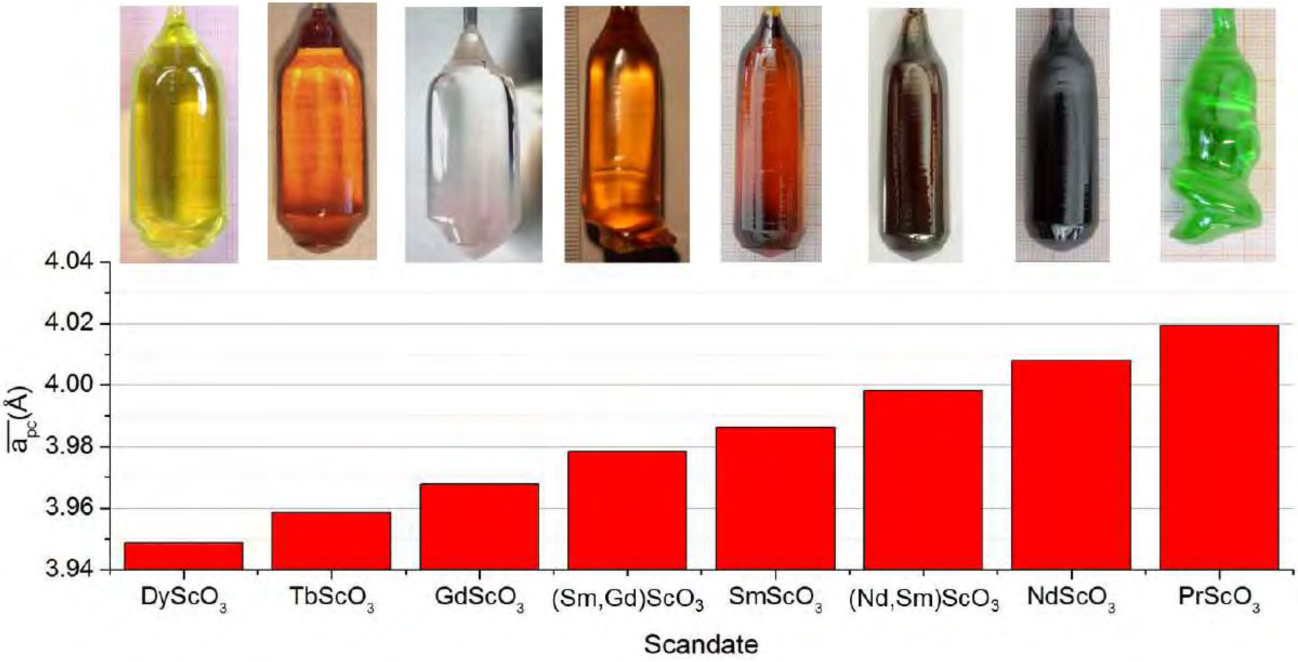

Fig. 1: Pseudo-cubic lattice parameters of different rare earth scandate single crystals (from [4])

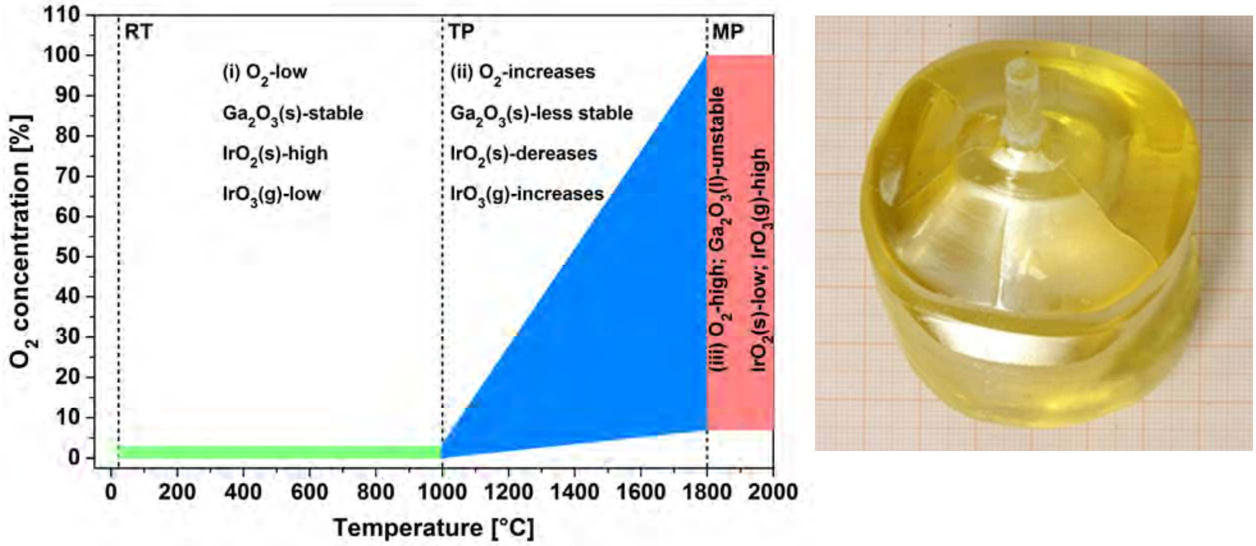

Fig. 2: Oxygen delivery vs. temperature for the growth of large diameter β-Ga2O3 single crystals from an Ir crucible (from [2]); 2-inch Al-doped β-Ga_2O_3 single crystal obtained by the Czochralski method (from [6])

[1] Z. Galazka, K. Irmscher, R. Uecker et al., Journal of Crystal Growth **404** (2014) 184
[2] Z. Galazka, R. Uecker, D. Klimm et al., ECS Journal of Solid State Science and Technology **6** (2017) Q3007
[3] R. Uecker, H. Wilke, D.G. Schlom et al., Journal of Crystal Growth **295** (2006) 84
[4] C. Guguschev, J. Hidde, T.M. Gesing et al., CrystEngComm **20** (2018) 2868-2876
[5] K. Tetzner, E.B. Treidel, O. Hilt et al., IEEE Electron Device Letters **40** (2019) 1503
[6] Z. Galazka, S. Ganschow, A. Fiedler et al., Journal of Crystal Growth 486 (2018) 82-90
[7] Z. Galazka, K. Irmscher, R. Schewski et al., Journal of Crystal Growth **529** (2020) 125297
[8] Z. Galazka, S. Ganschow, R. Schewski et al., Applied Physics Letters Materials **7** (2019) 022512
[9] H.J. Haeni, P. Irving, W. Chang et al., Nature **430** (2004) 758
[10] R. Uecker, R. Bertram, M. Brützam et al., Journal of Crystal Growth **457** (2017) 137–142
[11] C. Guguschev, D. Klimm, M. Brützam et al., Journal of Crystal Growth **528** (2019) 125263
[12] J. Pejchal, C. Guguschev, M. Schulze et al., Optical Materials **98** (2019) 109494
[13] K.T. Stevens, W. Schlichting, G. Foundos et al., Laser Technik Journal (Wiley) 03/2016, p. 18

Growth of high-melting sesquioxides for laser applications

A. Uvarova, C. Guguschev, M. Bickermann and C. Kränkel

Leibniz-Institut für Kristallzüchtung, Max-Born-Straße 2, 12489 Berlin, Germany
E-mail: anastasia.uvarova@ikz-berlin.de

Lasers in the mid-infrared range are attractive in fields like laser surgery or atmospheric detection, due to the strong absorption of water in this spectral region. To achieve good beam quality and stable high-power laser operation, good mechanical, optical, and thermal properties are essential for potential laser materials. The rare-earth sesquioxide crystals Lu_2O_3, Sc_2O_3, and Y_2O_3 have been shown to be very suitable for high-power mid-infrared laser operation due to their high thermal conductivity and low phonon energies.

Despite these promising results, the growth of sesquioxide crystals with high optical quality is very challenging due to their high melting temperatures of more than 2400 °C. These materials were previously grown by the heat exchanger method from rhenium crucibles, as this is the only crucible material that is suitable for such crystals [1]. This method has shown good results, but the Re-crucibles are very sensitive to oxygen, which requires a very precise control of the growth atmosphere. Moreover, the fabrication of Re-crucibles is very expensive and thus this growth method is not suitable for commercial use.

Here, we report on the application of the optical floating zone technique (OFZ) for the growth of high-melting sesquioxide crystals to avoid the use of expensive and sensitive crucible materials. This method has several advantages compared to previous growth methods. It is crucible free and does not require zirconica insulation. Therefore, high oxygen partial pressures and free choice of the growth atmosphere are possible.

By using our high-pressure high-temperature OFZ furnace undoped Lu_2O_3, as well as Er^{3+} and Yb^{3+}-doped Lu_2O_3 crystals were grown (Fig. 1). The growth experiments were carried out under Ar atmosphere at elevated pressure, the growth speed was varied between 2 mm/h and 7.5 mm/h at a lamp power of 5 kW. The pressed powder feeding rods were made from 5N purity powders. The doped rods were prepared by mixing Lu_2O_3 and Er_2O_3 or Lu_2O_3 and Yb_2O_3 powders, respectively, by using a 3-dimensional mixer. All rods were pressed in an isostatic press and then sintered in the oven.

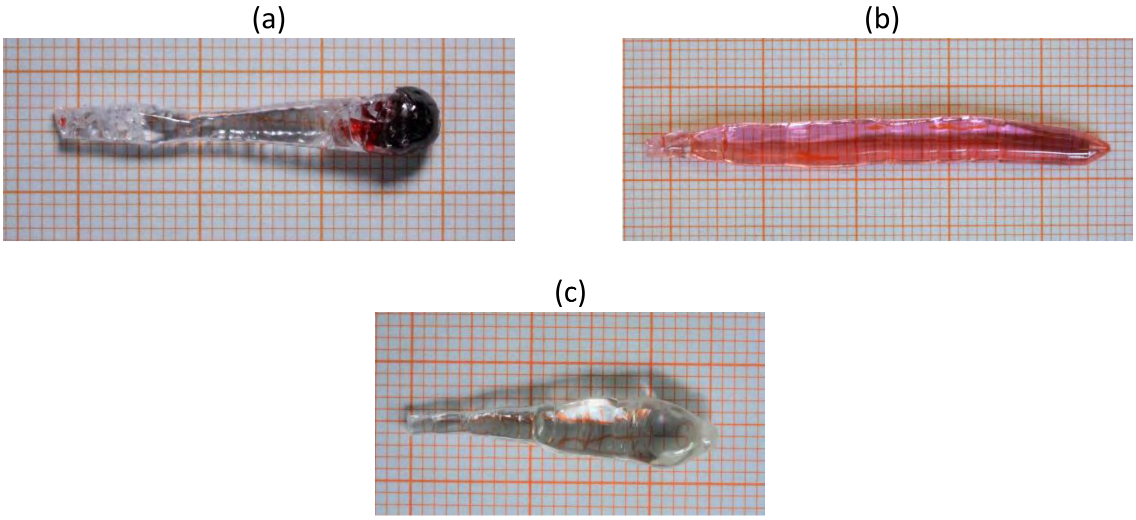
(a)
(b)
(c)

Fig. 1: Lu_2O_3 (a), Er^{3+} (b) and Yb^{3+}-doped Lu_2O_3 (c) crystals grown by the optical floating zone method.

In future, we aim to utilize these crystals for laser experiments to advance the progress in 3 µm laser operation with Er^{3+} -doped and 1 µm laser operation with Yb^{3+} -doped sesquioxides. We are convinced that the OFZ-technique is a well suited method for the growth of rare-earth doped sesquioxide crystals for laser applications.

[1] R. Peters, C. Kränkel, K. Petermann, and G. Huber, "Crystal growth by the heat exchanger method, spectroscopic characterization and laser operation of high-purity Yb:Lu_2O_3". J Cryst. Growth, 310(7-9), 1934-8, 2008

COMMEMORATIVE EVENT
50 YEARS DGKK
Schüler Preis
DGKK Nachwuchspreis
DGKK Preis

Thursday 12.03.2020

14:50 – 17:50

Solution Growth as a Powerful Tool for the Solid-State Physicist

A. Jesche [a]

[a] *EP VI, Center for Electronic Correlations and Magnetism, Institute of Physics,*
University of Augsburg, D-86159 Augsburg, Germany
E-mail: anton.jesche@physik.uni-augsburg.de

Summary

Whether for optimization of sample size and quality, detailed substitution series or exploratory work: solution growth is a versatile tool that offers many benefits. Once a suitable solvent (or flux) is found, the growth can be performed at reduced reaction temperature, reduced vapor pressure, and with small amounts of material (compared to using mirror furnaces, Czochralski or Bridgeman methods). Furthermore, an 'in situ purification' of the starting materials is often associated with crystallization from solutions.

I'm going to show how the successful single crystal growth from solution allowed for immediate progress in understanding various, primarily magnetic and superconducting materials. A couple of representative single crystals is shown in Fig. 1.

First example is the prominent family of FeAs high-temperature superconductors with critical temperatures of more than 50 K. Elevated synthesis temperatures beyond 1000°C in combination with the high vapor pressure of As pose a particular challenge. FeAs self-flux [1], KI salt flux [2], and Sn flux [3] were successfully applied to grow single crystals of several millimeter along a side. Those samples allowed to solve the magnetic structure and revealed important similarities and differences to the cuprate superconductors.

A significant number of binary systems with known crystal structure but unknown physical properties were grown as single crystals and investigated by temperature-dependent magnetization, specific heat and electric transport. Interesting and unexpected was, for example, the observation of strong quantum oscillations in the large-unit-cell compound $Cu_{13}Ba$ [4] and nearly-itinerant ferromagnetism in $CaNi_2$ and $CaNi_3$ [5].

The latter were grown from Ca-rich flux that is highly reactive and required some effort in designing suitable crucibles that were made from Nb or Ta. Such crucibles were also used to grow single crystals from Li flux. Several Li-based materials and in particular various nitrides were successfully grown [6], for example pure and transition-metal doped Li_3N, Li_4SrN_2, and $LiSr_2CoN_2$. A significant increase of the solubility of transition metals in Li is caused by the presence of N.

A completely unexpected side product was the growth of single crystalline α-Fe in Li-N flux [7]. We have found well facetted, rhombic dodecahedral α-Fe single crystals with diameters in the range of millimeters.

Furthermore, there is ongoing progress in the development of a 'feedback' furnace that allows for the in-situ detection of nucleation from a melt [8]. Liquidus temperature and other phase transitions are determined directly in the crystal growth apparatus leading to significantly improved process control and efficiency. Larger single crystals can be obtained by seed selection and slow cooling rates in the vicinity of the liquidus as shown for α-PdBi.

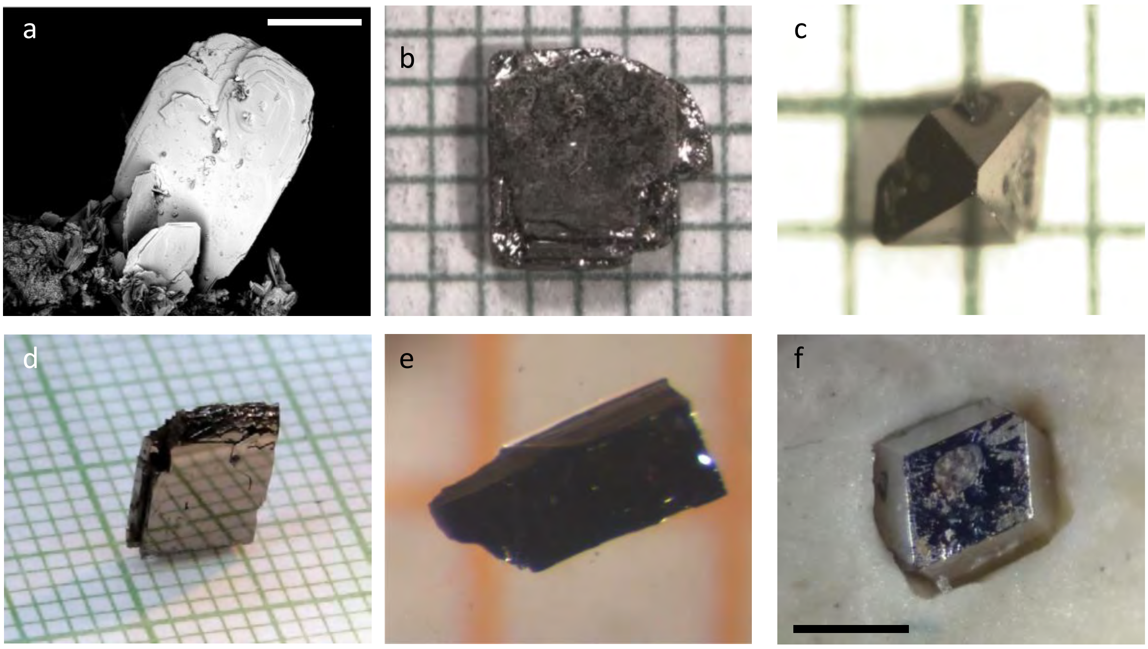

Fig. 1: Selection of single crystals obtained from high-temperature solution growth. a) CeFeAsO grown from KI flux. b) $Cu_{13}Ba$ grown from $Ba_{38}Cu_{62}$. C) $CaNi_2$ grown from $Ca_{67}Ni_{33}$. d) Li_3N grown from $Li_{90}N_{10}$. e) Fe-substituted Li_4SrN_2 grown from Li-rich flux. f) α-Fe grown from $Li_{84}N_{12}Fe_3$. Scalebar in a) and f) is 0.5 mm, all other samples are shown on millimeter grid.

To summarize, "the 'we find solutions' approach is based on the development of broadly versatile melts that will allow for the explorations of a new sets of phase spaces; new pathways into a poorly explored part of the forest... hic sunt leones." [9]

Acknowledgment
C. Krellner, C. Geibel, P.C. Canfield, A.A. Tsirlin, and P. Gegenwart are acknowledged for various fruitful conversations. The author thanks R. Weise, A. Herrnberger, and K. Wiedenmann for technical support. A cooperative project with the ScIDre GmbH (Dresden) was funded by the ZIM program of the German Ministry for Economic Affairs and Energy (BMWi). This work was supported by the Deutsche Forschungsgemeinschaft (DFG, German Research Foundation) - Grant No. JE748/1.

[1] M. Kumar, M. Nicklas, A. Jesche, N. Caroca-Canales *et al.* Phys. Rev. B **78**, 184516 (2008)
[2] F. Nitsche, A. Jesche, E. Hieckmann, T. Doert, and M. Ruck, Phys. Rev. B **82**, 134514 (2010)
[3] A. Jesche, C. Krellner, M. de Souza, M. Lang, and C. Geibel, Phys. Rev. B **81**, 134525 (2010)
[4] A. Jesche, S.L. Bud'ko, and P.C. Canfield, J. Alloys Compd. **587**, 705–709 (2014)
[5] A. Jesche, K.W. Dennis, A. Kreyssig, and P.C. Canfield, Phys. Rev. B **85**, 224432 (2012)
[6] A. Jesche and P.C. Canfield Philos. Mag. **94**, 2372–2402 (2014)
[7] M. Fix, H. Schumann, S.G. Jantz, F.A. Breitner *et al.* J. Cryst. Growth **486**, 50 (2018),
[8] A.G.F. Schneider, P. Sass, R. Schöndube, and A. Jesche Cryst. Res. Technol. 1900109 (2019)
[9] P.C. Canfield, Prog. Phys. **83**, 016501 (2020)

MOVPE GROWTH OF GaAs WITH GROWTH RATES UP TO 280 µm/h

R. Lang [a], F. Habib [b], M. Dauelsberg [b], F. Dimroth [a], D. Lackner [a]

[a] *Fraunhofer Institut für Solare Energiesysteme, Heidenhofstraße 2, 79110 Freiburg, Germany*
[b] *AIXTRON SE, Dornkaulstraße 2, 52134 Herzogenrath, Germany*
E-mail: robin.lang@ise.fraunhofer.de

Metal organic vapor phase epitaxy (MOVPE) of III-V compound semiconductors is a well-established technique used in industry for the production of multi-junction solar cells, LEDs, or lasers. MOVPE grown III-V multi-junction solar cells outperform all other solar cells in terms of efficiency. Still, the epitaxial production process is time consuming and expensive due to moderate growth rates and the inefficient use of the precursor materials. In this work, we address both issues simultaneously by increasing the growth rate and optimizing the process conditions of the reactor chamber. Additionally, we show the influence of high growth rates on material and solar cell properties.

All samples were grown with an AIXTRON CRIUS Close-Coupled Showerhead reactor in a 7x4" configuration. In this reactor design, the gap distance between ceiling and susceptor can be adjusted. Standard precursors including TMGa, TMIn, TMAl, PH_3, and AsH_3 were used. A dual-layer anti-reflection coating (ARC) was applied to the solar cells and they were measured under the AM1.5g spectrum.

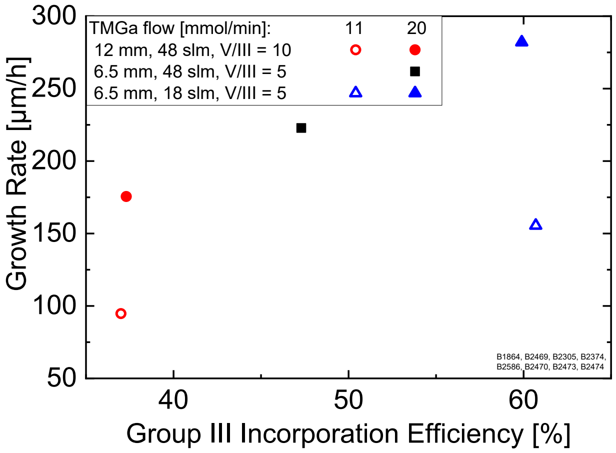

Fig. 1: GaAs growth rate plotted versus the incorporation efficiency of TMGa, calculated for one 12" wafer for different reactor conditions.

We demonstrate that growth rates up to 280 µm/h for GaAs with group III incorporation efficiencies above 60 % are possible using MOVPE (see Fig. 1) [1]. These values were achieved by increasing the concentration gradient between the showerhead and the substrate and therefore the material transport to the wafer surface. In this reactor type, the concentration gradient can be increased by reducing the process gap height as well as the total H_2 carrier gas flow. The experimental results could be reproduced both by accurate numerical simulation [2] and with a simple calculation using a control volume ansatz. Furthermore, the influence of the growth rate on properties like surface morphology, surface roughness, growth rate homogeneity and background doping was studied. In terms of solar cell properties, the minority carrier diffusion length and the solar cell performance were investigated up to growth rates of 140 and 100 µm/h, respectively [3] (see Fig. 2 and Table 1).

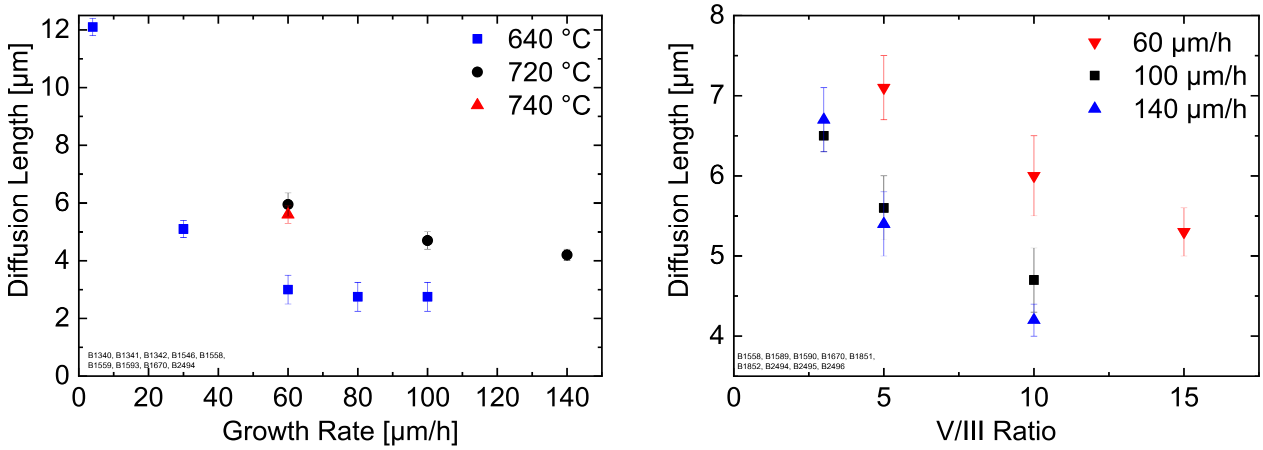

Fig. 2: Diffusion length in $2 \cdot 10^{17}$ cm^{-3} doped p-GaAs plotted versus the growth rate for different growth temperatures at a V/III ratio of 10 (A) and versus the V/III ratio for different growth rates at a growth temperature of 720°C (B).

Table 1: Best 4 cm^2 cell results (measured under the AM1.5g spectrum).

Growth Rate [µm/h]	T_G [°C]	V/III Ratio	V_{OC} [V]	J_{SC} [mA/cm^2]	FF [%]	η [%]
4	640	10	1.055	28.6	81.6	24.6
60	720	5	1.036	28.4	79.7	23.5
80	720	5	1.021	28.3	80.9	23.4
100	720	5	1.019	28.3	81.1	23.3
100	720	3	1.028	28.5	80.7	23.6

We found that an increase in the growth rate leads to a reduction of the diffusion length from 12 to 2.5 µm if all other parameters are kept constant. This is attributed to an increase in the amount of EL2 defects which is connected to As antisites (As_{Ga}) [4]. Higher growth temperatures and lower V/III ratios can suppress the formation of As_{Ga} and thus the diffusion length recovers. In the end, we achieved a diffusion length of more than 6 µm at a growth rate of 140 µm/h. The combination of high growth rates and low V/III ratios opens up opportunities for significant cost reduction for the III-V epitaxy growth.

Solar cell measurements reflect the diffusion length results (Table 1). At a growth rate of 100 µm/h, an open-ciruit voltage of 1.028 V and an efficiency of 23.6 % under the AM1.5g spectrum were achieved at a V/III as low as three. This is only 1.0 $\%_{abs}$ below a reference solar cell grown at a growth rate of 4 µm/h. The results show the potential of using MOVPE to reach lower cost GaAs epitaxy through the optimization of growth conditions.

Acknowledgment

The authors would like to acknowledge financial support by the German Federal Ministry of Education and Research under Grant “MehrSi” 03SF0525A and by the Marie Sklodowska-Curie “ENHANCE” Grant Agreement 722496.

[1] R. Lang, F. Habib, M. Dauelsberg, F. Dimroth, D. Lackner, submitted to Journal of Crystal Growth

[2] D. Brien, M. Dauelsberg, K. Christiansen, J. Hofeldt, M. Deufel, M. Heuken, Journal of Crystal Growth, **303**, 1, 330-333 (2007)

[3] R. Lang, J. Schön, F. Dimroth, D. Lackner, IEEE Journal of Photovoltaics, **8**, 6, 1596-1600 (2018) [3]

[4] K. J. Schmieder, E. A. Armour, M. P. Lumb, M. K. Yakes, Z. Pulwin, J. Frantz, R. J. Walters, IEEE Journal of Photovoltaics, **7**, 1, 1596-1600 (2017)

The “amazing” group-III nitrides – epitaxy for optical and electronic applications

Stacia Keller[a]

[a] *Electrical & Computer Engineering Department, University of California Santa Barbara,*
Santa Barbara, CA 93106, USA
E-mail: stacia@ece.ucsb.edu

In the past decades group-III nitride technology has developed at an enormous pace. Optical devices such as LEDs and lasers have become part of everyday life in light bulbs, street lights, automotive lights, or digital cinema. Less visibly, electronic applications have emerged and (Al,Ga)N transistors are utilized in base stations, communi cations and RADAR. The application of (Al,Ga,In)N materials for electronic components is, however, still evolving. The large band gap, the high breakdown field, and the high electron mobility make group-III nitride based transistors attractive in particular for high power and high frequency applications.

One current direction of research is the exploration of nitride based transistors for 5G communication networks. In this area, new developments in epitaxial growth have led to a breakthrough in the device performance. In difference to traditional group-III nitride devices, which are typically based on epitaxial layers grown in the Ga-polar (0001) direction of the hexagonal lattice, these novel devices are fabricated via growth in the N-polar (000-1) direction, taking advantage of the opposite direction of the internal electric fields in N- compared to Ga-polar III-N heterostructures. While N-polar nitrides were explored early on, their utilization for device applications was hampered by their poor structural properties and high residual impurity concentrations. In particular films grown by metal-organic chemical vapor deposition, the most common epitaxial technique used for the deposition of III-N heterostructures, exhibited dense arrays of surface defects, which were believed to be immanent to the N-polar growth direction. A closer look at the impact of the epitaxial growth parameters, however, indicated that limitations in the surface mobility of adsorbed species may play a role in the defect formation. Adjustments in the growth procedure allowed the deposition of high purity N-polar III-N films on sapphire, SiC, and (111) silicon substrates and enabled the fabrication of N-polar transistors demonstrating an record output power density of 8.8 W/mm at 94 GHz with a power added efficiency of 27%. [1,2]

Another area of intense research is the fabrication of micro-LEDs for display applications, which led to an increased interest in nitride LEDs with InGaN active regions emitting at wavelength longer than green. The demonstration of high performance LEDs emitting in the yellow and red, however, poses several challenges, one being the large 10 % lattice mismatch between InN and GaN. In order to mitigate the lattice mismatch between base material and active region, substrates with a lattice constant larger than GaN are very attractive. One possible path is the fabrication of relaxed InGaN pseudo-substrates. Two approaches will be discussed. The first involves the coalescence of relaxed III-nitride nano-features, utilizing the natural relaxation observed in the nanoscale. [3] The second, more recently pursued technique takes advantage of the reduced mechanical stiffness of porous GaN, allowing the demonstration of relaxed and partially relaxed InGaN-on-porous-GaN 10 µm x 10 µm tile arrays. [4] Such pseudo-substrates have the potential to catalyze the development of full color micro-LED arrays.

[1] S. Keller et al., Semicond. Sci. Technol. **29**, 113001 (2014).
[2] B. Romanczyk et al., IEEE Electron Device Letters, Early Access Article DOI 10.1109/LED.2020.2967034 (2020).

[3] S. Keller et al., Semicond. Sci. Technol. **30**, 105020 (2015).
[4] S. Pasayat et al., Materials **13**, 213 (2020).

Session 7

Friday 13.03.2020

8:30 – 10:20

Model experiments for crystal growth

K. Dadzis [a], O. Pätzold [b], G. Gerbeth [c]

[a] *Leibniz-Institut für Kristallzüchtung (IKZ), Max-Born-Straße 2, 12489 Berlin, Germany*
[b] *Institute of Nonferrous Metallurgy and Purest Materials, TU Bergakademie Freiberg, Leipziger Str. 34, 09599 Freiberg, Germany*
[c] *Institute of Fluid Dynamics, Helmholtz-Zentrum Dresden - Rossendorf, Bautzner Landstraße 400, 01328 Dresden, Germany*
E-mail: kaspars.dadzis@ikz-berlin.de

Summary

Numerical simulations are widely used for process development and equipment design for crystal growth both on research and industrial scales. The underlying physical models require measurement data for validation. However, many crystal growth processes take place at high temperatures in a vacuum-sealed atmosphere, which significantly limits in-situ observation. Therefore, dedicated *model experiments* are applied, where the relevant physical phenomena are transferred (more exactly – scaled) to a model system working with a model material and having an appropriate in-situ access. We have recently reviewed the use of such model experiments to investigate melt and gas flows in crystal growth [1]. Two prominent examples are Czochralski (CZ) growth and directional solidification (DS) of silicon.

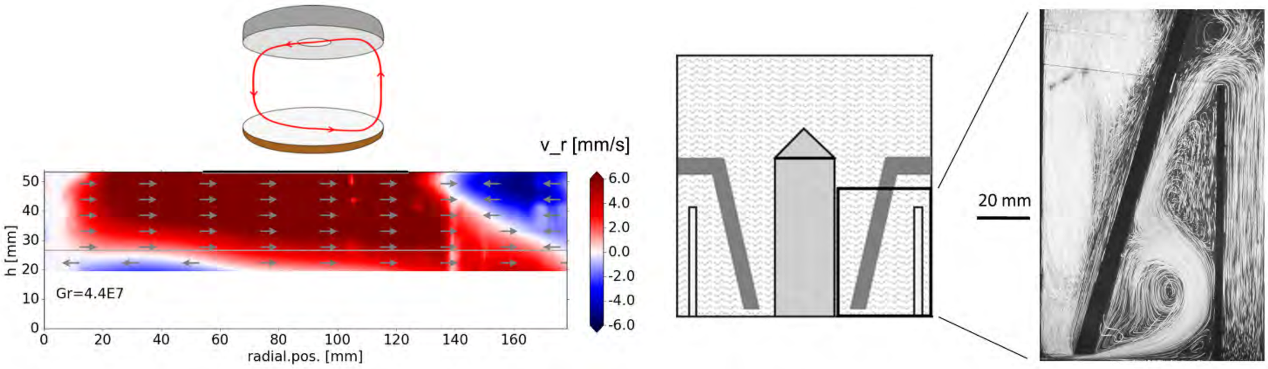

Fig. 1. Velocity measurements in model experiments for the CZ process: melt flow with an asymmetric structure (left); gas flow around the heat shield (right). See [1] for details.

Melt flow in the CZ Si growth has been modelled using liquid metal alloys such as GaInSn in heated containers with diameters up to 800 mm (see [1] and references therein). Early studies were focusing on the influence of various AC and DC magnetic fields and performed detailed measurements of the temperature field, which enabled the validation of turbulence models [2]. Application of ultrasonic velocity measurements recently revealed the presence of unexpected asymmetric flow patterns, which have not been fully explained by numerical simulation yet (see Fig. 1). What are appropriate boundary conditions for the temperature and velocity? Which turbulence models and discretization parameters are suitable? Such questions are still under active discussion today as demonstrated by recent simulations for the 300 mm CZ Si process [3]. Gas flows in CZ growth have been modelled using isothermal model liquids to describe the forced flow around the heat shield (see Fig. 1). While no comparisons with simulations have been published yet, the experiments have provided important hints about the long-range influence of inlet conditions and about the presence of 3D instabilities.

Model experiments with liquid metals for the melt flow in DS Si growth under AC magnetic fields have reached melt width up to 420 mm (see [1] and references therein). Advanced ultrasonic measurements of the 2D velocity fields in an experimental parameter study have enabled the classification of a large number of flow structures [4]. Although the corresponding numerical models still need further validation for the interaction with the solid-liquid boundary in particular, the confidence in the modeling results has been greatly improved.

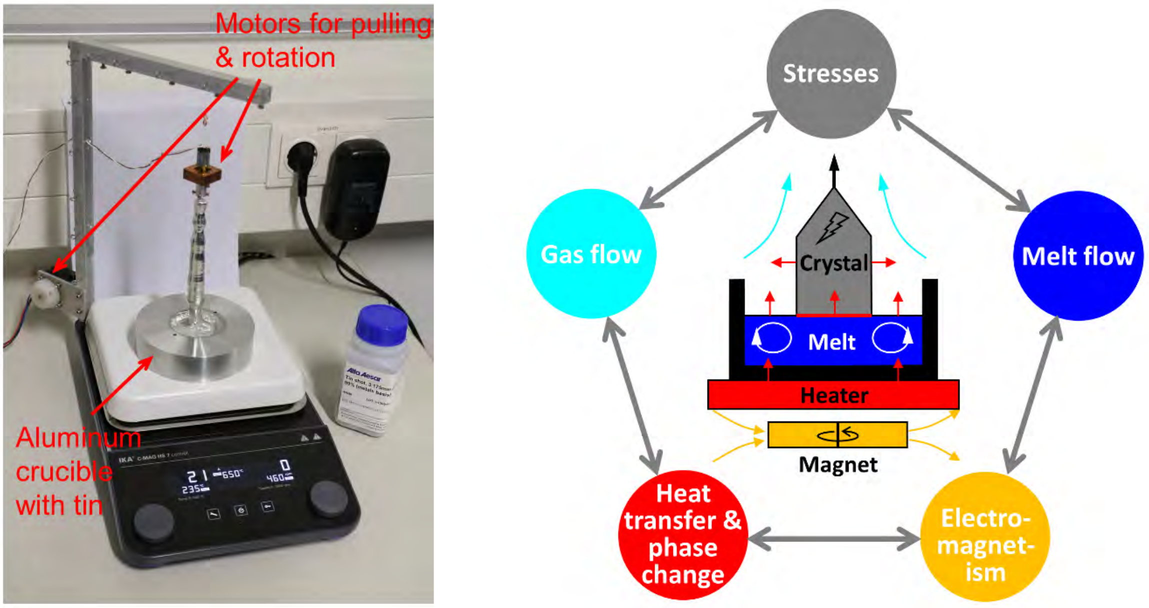

Fig. 2. Multi-physical model experiments for crystal growth: demo setup with CZ growth of Sn (left) and sketch of physical phenomena (right).

Melt and gas flows in crystal growth are a part of a larger landscape of interacting physical phenomena on several time and length scales. This physics landscape is common to many crystal growth processes – from the century-old experiments by Jan Czochralski with molten metals to industrial CZ pullers for 300 mm Si monocrystals. Fig. 2 shows a modern version of Czochralski's experiment and selects the key physical phenomena. It is important to realize that every crystal growth experiment needs to manage all these aspects. And every complete crystal growth simulation needs to include <u>validated</u> models (also, <u>validated</u> simplifications) of all these aspects. But how can we perform the necessary in-situ measurements for the validation of such coupled models? Note that the requirements for the modeling accuracy increase if we want to analyze complex phenomena such as transport of oxygen in solid, liquid and gas phases in CZ growth of Si.

These questions are being addressed within the Starting Grant NEMOCRYS funded by the European Research Council (ERC) for the time period Feb 2020 – Jan 2025 at the IKZ. We will develop accessible multi-physical model experiments for crystal growth and integrate modern measurement techniques (infrared imaging, ultrasonic velocimetry, etc.). The obtained in-situ measurement data will be used to reach a new level of physical understanding and establish a new generation of multi-physical models for crystal growth processes.

[1] K. Dadzis, O. Pätzold, G. Gerbeth, Cryst. Res. Technol., 1900096 (2019).
[2] A. Krauze, N. Jekabsons, A. Muiznieks, A. Sabanskis, U. Lacis, J. Cryst. Growth, **312**, 3225–3234 (2010).
[3] V. Kalaev, J. Cryst. Growth, **532**, 125413 (2020).
[4] N. Thieme, M. Keil, D. Meier, P. Bönisch, K. Dadzis, O. Pätzold, M. Stelter, L. Büttner, J. Czarske, J. Cryst. Growth, **522**, 221–229 (2019).

NUMERICAL MODELING OF METALLIC IMPURITY INCORPORATION DURING DIRECTIONAL SOLIDIFICATION OF MULTI-CRYSTALLINE SILICON ASSISTED BY EXPERIMENTAL PROOF

S. Schwanke[a]*, K. Schuck[a], T. Jung[a], M. Trempa[a], C. Kranert[b], C. Reimann[a,b], M. Kuczynski[c], G. Schroll[c], J. Sans[c], J. Stenzenberger[d], K. Hesse[d], J. Heitmann[b], J. Friedrich[a,b]

[a]Fraunhofer IISB, Schottkystr. 10, 91058 Erlangen, Germany
[b]Fraunhofer THM, Am St.-Niclas-Schacht 13, 09599 Freiberg, Germany
[c]AlzChem Trostberg GmbH, Dr.-Albert-Frank-Str. 32, 83308 Trostberg, Germany
[d]Wacker Chemie AG, Johannes-Hess-Straße 24, 84489 Burghausen, Germany

E-mail: Stanislaus.schwanke@iisb.fraunhofer.de

Summary

During the crystallization process of multi-crystalline silicon (mc-Si) metal impurities (like Fe, Co etc.) are mainly incorporated into the silicon melt and hence into the ingot via diffusion from the quartz crucible through the silicon nitride (Si_3N_4) coating or from the coating itself. As a consequence, the highly contaminated peripheral areas of the grown ingots known as "redzones" cannot be used for further production of solar cells resulting in a high wafer yield loss, as well as the ingot center is limited in electrical performance due to fast diffusing metal impurities.

In order to get a better understanding of the metal impurity input during the crystallization process two numerical models were developed and evaluated by comparison to real annealing and crystallization experiments. The 1D model, which was written in the programming language Python [1], describes the solid-state diffusion of metals from Si_3N_4 coated crucible substrates into silicon blocks during annealing experiments and was used to identify suitable diffusion parameters. Afterwards these parameters were transferred to a 2D crystallization model, which is based on a self-written solver using the finite volume method and is implemented in the C++ program package OpenFOAM [2]. For validation of the numeric models several annealing experiments using mono-crystalline Cz blocks 70x70x55mm^3 in size were performed and mc-Si ingots with a weight of 15kg were grown in a Vertical Gradient Freeze (VGF) furnace, while different consumables (ceramic silica crucible, Si_3N_4 coating and silicon feedstock) with varying purity levels were used. The numerically calculated metal profiles along the block/ingot height were compared to measured Fe_i-profiles and metal concentrations determined by neutron activation analysis (NAA). Furthermore, numerically observed differences in the metal content between the grown ingots were qualitatively compared to the trends derived from carrier-lifetime measurements.

It will be shown that the trends from the real experiments can be directly predicted using the numerical models. Afterwards, the numerical crystallization model is scaled up to the industrial G6 scale and an overview about the correlation between the purity variations of the raw materials and the effect on the red zone expansion as well as the lifetime values of the center region will be shown. Purity variations of the Si_3N_4 coating and feedstock come only into effect in modern setups containing crucible diffusion barriers. In this case, the redzone expansion among others can be decreased down to 35%, if the Fe concentration of the coating would be reduced by one order of magnitude, while the full potential is limited by the contamination level of the silicon feedstock.

Acknowledgment
These research and development activities were carried out within the SYNERGIE project (0324150) funded by the German Federal Ministry for Economic Affairs and Energy.

[1] Van Rossum, G., Python programming language, In USENIX Annual Technical Conference (2007)
[2] OpenFOAM 4.x UserGuide, 2011-2019 OpenFOAM Foundation Ltd., Berkshire, UK

Forced convection by high-speed rotation in Czochralski growth from high-temperature solutions

O. Harder [a], P. Eschenbacher [a], E. Hanfstaengl [a], K. Dadzis [b], P. Gille [a]

[a] *Sektion Kristallographie, Ludwig-Maximilians-Universität München, Theresienstraße 41, 80333 München, Germany*
[b] *Leibniz-Institut für Kristallzüchtung (IKZ), Max-Born-Straße 2, 12489 Berlin, Germany*
E-mail: oliver.harder@campus.lmu.de

Summary

In crystal growth of intermetallics, the Czochralski method has proved to be a powerful technique for bulk single crystals [1]. Many intermetallic compounds show peritectic melting behavior and can, therefore, only be crystallized from incongruent melts below their decomposition temperature. Combined with a restricted solubility, mass transport in the solution next to the growth interface is the limiting factor for growth rates and inclusion-free single crystal growth. Various techniques of forced convection, e.g. ACRT [2] or IRB [3], are known from literature to effectively suppress inclusion formation due to increased mass transport. Since the Czochralski method uses crystal and crucible counter-rotation anyway, we carried out a combined experimental and numerical modelling study to investigate the influence of high crystal rotation rates on mass transport in the Czochralski growth of intermetallic compounds from metallic solutions.

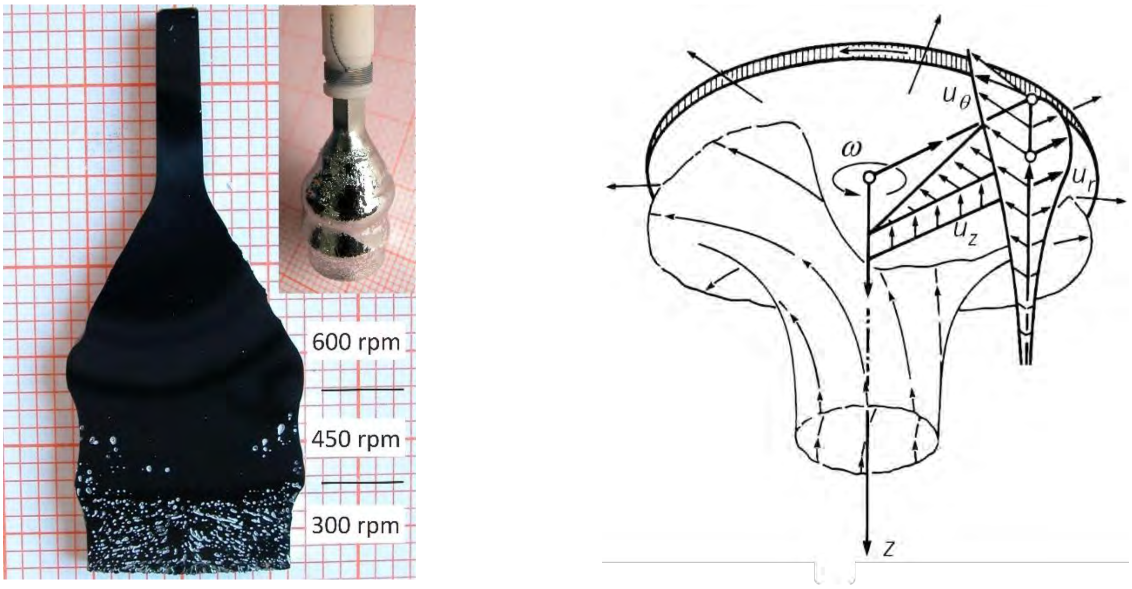

Fig. 1: Ga_3Ni_2 single crystal and inclusion distribution at varying crystal rotation rates (left). Schematic drawing of the rotating-disk model according to Hurle [5] (right).

As a first approximation, the rotating crystal can be described as a rotating disc attached to the melt surface. In this model, mass transport in the melt close to the crystal is dominated by diffusion in a boundary layer while convection dominates the remainder of the melt. This general case was analytically solved long time ago [4] and has been treated for Czochralski growth purposes by Hurle [5]. Its key idea is a reduced diffusion boundary layer (also named Ekman layer) thickness δ depending on the disc's rotation rate ω according to $\delta \sim (\nu/\omega)^{1/2}$ for a melt with kinematic viscosity ν.

Experimentally, several single crystal growth experiments were conducted in a modified self-built Czochralski apparatus using crystal rotation rates of up to 600 rpm. Ga_3Ni_2 and Ga_7Pd_3 served as model compounds due to their well-known tendency for severe inclusion formation at usual growth conditions. Despite such conditions, inclusion-free single crystal growth of Ga_3Ni_2 and Ga_7Pd_3 could be demonstrated with crystal rotation rates exceeding 400 rpm.

Further understanding about the impact of rotation rates and changes in rotation rates on the crystal growth dynamics was gained from experiments. As expected, there seems to be a critical rotation rate at which a system of formerly inclusion-free growth changes to the usual state of high inclusion density when the crystal rotation rate is lowered. Additionally, we could demonstrate that a state of abundant inclusions can return to one of inclusion-free growth. Lastly, we observed the impact of a sudden change in rotation rates on crystal growth dynamics.

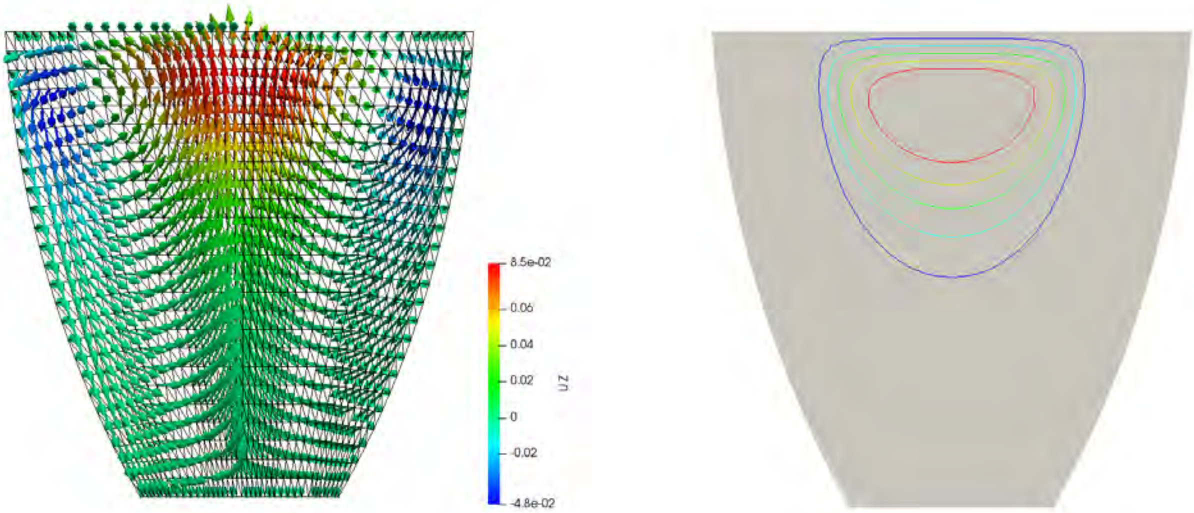

Fig. 2: Velocity vector field (in m/s) of fluid flow in a crucible (ratio of crystal to crucible radii 0.7) established by a crystal rotating with 600 rpm (left). Isolines of the vertical velocity component indicating the geometry of the boundary layer (right).

Numerical simulations with the computational fluid-dynamics package OpenFOAM were primarily used to investigate and support the experimental findings. Their most important result is the extension of the model of a uniform boundary layer thickness proposed by Hurle [5] to one of a radially outwards increasing boundary layer thickness. Hence, the three-phase coexistence line has been found to be the experiment's most vulnerable region. Further results concern the impact of experimental parameters on mass transport. Experimental confirmation of these predictions was achieved by single crystal growth in a wider range of temperatures and rotation rates.

Acknowledgment

We are very grateful for the surface polishing of the samples by Stefanie Hoser. Experimental contributions by Christina Glassl are gratefully acknowledged.

[1] P. Gille, in: Crystal Growth of Intermetallics, P. Gille, Yu. Grin (Eds.), de Gruyter, Berlin/Boston, 61-90 (2019).
[2] H.J. Scheel, J. Crystal Growth, **13/14**, 560-565 (1972).
[3] M. Pillaca et al., J. Crystal Growth, **475**, 346-353 (2017).
[4] T. v. Kármán, Z. Angew. Math. Mechan., **1**, 233-252 (1921).
[5] D.T.J. Hurle, in: Advanced Crystal Growth, P.M. Dryburgh et al. (Eds.), Prentice Hall, 97-123 (1987).

Theoretical analysis, critique and validity limits of Haasen-Alexander-Model for predicting the dislocation density

D.V. Berkov

Genearl Numerics Research Lab, Moritz-von-Rohr-Str. 1ª, D-00745 Jena, Germany
E-mail: d.berkov@general-numerics-rl.de

In this talk we analyze in detail the widely used phenomenological Haasen-Alexander (HA) model [1,2] and its extension - Haasen-Alexander-Sumino (HAS) [3,4] model, which are used for predicting the dislocation density in crystals. We recall that both the original model and its extension are based on four equations of the meso- and macroscopic dislocation dynamics, namely:

- The Orowan law relating the **plastic** shear rate ε_p, density of mobile dislocations n_m and the dislocation velocity v:

$$\frac{d\varepsilon_p}{dt} = \frac{1}{F} n_m \cdot v \cdot b \qquad \text{(A)}$$

- The empirical law relating the growth rate of the dislocation density dn_m/dt to the effective stress τ_{eff}, the density n_m itself and the dislocation velocity v:

$$\frac{dn_m}{dt} = K \cdot \tau_{\text{eff}}^{\lambda} \cdot n_m \cdot v \qquad \text{(B)}$$

- The Arrhenius-type relation between the dislocation velocity v and the effective stress τ_{eff} via the activation energy of the dislocation motion Q:

$$v = v_0 \exp\left[-Q / k_B T\right] \cdot \tau_{\text{eff}}^{m} \qquad \text{(C)}$$

- The definition of the effective stress τ_{eff} via the applied stress τ_{ext} and the ‚hardening' term τ_{h}:

$$\tau_{\text{eff}} = \max\left(S \cdot \tau_{\text{ext}} - \tau_{\text{h}},\ 0\right), \quad \text{with } \tau_{\text{h}} = \alpha \cdot Gb \cdot \sqrt{n_m} \qquad \text{(D)}$$

Whereas the Orowans law is a direct consequence of the definition of a plastic deformation due to the dislocation movement (factor ***F*** accounts for different contributions of different dislocation types), equations (B), (C) and (D) cannot be obtained from any basic physical principles and should be viewed as empirical relations based on more or less uncontrollable assumptions. In particular, non-linear dependencies on the effective stress on the r.h.s. in Eqs. (B) and (C) are purely phenomenological and have no proper physical basis.

The most important point, however, is the absence of any physical justification for the functional form of the dependence of the hardening term $\tau_{\text{h}} \sim \sqrt{n_m}$ on the dislocation density n_m used in the key equation (D) of the HAS model. First, we point out, that in the original work of Haasen [1] this dependence was introduced on a purely phenomenological basis to explain the non-monotonicity of the stress-strain dependence. Haasen made an attempt to explain this term stating that the 'effective' stress is the sum of the external stress and the **average dislocation-induced stress**.

However, we show that this explanation is incorrect, because components of the dislocation-induced stress are **odd** functions of Cartesian coordinates, so that for the random (and most other kinds of) dislocation arrangement the **average dislocation-induced stress is zero**.

Next, we analyze the possibility that the 'effective' stress is the sum of the external stress and **the standard deviation** of the dislocation-induced stress. The latter quantity would indeed be proportional to $\sim\sqrt{n_m}$ (according to the central limit theorem), but this interpretation would be incorrect nevertheless, because the **random variable cannot be replaced** (even after averaging) **by its standard deviation** in any physical application.

The only possibility to assign a real physical meaning to the hardening term is to suggest, that **material 'hardening' is due to the presence of other (immobile!) dislocations** which generate a stress landscape for mobile dislocations. However, in this case the dislocation density in the hardening term would be different from the density of moving dislocations (these two dislocation populations are entirely different), which would also mean the failure of the HAS model.

Finally, we analyze the extended HAS model and summarize its advantages and further limitations. To the most serious limitations (in addition to the discussed above) belong:

- A very large number of freely adjustable parameters in the basic HA model; this number is even larger in the extended version, where many dislocation types and glide planes are taken into account.
- Complicated dislocation interactions (elastic forces, jogs, intersections etc.) are 'squeezed' into a single 'hardening' parameter ***a***
- Any structures in the dislocation arrangement (cellular structures, dislocation walls etc.) are neglected
- All model parameters have to be determined experimentally anew not only for each new material, but also for each new type of the growth process
- These model parameters should be, strictly speaking, time-dependent due to the possible appearance of new dislocation structures during the growth and annealing processes
- The model is not applicable to crystals with the low dislocation density, because the dislocation configuration in such crystals should be described in terms of separated dislocations.

Following the line of arguments presented above, we strongly recommend the development and usage of really physical models, where the complicated matter of the dislocation interaction and multiplication is treated based on established physical relations.

ACKNOWLEDGMENT. The author acknowledges the financial support of BMWi (grant Nu. 03ET1331A)

[1] P. Haasen, *Zeitschrift für Physik* **167** (1962) 461
[2] H. Alexander, P. Haasen, *Solid State Physics* **22** (1969) 27
[3] M. Suezawa, K. Sumino and I. Yonenaga, *phys. stat. sol.* (*a*) **51** (1979) 217
[4] K. Sumino, I. Yonenaga, *phys. stat. sol. (a)* **138** (1993) 573

Session 8

Friday 13.03.2020

11:00 – 12:50

Towards 80 mm dia. ultra-high purity germanium single crystals by Czochralski growth

Alexander Gybin, Kevin-Peter Gradwohl, Jozsef Janicskó-Csáthy, Natasha Dropka, Uta Juda,
Jörg Fischer and Radhakrishnan Sumathi*

Leibniz-Institut für Kristallzüchtung (IKZ), Max-Born-Str. 2, 12489 Berlin, Germany

**e-mail:* radhakrishnan.sumathi@ikz-berlin.de

Summary

High-purity germanium (HPGe) single crystals are very promising for their applications as radiation, spectroscopy detectors and are mostly used in experiments dealing with highest resolution, like dark matter research, neutrinoless events (e.g. LEGEND), and as best solution for precise gamma and x-ray spectroscopy. In comparison to silicon (Si), germanium (Ge) is much more efficient for radiation detection due to its high mass number, needing less energy for electron-hole pair creation and can have a larger depletion region (cm thickness) for total absorption. Growing "detector-grade" HPGe single crystals, with engineered structural defects and controlled properties, uniform throughout the crystal, represents one of the challenging tasks in these type of semiconductor materials' crystal growth. For low background and high-resolution detection, the impurity concentration in the crystal should be ultra-low ($n < 10^{10}$ cm^{-3}). Numerous process steps are involved to obtain ultra-pure Ge source material and to cultivate single crystals. Additional challenges arise as Ge is one of the few substances that expands as it solidifies.

We have been establishing the following principal process steps at IKZ, all in-house under a single roof, to obtain HPGe crystals: (i) Reduction of GeO_2 to Ge for preparing poly-crystalline Ge bars, (ii) multi-zone-refining of the starting Ge metal bars up to ultra-high purity (12 N); (iii) Czochralski (Cz) growth of single crystals. The most challenging steps are, zone refining to reach the unprecedented purity and the Cz growth, both in H_2 atmosphere. In order to obtain the required purity level, the growth equipment has been specially constructed with an inductive heating set-up. However, it makes the control of the thermal field much more complicated as compared to resistive heating systems. The suitability of the constructed equipment has been tested for growing 2-inch crystals, before implementing a scaling-up process to grow larger diameter (≈ 3-inch), massive crystals of few kgs in weight. For higher sensitivity and larger volume for detecting dark matter events, large diameter HPGe crystals are prerequisite.

The 3-inch diameter crystals are grown along the [100] direction (Fig.1a), which allow the dislocations to glide out and terminate at the crystal surface. The dislocation densities in these crystals are relatively higher ($\approx 10^4$ cm^{-2}), but uniform all along the grown crystals. The 2-inch crystals grown under well-optimised conditions, usually have a dislocation density in the mid. 10^3 cm^{-2}, which is in the required range ($10^2 - 10^4$ cm^{-2}) for the applications. [111] oriented crystals were also grown (Fig. 1b, nice facets seen from the top view). During the scaling-up process of massive crystals, further optimisation of the hot-zone and growth parameters are decisive. The most influencing factor in HPGe crystal growth is the process gas (H_2) environment, which makes the thermal field difficult to be controlled and thereby the temperature gradient in the growth regime. The H_2 atmosphere is used to reduce the oxides and minimize trapping centers. H_2 has a large thermal conductivity, low viscosity and also large convective heat transfer coefficient. Further, its purity, flow rate, convection, etc., will

additionally play a role on the final impurity concentration and defect density in the crystals. In our growth equipment, all the internal parts were home-designed and constructed specifically to take care of the concerns of high purity. A realistic three-dimensional computer-aided-design (3D-CAD) model was used to define the geometry, and for a good understanding of the thermal field and transport kinetics, computational fluid dynamics (CFD) simulations have been carried out (Fig.1c).

The grown crystals were investigated in the limelight of crystal perfection, defect density, defect nature and concentration of impurities. Different segregation coefficients of acceptors (B, having a very high segregation coefficient in Ge, $k_0 > 17$) and donors (P, very low $k_0 \approx 0.08$) give raise to a p-n transition around the middle part of the crystal. The shape of the solid-melt interface during the growth process is also important to predict the radial homogeneity of the wafers. The detailed properties obtained from various measurements will be presented, especially for large diameter crystals. The issues related to the diameter enlargement and retaining the control over purity and defect density will also be elucidated.

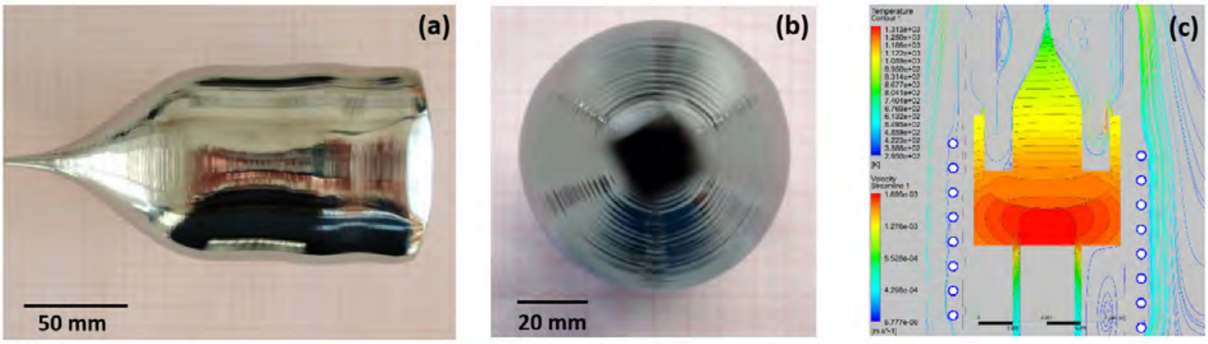

Fig. 1: a) Photo of a 3-inch dia. [100] HPGe crystal grown at IKZ; b) [111] oriented HPGe crystal; c) Numerical simulation of temperature field and gas convection in the crystal growth system.

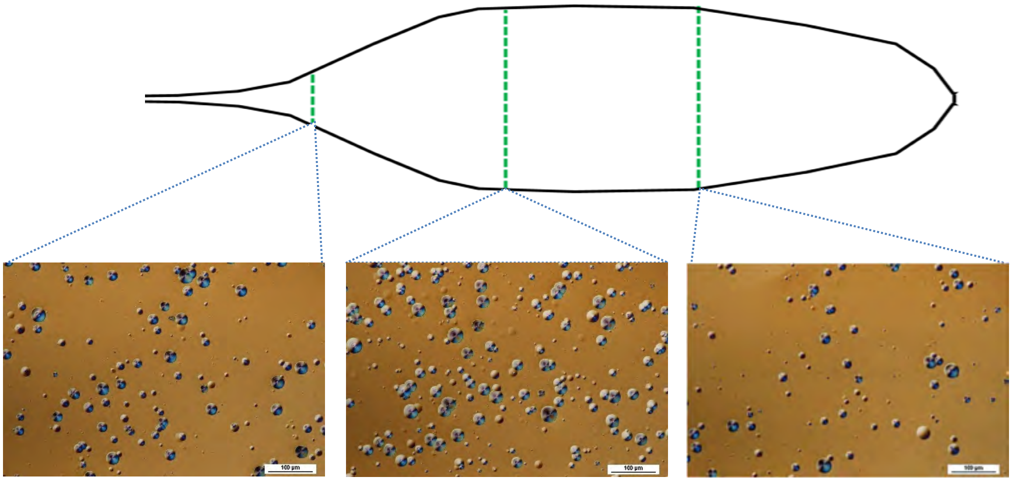

Fig. 2: Controlled EPD in the crystal grown in the newly scaled-up system. Top: Sketch showing the places where the samples were taken for EPD analyses; Bottom: Etched surfaces of the wafers cut from their respective top, middle, and bottom parts.

Acknowledgment

Authors gratefully acknowledge the German Federal Ministry for Education and Research (BMBF) for the financial support through a research grant (number 05A17BC1).

Formation of vacancy related defects in high-purity germanium

K.-P. Gradwohl [a], A. Gybin [a], J. Janicsko-Csathy [a], M. Roder [b], A. Danilewsky [b], R.R. Sumathi [a]

[a] *Leibniz-Institut für Kristallzüchtung, Max-Born-Str. 2, 12489 Berlin, Germany*
[b] *Kristallographie, ALU Freiberg, Hermann-Herder-Str. 5, 79104 Freiburg, Germany*
E-mail: radhakrishnan.sumathi@ikz-berlin.de

Large mass radiation detectors with high resolution can be fabricated from high-purity germanium. The production of such detectors has recently gained large interest, since they might aid in the search of the neutrinoless double beta decay within the experimental program of the LEGEND collaboration [1]. For these applications, Ge single crystals with a very high crystalline perfection are required, to say more precisely, a high purity (net concentration of electrically active impurities $< 10^{10}$ cm^{-3}) and a homogeneous distribution of less structural defects such as dislocations and voids are required.

[100] single crystals of HPGe with a diameter of 2-inch were grown in pure H_2 atmosphere by the Czochralski method as described elsewhere [2]. The structural defects in these crystals were investigated by white beam X-ray imaging conducted at the topography station at the imaging cluster of the Karlsruhe Research Accelerator (KARA) synchrotron – a 2.5 GeV electron storage ring situated at Karlsruhe Institute of Technology (KIT), Germany [3]. The top part of the crystal was mostly dislocation-free and the dislocation density increases towards the tail of the crystal to a value of 2600 cm^{-2}, as can be seen in the X-ray topographs of Fig. 1. In a Ge crystal, the equilibrium vacancy (V) concentration at the melting point which ultimately originates from the growth process is 10^{15} cm^{-3}, while the concentration of self-interstitials is only around 10^{9} cm^{-3}, which has been shown by first-principles calculations [4] as well as experimentally [5]. Hence, the mechanism $Ge_i + V_{Ge} \rightarrow Ge_{Ge}$ (Frank-Turnbull) does not noticeably reduce the concentration of Vs in the crystal. Vs can only be absorbed in parts of the crystal with dislocations of partly edge character, which consequently climb. Consequently, dislocation-free crystals exhibit huge excess Vs, which tend to form clusters (e.g. voids) or even electrically active V-related complexes when grown under H_2 atmosphere. We have observed that these Vs cluster into voids in the dislocation-free parts of the crystal, while no voids can be observed in parts with moderate dislocation density. The voids are identified by a black-white contrast in the topographs (Fig.1a), which is caused by a dynamical diffraction effect. It results from a modulation of the diffracted intensity, induced by a shift of the tie point position on the dispersion surface by the bending of lattice planes, due to the tensile strain around voids [6]. We estimate that the void density in the top part of the crystal is $< 10^{5}$ cm^{-3} and therefore very hard to detect them directly by microscopy.

The comparison of etching features originating from a modified CP-4 etch of samples from dislocation-free with non-dislocation-free samples of the crystal showed clear differences, indicating different defect structures. Charge carrier lifetime in dislocation-free wafers, laterally mapped by microwave detected photoconductivity (MDP), was determined to be less than 100 µs, which is only a fraction of the typical lifetime (>500 µs) in comparable samples with a moderate dislocation density along with homogeneous distribution. At the middle of the wafers the charge carrier lifetime of dislocation-free crystals can even locally drop below 20 µs. Since this behavior is not explicable by the simple presence of voids, further vacancy-related defects such as V-H complexes or vacancy condensation in the form of intrinsic stacking faults may exist in the crystals.

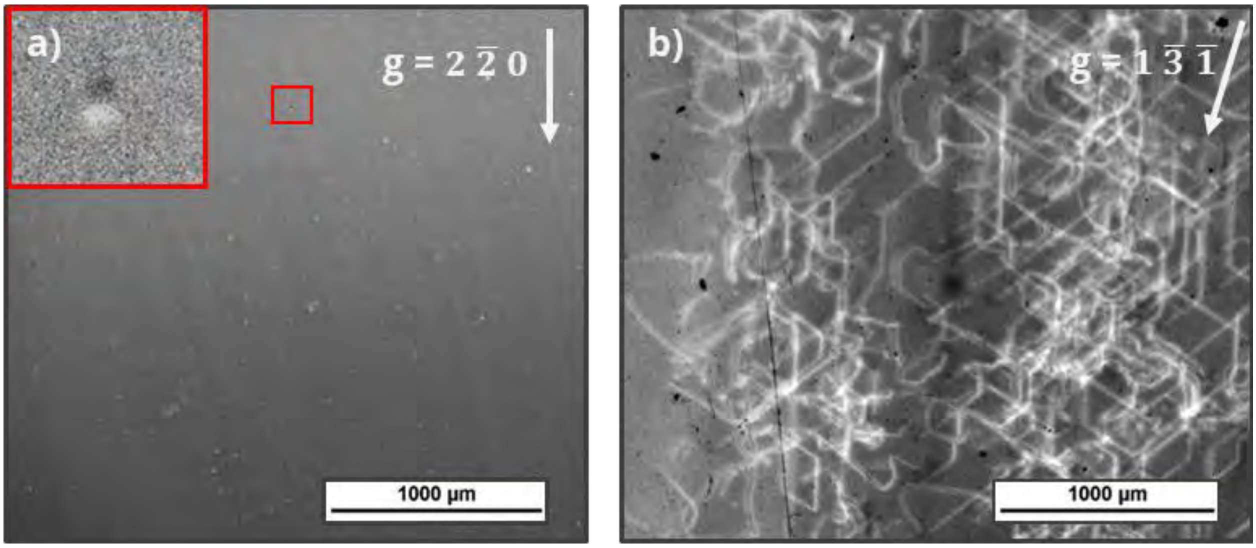

Fig. 1: White beam X-ray topographs of [100] Cz-Ge grown in H_2 atmosphere. (a) depicts an almost dislocation-free part of the crystal (>1 cm^2) with a void depicted in the inset, while (b) shows a part of the same crystal with a moderate dislocation density of 2600 cm^{-2} and no indication of voids.

Acknowledgment

We thank the Karlsruhe Institute of Technology for the beam time at the Karlsruhe Research Accelerator synchrotron for investigation of our samples in the framework of the BIRD contract. We acknowledge the support by the German Federal Ministry for Education and Research (BMBF) within the collaborative project under the grant number 05A2017-GERDA.

[1] N. Abgrall, et al., AIP Conference Proceedings, **1894**, No. 1 (2017)
[2] N. Abrosimov, M. Czupalla, N. Dropka, J. Fischer, A. Gybin, K. Irmscher, J. Janicskó-Csáthy, U. Juda, S. Kayser, W. Miller, M. Pietsch, F. M. Kießling, Journal of Crystal Growth, **532**, 125396 (2020)
[3] A. Rack, T. Weitkamp, S. Bauer Trabelsi, P. Modregger, A. Cecilia, T. dos Santos Rolo, T. Rack, D. Haas, R. Simon, R. Heldele, M. Schulz, B. Mayzel, A. N. Danilewsky, T. Waterstradt, W. Diete, H. Riesemeier, B. R. Müller, T. Baumbacha, Nuclear Instruments and Methods in Physics Research Section B: Beam Interactions with Materials and Atoms, **267.11**, 1978-1988 (2009)
[4] P. Śpiewak, K. Sueoka, J. Vanhellemont, K. J. Kurzydłowski, K. Młynarczyk, P. Wabiński, I. Romandice, Physica B: Condensed Matter, **401**, 205-209 (2007)
[5] J. Vanhellemont, P. Śpiewak, K. Sueoka, Journal of Applied Physics, **101**, 036103 (2007)
[6] T. Tuomi, R. Rantamäki, P. J. McNally, D. Lowney, A. N. Danilewsky, P. Becker, Journal of Physics D: Applied Physics, **34**, 10A (2001)

$CaWO_4$ CRYSTAL GROWTH FOR THE CRESST DARK MATTER SEARCH

A. Kinast [a], A. Erb [a,b], F. Hamilton [a], M. Kaznacheeva [a], A. Langenkämper [a],
E. Mondragon [a], T. Ortmann [a], L. Pattavina [a], W. Potzel [a], S. Schönert [a],
R. Strauss [a] and V. Wagner [a]

[a] *Physik Department, Technische Universität München, James-Franck-Str. 1, 85748 Garching, Germany*
[b] *Walther-Meißner-Institut, Bayerische Akademie der Wissenschaften, Walther-Meißner-Straße 8,*
85748 Garching, Germany

E-mail: angelina.kinast@tum.de

Summary

The CRESST (**C**ryogenic **R**are **E**vent **S**earch with **S**uperconducting **T**hermometers) experiment is searching for elastic scattering of light dark matter particles using $CaWO_4$ single crystals. It is located deep underground at the Laboratori Nazionali del Gran Sasso (LNGS) in Italy and surrounded by several layers of active and passive shielding to reduce various backgrounds such as cosmic radiation or radiation from radioactive decays. CRESST is the world leading experiment in the mass range up to 0.5 GeV/c^2. A low detector threshold and a low background have a crucial impact on the sensitivity [1]. For both, the quality of the $CaWO_4$ crystals is essential. In order to fulfill the requirements of CRESST, a dedicated Czochralski crystal growth facility (see fig 1a) has been set up at the Technical University of Munich (TUM), starting from the production of the $CaWO_4$ powder from the raw materials $CaCO_3$ and WO_3 up to the final steps of cutting the detector crystals from the ingot [2]. An important milestone was the growth of the crystal TUM40 (see Fig. 1b,c) which showed an exceptional performance and a much higher radio-purity compared to commercially purchased crystals Daisy (dashed red line) and VK31 (dashed black line) [3],[4].

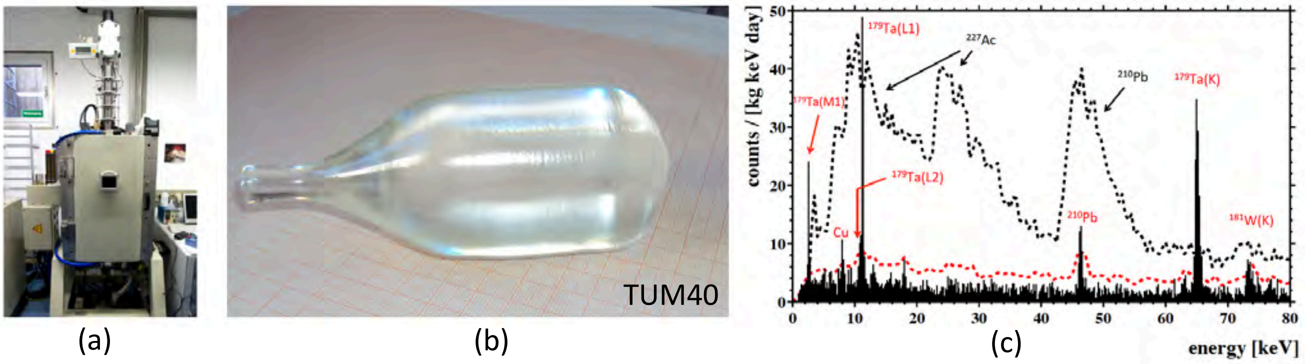

(a) (b) (c)

Fig. 1: (a) Picture of the Czochralski furnace in which the $CaWO_4$ single crystals are grown at TUM. The facility is exclusively used for $CaWO_4$ crystal growth to avoid cross contamination from impurities of other materials. (b) The $CaWO_4$ crystal ingot TUM40.
(c) Histogram of the low-energy events of the detector TUM40 (black bars) recorded during CRESST-II Phase 2. The most prominent peaks are labelled. In comparison the two commercially bought crystals Daisy (dashed red line) and VK31 (dashed black line). Figure from [4].

In order to further improve the quality of the $CaWO_4$ crystals two approaches are followed. First and most important the improvement of the crystals' radiopurity by two orders of magnitude. For this a synthetization of the $CaWO_4$ powder via a precipitation reaction (see Fig. 2a) as well as an extensive powder purification for both the raw materials and the synthesized $CaWO_4$ powder has been developed and conducted at TUM. Screening of the powder using HPGe detectors shows a significant improvement of the radiopurity.
The second way to improve the crystal quality is the reduction of internal stress which is introduced to the crystal lattice from temperature gradients during the growth. To target this, a simulation of the temperature distribution in the furnace was developed with the help of the Leibniz-Institut für Kristallzüchtung (IKZ) using COMSOL Multiphysics (see Fig. 2b). The Czochralski setup was adapted accordingly and first measurements of the crystals in a stress birefringence setup show promising results.

In August 2019 the crystal TUM93 was grown from the first batch of the extensively chemically purified powder. Three CRESST detector crystals have been cut from the ingot and installed in the CRESST setup. This is an important milestone to reach the goals of the CRESST dark matter search.

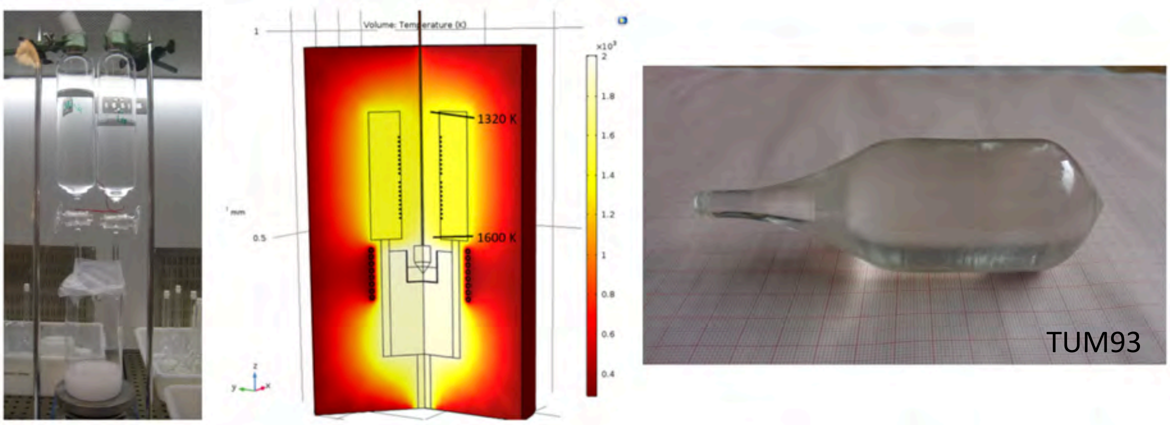

(a) (b) (c)

Fig. 2: (a) Picture of the precipitation reaction of the $CaWO_4$ powder from the raw materials $CaCO_3$ and WO_3 which are brought in an aqueous solution and are chemically purified prior to the reaction.
(b) Temperature distribution during the Czochralski growth. This simulation was performed with the program COMSOL Multiphysics in order to understand the temperature gradients during the growth better which are causing stress in the crystal lattice. The setup was then modified accordingly to lower these gradients.
(c) The $CaWO_4$ crystal TUM93 which was grown from the first batch of an extensively chemical purified powder. Three detector crystals have been cut from the ingot. They are currently operated in the ongoing CRESST run.

Acknowledgments

This research was supported by the DFG cluster of excellence Origins, by the BMBF Verbundprojekt 05A2017 CRESST-XENON and by the SFB1258.

[1] A. H. Abdelhameed, et al, *arXiv:1904.00498* (2019).
[2] A. Erb, J.-C. Lanfranchi, **CrystEngComm**, 15.12 (2013): 2301-2304.
[3] R. Strauss, et al., **The European Physical Journal**, C 75.8 (2015): 352.
[4] R. Strauss, et al., **Journal of Cosmology and Astroparticle Physics**, 2015.06 (2015): 030.

Investigation of particle incorporation in a transparent melt system under µg conditions

T. Jauß[a], T. Sorgenfrei[a]

[a]*Kristallographie, Albert-Ludwigs-Universität Freiburg, Hermann-Herder-Straße 5, 79104 Freiburg, Germany*

E-mail: thomas.jauss@fmf.uni-freiburg.de

The incorporation of foreign phase particles during crystal growth is a common occurrence, for example during the directional solidification of multi crystalline silicon for photovoltaic applications or string casting processes. These foreign phases generate several limitations, starting with acting as sources for dislocation clusters, disturbing the post growth material processing like wafering during wire sawing, and may be responsible for electrical problems, i.e. for solar cells by acting as shunts, short-circuiting the device. During earlier investigations of the incorporation behavior of silicon carbide (SiC) and silicon nitride (Si_3N_4) particles into growing silicon crystals [1, 2], we experienced the need to study the local reaction of the approaching phase boundary to the particle in front of it more in detail. With silicon as an opaque crystal and equally opaque melt, the only available way to investigate is post growth, and therefore, it is impossible to see the incorporation of a particle at the time of its engulfment. This requirement leads to the use of a transparent melt system with direct visual observability of the particles in the melt, in front of the phase boundary, and during the engulfment process.

The model system studied in this work is ice-water-glass-polystyrene. H_2O shows a clear and planar solid-liquid phase front while it can be crystallized in a suitable range of growth velocities. Different species of spherical particles were used to investigate the influence of different material parameters like density (density ratio to surrounding fluid), heat capacity, heat conductivity, etc. Hollow spheres of glass (9-13 µm diameter) and spheres of polystyrene (10, 30, and 100 µm diameter) were engulfed by a moving ice/water phase boundary. This setup was used under terrestrial conditions as well as on board of the TEXUS 56 sounding rocket payload, under microgravity conditions.

During the experiments, we could observe that in this system, similar to the Si-SiC-Si_3N_4 system, a critical growth velocity exists, below which a particle gets pushed along by the solid liquid interface, and above which a particle gets incorporated. Further, we could observe that the moving phase boundary also enriches the particles in front of itself, while it only incorporates particles with the "correct" radius (Fig 1).

As mentioned above, the focus of this work lies in the investigation of the direct, short-term, and local response of the moving phase boundary on the stationary/static particle in the fluid while getting closer. In µg as well as in reference experiments on ground it was observed that there is no determinable reaction of the phase boundary like forming hillocks or trenches, when a particle is engulfed and incorporated. The growth front stays flat, while the particle is overgrown laterally (Fig 2). This behavior is also in accordance to a silicon crystal engulfing a SiC particle (Fig 3). The acquired data points can now be used to further calibrate and validate quantitative FEM-models, so numerical predictions about particle incorporation can be made.

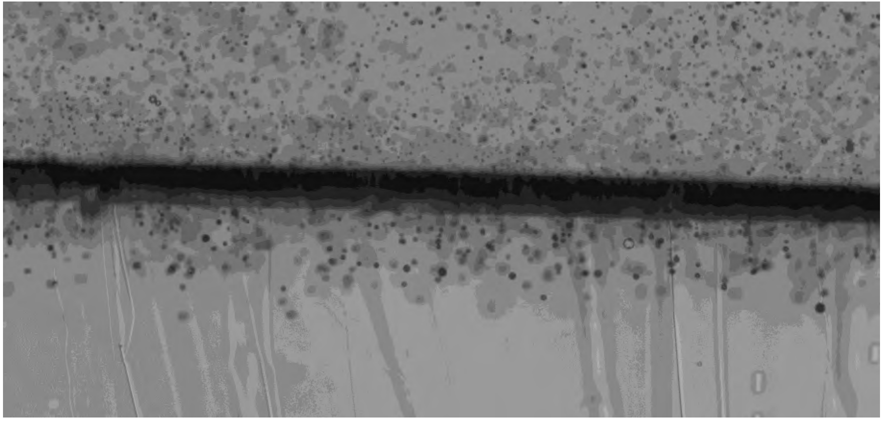

Fig. 1: Hollow glass sphere particles incorporated as a horizon by the moving ice-water phase boundary.

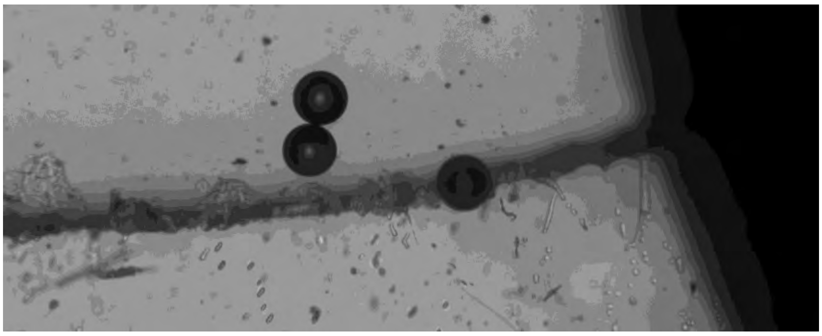

Fig. 2: Polystyrene particles with 30 µm diameter are engulfed by the moving ice-water phase boundary without determinable deformation of the phase boundary into hillocks or trenches.

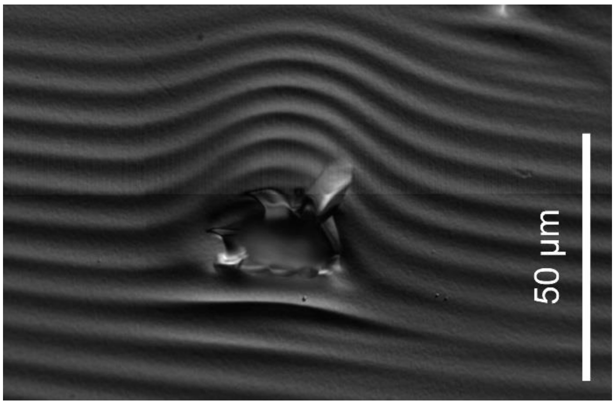

Fig. 3: SiC particle engulfed during growth. The striations indicate no reaction of the phase boundary to the particle prior to engulfment

Acknowledgment

We would like to thank Ms. Nadine Pfändler for her work during the preparations and execution of the TEXUS 56 sounding rocket mission. Our thanks also go to the teams of Airbus D&S, OHB, and SSC for their invaluable technical support. Financial support by DLR/BMWi under FKZ 50WM1756 is gratefully acknowledged.

[1] J. Friedrich, C. Reimann, T. Jauss, A. Cröll, T. Sorgenfrei, J Cryst Growth, **447**, 18-26 (2016)

[2] J. Friedrich, C. Reimann, T. Jauss, A. Cröll, T. Sorgenfrei, Y. Tao, J.J. Derby, J Cryst Growth, **475**, 33 (2017)

Posterprize

A prize for the best poster presented during the poster session on Wednesday March 11, 2020 will be given by DGKK.

The winner will receive the volume “Fundamentals: Thermodynamics and kinetics” of the Handbook of Crystal Growth.
The volume is sponsored by Elsevier